

เมลามีนเซ็นเซอร์แบบเรืองแสงจากแนพทาลีไมด์-กรดไซยานูริกคอนจูเกต



นางสาวจิตรานุช เฟิงส์สวัสดิ์

จุฬาลงกรณ์มหาวิทยาลัย

CHULALONGKORN UNIVERSITY

บทคัดย่อและแฟ้มข้อมูลฉบับเต็มของวิทยานิพนธ์ตั้งแต่ปีการศึกษา 2554 ที่ให้บริการในคลังปัญญาจุฬาฯ (CUIR)

เป็นแฟ้มข้อมูลของนิสิตเจ้าของวิทยานิพนธ์ ที่ส่งผ่านทางบัณฑิตวิทยาลัย

The abstract and full text of theses from the academic year 2011 in Chulalongkorn University Intellectual Repository (CUIR) are the thesis authors' files submitted through the University Graduate School.

วิทยานิพนธ์นี้เป็นส่วนหนึ่งของการศึกษาตามหลักสูตรปริญญาวิทยาศาสตรมหาบัณฑิต

สาขาวิชาปิโตรเคมีและวิทยาศาสตร์พอลิเมอร์

คณะวิทยาศาสตร์ จุฬาลงกรณ์มหาวิทยาลัย

ปีการศึกษา 2558

ลิขสิทธิ์ของจุฬาลงกรณ์มหาวิทยาลัย

MELAMINE FLUORESCENT SENSORS FROM NAPHTHALIMIDE-
CYANURIC ACID CONJUGATES

Miss Chittranuch Pengsawad



A Thesis Submitted in Partial Fulfillment of the Requirements
for the Degree of Master of Science Program in Petrochemistry and Polymer Science
Faculty of Science
Chulalongkorn University
Academic Year 2015
Copyright of Chulalongkorn University

| | |
|-------------------|---|
| Thesis Title | MELAMINE FLUORESCENT SENSORS FROM NAPHTHALIMIDE-CYANURIC ACID CONJUGATES |
| By | Miss Chittranuch Pongsawad |
| Field of Study | Petrochemistry and Polymer Science |
| Thesis Advisor | Associate Professor Paitoon Rashatasakhon, Ph.D. |
| Thesis Co-Advisor | Professor Mongkol Sukwattanasinitt, Ph.D. |

Accepted by the Faculty of Science, Chulalongkorn University in Partial
Fulfillment of the Requirements for the Master's Degree

.....Dean of the Faculty of Science
(Associate Professor Polkit Sangvanich, Ph.D.)

THESIS COMMITTEE

.....Chairman
(Professor Pattarapan Prasassarakich, Ph.D.)

.....Thesis Advisor
(Associate Professor Paitoon Rashatasakhon, Ph.D.)

.....Thesis Co-Advisor
(Professor Mongkol Sukwattanasinitt, Ph.D.)

.....Examiner
(Assistant Professor Varawut Tangpasuthadol, Ph.D.)

.....External Examiner
(Nakorn Niamnont, Ph.D.)

จิตรานุช เพ็งสวัสดิ์ : เมลามีนเซ็นเซอร์แบบเรืองแสงจากแนพทาลิไมด์-กรดไซยานูริกคอนจูเกต (MELAMINE FLUORESCENT SENSORS FROM NAPHTHALIMIDE-CYANURIC ACID CONJUGATES) อ.ที่ปรึกษาวิทยานิพนธ์หลัก: รศ. ดร. ไพฑูรย์ รัชตะสาคร, อ.ที่ปรึกษาวิทยานิพนธ์ร่วม: ศ. ดร. มงคล สุขวัฒนาสินธิ์, 83 หน้า.

การพัฒนาเซ็นเซอร์สำหรับเมลามีนเป็นแนวทางวิจัยที่มีความสำคัญเนื่องจากเมลามีนที่ตกค้างอยู่ในผลิตภัณฑ์นมและอาหารเด็กนั้นมีความเป็นพิษต่อมนุษย์โดยเฉพาะอย่างยิ่งสำหรับเด็กอ่อน งานวิจัยนี้ออกแบบและสังเคราะห์ฟลูออเรสเซนต์เซ็นเซอร์ใหม่ 5 ชนิด (F1 ถึง F5) ซึ่งมี 1,8-แนพทาลิไมด์เป็นฟลูออโรฟอร์และมีหมู่ไซยานูริกเป็นหน่วยตรวจจับสำหรับเมลามีน ได้พิสูจน์เอกลักษณ์สารเป้าหมายทุกชนิดด้วยเทคนิคโปรตอนและคาร์บอนนิวเคลียร์แมกเนติกเรโซแนนซ์ แมสสเปกโตรเมตรีความละเอียดสูง และการวิเคราะห์ธาตุองค์ประกอบ และศึกษาสมบัติเชิงแสงด้วยยูวีวิซิเบิลและฟลูออเรสเซนต์สเปกโตรสโกปี การค้นหาความจำเพาะโดยใช้สารละลายของ F3, F4 และ F5 ในตัวทำละลายผสมระหว่างน้ำกับไดเมทิลซัลฟอกไซด์พบว่าเกิดการเปลี่ยนสัญญาณฟลูออเรสเซนต์ได้ในภาวะที่มีเมลามีน โดยกลไกการเปลี่ยนแปลงสัญญาณเกิดจากการรวมตัวกันของฟลูออโรฟอร์และการแยกตัวจากกัน เมื่อเกิดพันธะไฮโดรเจนระหว่างเมลามีนกับหมู่ไซยานูริก เซ็นเซอร์ F3 และ F4 จะเกิดการระงับสัญญาณหลังการรวมตัวกันในตัวทำละลายน้ำ 90% ในไดเมทิลซัลฟอกไซด์ ส่งผลให้มีสัญญาณฟลูออเรสเซนต์ที่ต่ำลง และเมื่อเติมเมลามีนแล้วจะเกิดสัญญาณที่สูงขึ้นเมื่อฟลูออโรฟอร์เหล่านั้นแยกตัวออกจากกัน โดยเซ็นเซอร์ F4 มีขอบเขตของการตรวจวัดเมลามีนที่ 0.8 ส่วนในล้านส่วน แต่สำหรับเซ็นเซอร์ F5 นั้นมีพฤติกรรมที่ให้สัญญาณฟลูออเรสเซนต์ที่สูงขึ้นเมื่อเกิดการรวมตัวกันในตัวทำละลายผสมระหว่างน้ำกับไดเมทิลซัลฟอกไซด์ และเกิดการระงับสัญญาณเมื่อเมลามีนไปทำให้ฟลูออโรฟอร์เกิดการแยกตัวกัน โดยให้ค่าคงที่สเทิร์นโวลเมอร์ที่ 3×10^3 ต่อโมลาร์ และมีขอบเขตของการตรวจวัดเมลามีนที่ 3.2 ส่วนในล้านส่วน

สาขาวิชา ปีโตรเคมีและวิทยาศาสตร์พอลิเมอร์ ลายมือชื่อนิสิต

ปีการศึกษา 2558

ลายมือชื่อ อ.ที่ปรึกษาหลัก

ลายมือชื่อ อ.ที่ปรึกษาร่วม

5572241623 : MAJOR PETROCHEMISTRY AND POLYMER SCIENCE

KEYWORDS: FLUORESCENCE SENSOR / MELAMINE / CYANURIC ACID / 1,8-NAPHTHALIMIDE / AGGREGATION-CAUSED QUENCHING (ACQ) / AGGREGATION-INDUCED EMISSION ENHANCEMENT (AIEE) / DE-AGGREGATION

CHITTRANUCH PENGSAWAD: MELAMINE FLUORESCENT SENSORS FROM NAPHTHALIMIDE-CYANURIC ACID CONJUGATES. ADVISOR: ASSOC. PROF. PAITON RASHATASAKHON, Ph.D., CO-ADVISOR: PROF. MONGKOL SUKWATTANASINITT, Ph.D., 83 pp.

The development of melamine sensors is an important research theme because contaminating melamine in dairy products or infant powder is toxic to human health, especially for babies. In this research, five novel fluorescent sensors (F1 to F5) containing a 1,8-naphthalimide fluorophore and cyanuric moiety as melamine receptor are designed and successfully synthesized. All target compounds are characterized by ^1H and ^{13}C -NMR, High Resolution Mass Spectrometry, and Elemental Analysis. The photophysical properties are investigated by UV-Vis and fluorescence spectroscopy. The selectivity screenings in aqueous DMSO indicate that F3, F4 and F5 give selective fluorogenic changes in the presence of melamine. The sensing mechanism involves the fluorophore aggregation and de-aggregation by multivalent hydrogen-bonding between melamine with cyanuric moiety. The sensor F3 and F4 in 90% water in DMSO show Aggregation-Caused Quenching (ACQ) behavior which results in weak fluorescent emission. After the addition of melamine, the fluorescent signals are selectively enhanced based on the de-aggregation of fluorophore. The sensor F4 provided a detection limit for melamine at 0.8 ppm. On the other hands, the sensor F5 which exhibits an Aggregation-Induced Emission Enhancement (AIEE) in aqueous DMSO shows selective florescence quenching toward melamine upon de-aggregation. The Stern-Volmer constant (K_{sv}) for signal quenching by melamine is $3 \times 10^3 \text{ M}^{-1}$ with the detection limit of 3.2 ppm.

Field of Study: Petrochemistry and
Polymer Science

Student's Signature

Advisor's Signature

Academic Year: 2015

Co-Advisor's Signature

ACKNOWLEDGEMENTS

First of all, I would like to express my sincere gratitude to my thesis advisor, Associate Professor Dr. Paitoon Rashatasakhon and my co-advisor, Professor Dr. Mongkol Sukwattanasinitt for giving me the opportunities, invaluable advice, guidance and encouragement throughout the course of this research. Sincere thanks are also extended to Assistant Professor Dr. Anawat Ajavakom, Assistant Professor Dr. Sumrit Wacharasindhu and Dr. Sakulsuk Unarunotai for their generous advice, invaluable guidance and encouragement.

I would like to gratefully acknowledge the committee, Professor Dr. Pattarapan Prasassarakich, Assistant Professor Dr. Varawut Tangpasuthadol and Dr. Nakorn Niamnont for their kindness, valuable suggestion and recommendations.

I would like to express my gratitude to Material to Material Advancement via Proficient Synthesis group (MAPS), Department of Chemistry, Faculty of Science, Chulalongkorn University for providing the chemicals and facilities throughout the course of study.

A deep affectionate gratitude is acknowledged to my beloved family for their understanding, encouragement and support throughout the education course. I especially thank Ms. Pornpat Sam-ang, Ms. Kunnigar Vongnam and Ms. Kanokthorn Boonkitpatarakul for their training, helps, suggestions and guidance. Moreover, I would like to thanks everyone in MAPS group for a great friendship, spirit, smile, good wish and their helps.

Finally, I would like to express my thankfulness to my beloved parents who always stand by my side during both of my pleasant and hard time. I would not be able to reach this success without them.

CONTENTS

| | Page |
|--|-------|
| THAI ABSTRACT | iv |
| ENGLISH ABSTRACT | v |
| ACKNOWLEDGEMENTS | vi |
| CONTENTS | vii |
| LIST OF FIGURES | xi |
| LIST OF SCHEMES | xvii |
| LIST OF TABLES | xviii |
| LIST OF ABBREVIATIONS | xix |
| CHAPTER I INTRODUCTION..... | 1 |
| 1.1 Melamine..... | 1 |
| 1.2 Fluorescence | 2 |
| 1.2.1 Principle of fluorescence | 3 |
| 1.2.2 Fluorescent chemosensors | 4 |
| 1.2.2.1 Fluorescence Quenching | 4 |
| 1.2.3 Mechanism of fluorescent signal changes..... | 5 |
| 1.2.3.1 Photo induced-electron transfer (PET)..... | 5 |
| 1.2.3.2 Internal charge transfer (ICT)..... | 6 |
| 1.2.3.3 Aggregation-caused quenching (ACQ)..... | 7 |
| 1.2.3.4 Aggregation-induced emission enhancement (AIEE)..... | 7 |
| 1.3 Naphthalimide derivatives as fluorescent sensors..... | 8 |
| 1.4 Chemical sensor for the detection of melamine | 9 |
| 1.5 Objective of the this research | 13 |

| | Page |
|--|------|
| CHAPTER II EXPERIMENTAL | 14 |
| 2.1 Chemical and Materials..... | 14 |
| 2.2 Analytical Instruments..... | 14 |
| 2.3 Synthesis and Characterizations..... | 15 |
| 2.3.1 Synthesis of 1a | 15 |
| 2.3.2 Synthesis of 2a | 15 |
| 2.3.3 Synthesis of F1 | 16 |
| 2.3.4 Synthesis of 1b..... | 17 |
| 2.3.5 Synthesis of 2b..... | 17 |
| 2.3.6 Synthesis of 3b..... | 18 |
| 2.3.7 Synthesis of F2 | 19 |
| 2.3.8 Synthesis of 1c | 20 |
| 2.3.9 Synthesis of 2c | 20 |
| 2.3.10 Synthesis of 3c | 21 |
| 2.3.11 Synthesis of F3..... | 21 |
| 2.3.12 Synthesis of 1d..... | 22 |
| 2.3.13 Synthesis of 2d..... | 23 |
| 2.3.14 Synthesis of 3d..... | 23 |
| 2.3.15 Synthesis of F4..... | 24 |
| 2.3.16 Synthesis of 1e..... | 24 |
| 2.3.17 Synthesis of 2e..... | 25 |
| 2.3.18 Synthesis of F5..... | 25 |
| 2.4 Photophysical properties..... | 26 |

| | Page |
|--|------|
| 2.4.1 UV-Visible spectroscopy | 26 |
| 2.4.1.1 Molar extinction coefficient (ϵ) | 26 |
| 2.4.2 Fluorescence spectroscopy | 27 |
| 2.4.2.1 Fluorescence quantum yield | 27 |
| 2.5 Fluorescence sensor study | 28 |
| 2.5.1 Melamine sensors | 28 |
| 2.5.2 Interference behaviors from relative structure of melamine | 28 |
| 2.5.3 Effect of water content | 28 |
| 2.5.4 Time-dependent effect | 28 |
| 2.5.5 Surfactant study | 29 |
| 2.5.6 pH effect | 29 |
| 2.5.7 Limit of detection | 29 |
| CHAPTER III RESULTS AND DISCUSSION..... | 30 |
| 3.1 Synthesis and characterization | 30 |
| 3.2 Photophysical properties of F1 to F5 | 34 |
| 3.3 Screening of F1 to F3 toward melamine..... | 36 |
| 3.4 Screening of F4 and F5 towards melamine..... | 38 |
| 3.5 selectivity study of F4 and F5 toward melamine..... | 40 |
| 3.6 Proposed mechanism of F4 toward melamine | 41 |
| 3.7 Melamine detection optimization | 43 |
| 3.7.1 pH effect study..... | 43 |
| 3.7.2 Water content for detection of melamine..... | 44 |
| 3.7.3 Time-dependent study..... | 45 |

| | Page |
|--|------|
| 3.7.4 Surfactant study | 45 |
| 3.8 Interferences test | 46 |
| 3.9 Detection limit of F4 and F5 toward melamine | 48 |
| 3.10 ¹ H NMR experiment | 49 |
| CHAPTER IV CONCLUSION | 50 |
| 4.1 Conclusion | 50 |
| 4.2 Suggestion for future works..... | 50 |
| REFERENCES | 52 |
| VITA..... | 83 |



LIST OF FIGURES

| | |
|--|----|
| Figure 1.1 Structure of melamine. | 1 |
| Figure 1.2 The toxicity of melamine in the human body | 2 |
| Figure 1.3 Examples of fluorescent compounds..... | 3 |
| Figure 1.4 The Jablonski diagram | 4 |
| Figure 1.5 The format of fluorescent PET sensor. | 5 |
| Figure 1.6 General sensor designs by PET mechanism [22]..... | 6 |
| Figure 1.7 Potential energy surfaces of the ground state (S_0) is excited to and S_1 or S_2 and then relaxed to LE, and ICT (FC = Franck-Condon)..... | 7 |
| Figure 1.8 Planar molecules such as pyrene tend to aggregate just as discs pile up due to strong π - π stacking interactions, which commonly turn “off” light emission, whereas nonplanar propeller-shaped luminogens such as hexaphenylsilole (HPS) behave oppositely, with their light emissions turned “on” by aggregate formation, due to the restricted intramolecular rotation in the aggregates..... | 8 |
| Figure 1.9 Examples of chemosensors derived from 1,8-naphthalimides..... | 9 |
| Figure 1.10 Novel recognition and transducer components used for fabrication of sensor for melamine detection sensor..... | 9 |
| Figure 1.11 a) structure of CB7; Molecular modeling of the CB7-melamine complex. b) conformation of melamine; c) top-view of CB7-melamine complex; b) side-view of CB7-melamine complex. | 10 |
| Figure 1.12 Structure formula of florescent functional monomer..... | 10 |
| Figure 1.13 Mechanical representation of fluorescence enhancement..... | 11 |

| | |
|--|----|
| Figure 1.14 (left) excitation spectrum (a) and emission spectrum (b) of fluorescein and absorption spectrum of AuNPs; (right) Mechanism for the detection of melamine based on FRET..... | 12 |
| Figure 1.15 a) Structure of 1 ; b) Melamine-cyanuric acid adduct formed through multivalent hydrogen bonding; c) Concentration of melamine detected by the molecule 1 | 13 |
| Figure 3.1 ^1H NMR spectroscopy (400 MHz, DMSO- d_6) of F1 | 31 |
| Figure 3.2 ^1H NMR spectroscopy (400 MHz, DMSO- d_6) of F2 | 31 |
| Figure 3.3 ^1H NMR spectroscopy (400 MHz, DMSO- d_6) of F3 | 33 |
| Figure 3.4 ^1H NMR spectroscopy (400 MHz, DMSO- d_6) of F4 | 33 |
| Figure 3.5 ^1H NMR spectroscopy (400 MHz, DMSO- d_6) of F5 | 34 |
| Figure 3.6 Normalized absorption and emission spectra of F1 and F2 in CH_3CN | 35 |
| Figure 3.7 Normalized absorption and emission spectra of F3 and F5 in DMSO..... | 36 |
| Figure 3.8 Screening of F1 to F3 in organic solvent..... | 36 |
| Figure 3.9 Screening of F1 to F3 in aqueous media..... | 37 |
| Figure 3.10 Fluorescent spectra (left) and absorption spectra (right) of fluorophore F3 (500 μM) in DMSO and various water contents..... | 38 |
| Figure 3.11 Selectivity screening of F3 in aqueous media..... | 38 |
| Figure 3.12 Screening of F4 and F5 in aqueous media..... | 39 |
| Figure 3.13 Fluorescent spectra (left) and absorption spectra (right) of F4 (100 μM) in DMSO and various water contents..... | 39 |
| Figure 3.14 Fluorescent spectra (left) and absorption spectra (right) of F5 (10 μM) in DMSO and various water contents..... | 40 |
| Figure 3.15 Selectivity screening of F4 in aqueous media..... | 41 |
| Figure 3.16 Selectivity screening of F5 in aqueous media..... | 41 |

| | |
|---|----|
| Figure 3.17 Proposed behaviors of F4 after addition of melamine. | 42 |
| Figure 3.18 Absorption spectra of fluorophore F4 (100 μM) in 90% water in DMSO in the various melamine contents..... | 42 |
| Figure 3.19 Proposed behaviors of F4 after addition of melamine. | 43 |
| Figure 3.20 The fluorescence intensity of F3 (500 μM), F4 (100 μM) and F5 (10 μM) in 10% DMSO/ buffer pH 5-9. | 43 |
| Figure 3.21 The fluorescence intensity F3 (100 μM) upon addition of melamine | 44 |
| Figure 3.22 Fluorescence intensity in the absent of melamine (I_0) and in the presence of (I)..... | 44 |
| Figure 3.23 Time dependent change in fluorescence intensity of F3 , F4 and F5 upon addition of melamine 10 equivalent in 90% water in DMSO. | 45 |
| Figure 3.24 Surfactant study of fluorescence intensity of F5 (10 μM) toward various 100 μM surfactant (left), the fluorescence intensity of F5 in the presence of melamine 100 μM in SDC, DTAB and Triton X-100 (100 μM) (right)..... | 45 |
| Figure 3.25 The bar represent the fluorescence enhancement ratio (I/I_0) of F3 upon addition of melamine in the present of relative structures ($\lambda_{\text{ex}}=366$ nm; Medium = 90% water in DMSO; $[\text{F3}] = 0.5$ mM; $[\text{mel}] = 0.5$ mM; $[\text{relative structures}] = 5$ mM). | 46 |
| Figure 3.26 The bar represent the fluorescence enhancement ratio (I/I_0) of F4 upon addition of melamine in the present of relative structures ($\lambda_{\text{ex}}=366$ nm; Medium = 90% water in DMSO; $[\text{F4}] = 0.1$ mM; $[\text{mel}] = 0.1$ mM; $[\text{relative structures}] = 1$ mM). | 47 |
| Figure 3.27 The bar represent the fluorescence enhancement ratio (I/I_0) of F5 upon addition of melamine in the present of relative structures ($\lambda_{\text{ex}}=365$ nm; Medium = 90% water in DMSO; $[\text{F5}] = 0.01$ mM; $[\text{mel}] = 0.5$ mM; $[\text{relative structures}] = 5$ mM). | 47 |

| | |
|--|----|
| Figure 3.28 The fluorescence spectra (left), the fluorescence intensity change (I/I_0) of [F4] = 100 μM , versus [melamine] in condition = 90% water in DMSO. | 48 |
| Figure 3.29 The fluorescence spectra (left), the fluorescence intensity change (I/I_0) of [F4] = 100 μM , versus [melamine] in condition = 90% water in DMSO..... | 48 |
| Figure A.1 $^1\text{H-NMR}$ spectrum of 1a in CDCl_3 | 60 |
| Figure A.2 $^1\text{H-NMR}$ spectrum of 2a in CDCl_3 | 60 |
| Figure A.3 $^{13}\text{C-NMR}$ spectrum of 2a in CDCl_3 | 61 |
| Figure A.4 $^1\text{H-NMR}$ spectrum of F1 in CDCl_3 | 61 |
| Figure A.5 $^{13}\text{C-NMR}$ spectrum of F1 in DMSO-d_6 | 62 |
| Figure A.6 $^1\text{H-NMR}$ spectrum of 1b in CDCl_3 | 62 |
| Figure A.7 $^1\text{H-NMR}$ spectrum of 2b in CDCl_3 | 63 |
| Figure A.8 $^1\text{H-NMR}$ spectrum of 3b in CDCl_3 | 63 |
| Figure A.9 $^{13}\text{C-NMR}$ spectrum of 3b in CDCl_3 | 64 |
| Figure A.10 $^1\text{H-NMR}$ spectrum of F2 in DMSO-d_6 | 64 |
| Figure A.11 $^{13}\text{C-NMR}$ spectrum of F2 in DMSO-d_6 | 65 |
| Figure A.12 $^1\text{H-NMR}$ spectrum of 1c in CDCl_3 | 65 |
| Figure A.13 $^1\text{H-NMR}$ spectrum of 2c in CDCl_3 | 66 |
| Figure A.14 $^{13}\text{C-NMR}$ spectrum of 2c in CDCl_3 | 66 |
| Figure A.15 $^1\text{H-NMR}$ spectrum of 3c in CDCl_3 | 67 |
| Figure A.16 $^{13}\text{C-NMR}$ spectrum of 3c in CDCl_3 | 67 |
| Figure A.17 $^1\text{H-NMR}$ spectrum of F3 in DMSO-d_6 | 68 |
| Figure A.18 $^{13}\text{C-NMR}$ spectrum of F3 in DMSO-d_6 | 68 |
| Figure A.19 $^1\text{H-NMR}$ spectrum of 1d in CDCl_3 | 69 |
| Figure A.20 $^1\text{H-NMR}$ spectrum of 2d in CDCl_3 | 69 |

| | | |
|-------------|--|----|
| Figure A.21 | ^{13}C -NMR spectrum of 2d in CDCl_3 . | 70 |
| Figure A.22 | ^1H -NMR spectrum of 3d in CDCl_3 . | 70 |
| Figure A.23 | ^{13}C -NMR spectrum of 3d in CDCl_3 . | 71 |
| Figure A.24 | ^1H -NMR spectrum of F4 in DMSO-d_6 . | 71 |
| Figure A.25 | ^{13}C -NMR spectrum of F4 in DMSO-d_6 . | 72 |
| Figure A.26 | ^1H -NMR spectrum of 1e in CDCl_3 . | 72 |
| Figure A.27 | ^{13}C -NMR spectrum of 1e in CDCl_3 . | 73 |
| Figure A.28 | ^1H -NMR spectrum of 2e in CDCl_3 . | 73 |
| Figure A.29 | ^1H -NMR spectrum of 2e in CDCl_3 . | 74 |
| Figure A.30 | ^1H -NMR spectrum of F5 in DMSO-d_6 . | 74 |
| Figure A.31 | ^{13}C -NMR spectrum of F5 in DMSO-d_6 . | 75 |
| Figure A.32 | Elemental Analysis of F1 and F2 . | 76 |
| Figure A.33 | Elemental Analysis of F3 . | 77 |
| Figure A.34 | HRMS spectrum of F4 . | 78 |
| Figure A.35 | HRMS spectrum of F5 . | 78 |
| Figure A.36 | Molar absorption coefficient plot of F1 in CH_3CN . | 79 |
| Figure A.37 | Molar absorption coefficient plot of F2 in CH_3CN . | 79 |
| Figure A.38 | Molar absorption coefficient plot of F3 in DMSO . | 79 |
| Figure A.39 | Molar absorption coefficient plot of F4 in DMSO . | 80 |
| Figure A.40 | Molar absorption coefficient plot of F5 in DMSO . | 80 |
| Figure A.41 | Quantum yield plot of F1 in CH_3CN . | 81 |
| Figure A.42 | Quantum yield plot of F2 in CH_3CN . | 81 |
| Figure A.43 | Quantum yield plot of F3 in DMSO . | 81 |
| Figure A.44 | Quantum yield plot of F4 in DMSO . | 82 |

Figure A.45 Quantum yield plot of F5 in DMSO..... 82



LIST OF SCHEMES

| | |
|--|----|
| Scheme 3.1 Synthesis of F1 and F2..... | 30 |
| Scheme 3.2 Synthesis of F3, F4 and F5..... | 32 |



LIST OF TABLES

Table 3.1 Photophysical properties of **F1** to **F5**..... 34



LIST OF ABBREVIATIONS

| | |
|--------------------------|--------------------------------------|
| calcd | calculated |
| ^{13}C NMR | carbon-13 nuclear magnetic resonance |
| δ | chemical shift |
| J | coupling constant |
| $^{\circ}\text{C}$ | degree Celsius |
| CDCl_3 | deuterated chloroform |
| $\text{DMSO } d_6$ | deuterated dimethyl sulfoxide |
| DMSO | dimethylsulfoxide |
| DMF | N,N-dimethylformamide |
| CH_2Cl_2 | dichloromethane |
| d | doublet (NMR) |
| dd | doublet of doublet (NMR) |
| EtOAc | ethyl acetate |
| equiv | equivalent (s) |
| Hz | Hertz |
| HRMS | high resolution mass spectrum |
| h | hour (s) |
| MgSO_4 | magnesium sulphate |
| mg | milligram (s) |
| mL | milliliter (s) |
| mmol | millimole (s) |
| m.p. | melting point |

| | |
|--------------------|-----------------------------------|
| m/z | mass per charge |
| m | multiplet (NMR) |
| M.W. | molecular weight |
| M | molar |
| μL | microliter (s) |
| μM | micromolar (s) |
| ϵ | molar absorptivity |
| MsCl | methanesulfonyl chloride |
| MHz | megahertz |
| nm | nanometer (s) |
| ppm | parts per million |
| PBr ₃ | phosphorus tribromide |
| KOH | potassium hydroxide |
| ¹ H NMR | proton nuclear magnetic resonance |
| %yield | percentage yield |
| Φ | quantum yield |
| q | quartet (NMR) |
| rt | room temperature |
| s | singlet (NMR) |
| t | triplet (NMR) |
| TLC | thin layer chromatography |
| TEA | triethylamine |
| UV | ultraviolet |
| λ | wavelength |

CHAPTER I

INTRODUCTION

1.1 Melamine

Melamine ($C_3H_6N_6$) is a high nitrogen-containing compound (66% by mass) with a cyclic structure as shown in **Figure 1.1**. It has been widely used in many industrial applications, for examples, the production of melamine-formaldehyde resins which are used in plastic, paints, adhesives, and fire-retardants.

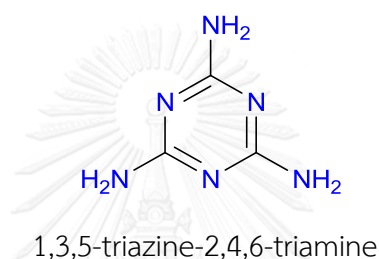


Figure 1.1 Structure of melamine.

Recently, melamine contamination was found in milk and dairy products as well as infant formula for the false increase of protein levels as determined by the nitrogen contents. Although melamine has low toxicity, it can be associated with cyanuric acid to form high molecular weight network complexes. These complexes have poor aqueous solubility and precipitate in the renal tubes, causing damage to the urinary system, development of kidney stones, renal failure and ultimate death [1, 2] (**Figure 1.2**). Therefore, the U.S. Food and Drug Administration (US-FDA) has set a safe contamination level of melamine at 1 mg.kg^{-1} for powdered infant milk formula and at 2.5 mg kg^{-1} for other foods [3]. While, the World Health Organization (WHO) has specified the tolerable daily intake for melamine to be 0.2 mg.kg^{-1} body weight per day [4].

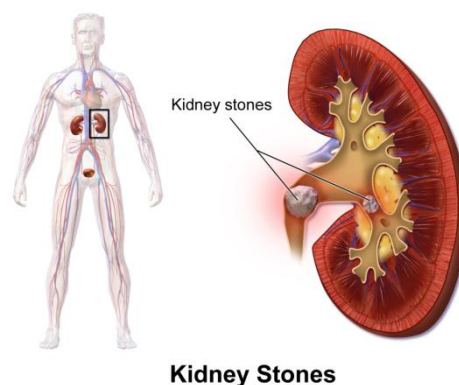


Figure 1.2 The toxicity of melamine in the human body

Nowadays, several methods for melamine detection have been reported such as Gas Chromatography mass spectrometry (GC-MS), High-Performance Liquid Chromatography (HPLC) [5, 6], Liquid chromatography–mass spectrometry (LC-MS) [7, 8], Enzyme-linked immunosorbent assay (ELISA) [9], Electrochemical method [10], Colorimetric technique [11], Nuclear magnetic resonance (NMR) spectroscopy [12], and Capillary electrophoresis (CE) [13]. Most of these methods are highly sensitive, but they require high-cost instruments, complicated sample preparation, and well-trained technicians or instrument users. Therefore, the development of a rapid, easy, and inexpensive method for melamine detection has become essential. With respect to its high sensitivity and reasonable instrument cost, fluorescence technique has become more favorable and desirable technique of detection.

1.2 Fluorescence

Fluorescence technique has widely been used in the field of chemistry and biological sciences due to its high selectivity, sensitivity, and rapid detection. With the made of portable devices, it can be applied easily for real-time and on-site applications. Good fluorescent compounds usually contain long π -conjugation and generally are planar which consequently allow electrons to delocalize through the entire conjugated system. Molecules with multiple aromatic rings usually have high rigidity with restricted C-C bond rotation. As a result, these molecules exhibit strong fluorescent signals. Examples of fluorescent compounds (fluorophores) are shown in **Figure 1.3** [14].

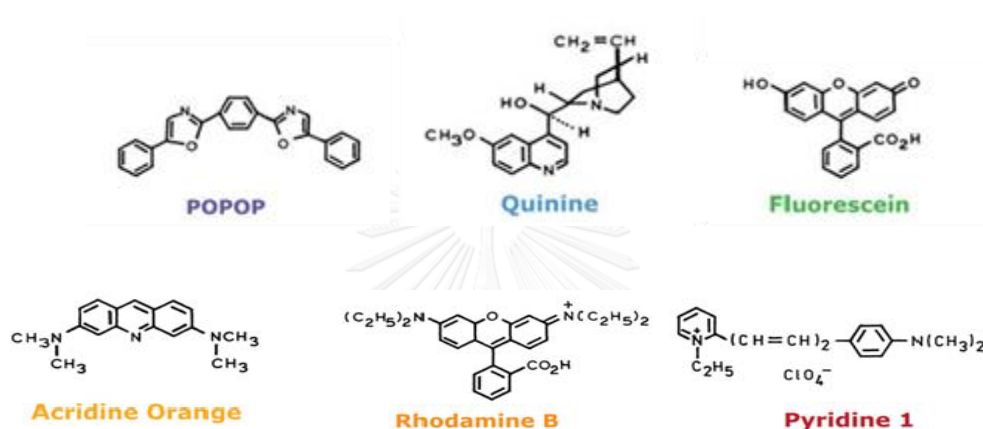
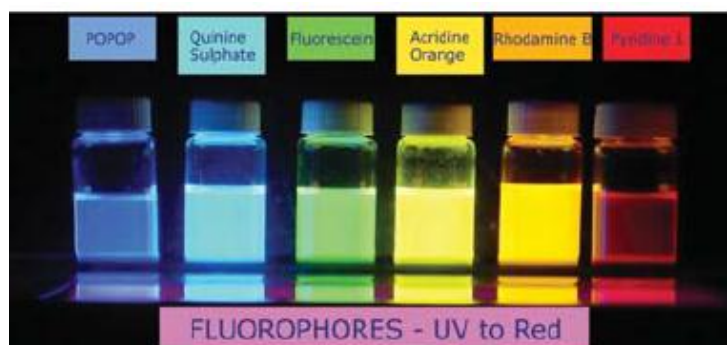


Figure 1.3 Examples of fluorescent compounds.

1.2.1 Principle of fluorescence

The fluorescence process involves the absorption and emission of light energy by the molecules and this process is usually illustrated by the Jablonski diagram (Figure 1.4). When molecules absorb sufficient amount of energy, they become unstable and can often be called as “molecules in excited states”. The excited molecules will first release some energy in the forms of molecular rotation and vibration, or thermal energy until they reach a semi-stable or locally excited state (LE) which is usually the lowest electronic excited state. The remaining energy will be released in the form of fluorescent light as the molecules completely return to the ground state (S_0) [14].

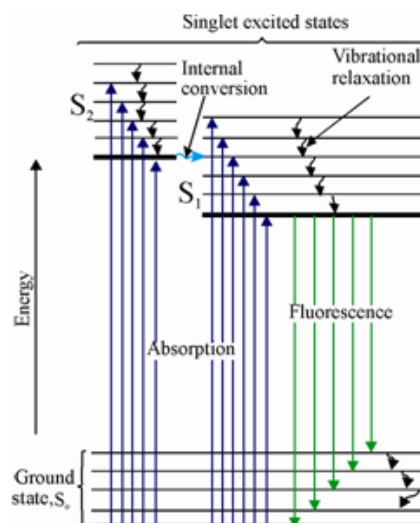


Figure 1.4 The Jablonski diagram

When the fluorescence spectroscopy is applied in chemosensors, the disturbance of fluorescent signals by analytes are usually detected and compared to the original intensity. There are several mechanisms of fluorescent signal changes, which involve how the sensors are designed and the interaction between sensors and analytes.

1.2.2 Fluorescent chemosensors

In general, a fluorescent sensor contains two major components which are a fluorophore and a receptor. The good receptor should be able to recognize a specific target substance which is known as the analyte. A selective binding between receptor and analyte depends on the size, shape, and binding energy. On the other hand, fluorophore part will serve as a signal transducer which reports the binding event. Typical mode of detection are fluorescence enhancement or signal turn-on and the fluorescence quenching of signal turn-off [14].

1.2.2.1 Fluorescence Quenching

The intensity of fluorescence can be decreased by several quenching processes. The fluorescence quenching is usually characterized by the Stern–Volmer equation [15].

$$\frac{I_0}{I} = 1 + k_q \tau_0 [Q] = 1 + K_{SV} [Q]$$

From equation, I_0 and I are the fluorescence intensities in the absence and presence of quencher, respectively; k_q is the bimolecular quenching constant; τ_0 is the lifetime of the fluorophore in the absence of quencher; and $[Q]$ is the concentration of quencher. The Stern-Volmer quenching constant is given by $K_D = k_q \tau_0$. Stern-Volmer constant will be represented by K_D when quenching is known to be dynamic and represented by K_{SV} when quenching is known to be static. Quenching data are usually presented as plots of I_0/I versus $[Q]$. This is because the I_0/I is expected to be linearly dependent upon the concentration of quencher. A plot of I_0/I versus $[Q]$ yields an intercept of one on the y-axis and a slope equals to K_{SV} .

1.2.3 Mechanism of fluorescent signal changes

According to the Jablonski's diagram, the highly rigid molecules give high fluorescent intensities at the shorter wavelength due to the lower degree of geometrical relaxation. In contrast, less rigid molecules can allow the excited molecules to vibrate and rotate more vigorously; therefore, a large portion of energy should be lost prior to returning to the ground state. Therefore, the emission wavelengths of less rigid molecules should be longer and the fluorescent intensities might be lower. Apart from the rigidity, several processes can also alter the fluorescent signals.

1.2.3.1 Photo induced-electron transfer (PET)

Photo-induced electron transfer (PET) often results in fluorescent signal quenching [16]. This phenomenon has been widely applied for fluorescent sensor [17-19]. The PET-based sensors consist of a fluorophore and a receptor linked by a spacer as shown in **Figure 1.5** [20].

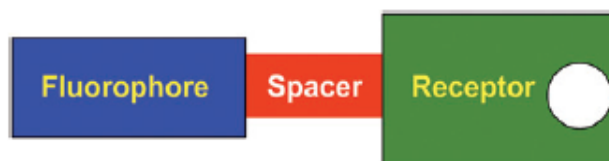


Figure 1.5 The format of fluorescent PET sensor.

The fluorophore-spacer-receptor can be classified into two modes: fluorescence “turn-off” and fluorescence “turn-on”. When the electron of the fluorophore is excited, the electron from HOMO of the receptor which has a higher energy will transfer to the lower singly occupied orbital of the fluorophore, resulting in a fluorescence quenching or fluorescence “turn-off” (**Figure 1.6**). When there is a binding between analyte and receptor; making the energy level of HOMO of the receptor lower than the fluorophore, there will not be the electron transfer between the two fragments. Therefore, the fluorescent signal will be greatly enhanced and it is called a fluorescence “turn-on” [21].

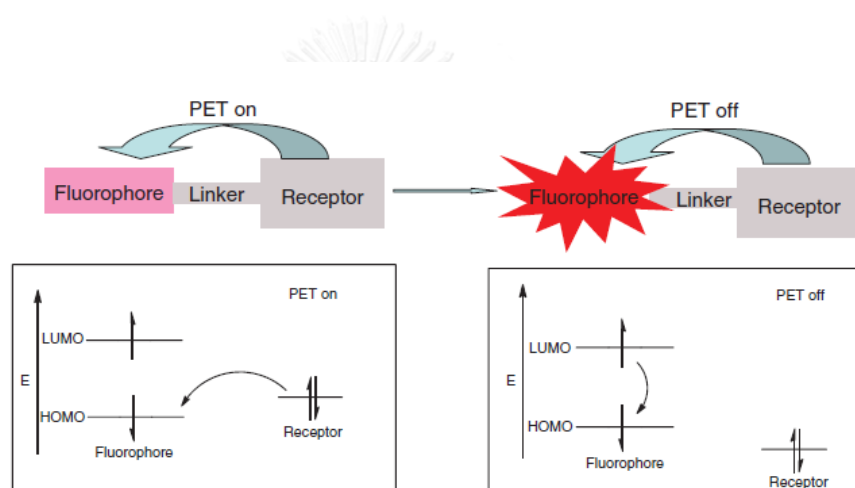


Figure 1.6 General sensor designs by PET mechanism [22].

1.2.3.2 Internal charge transfer (ICT)

Internal charge transfer (ICT) is an important and common process that changes fluorescent intensity [23]. It is a typical phenomenon occurring to the molecules that contain both electron-donating and electron-withdrawing groups. During this process, the molecules will not return from the locally excited state (LE) to the ground state, but they will populate at the more stable state called “ICT” state according to the Frank-Condon principle (**Figure 1.7**). Then, the emission energy will be lower and the molecules show a large Stoke shift and red-shifted emission. In some cases, the fluorescent signals disappear when the emitted energy is out of the UV-visible range [24]

interested [21]. In 2001, AIEE is a unique photoluminescence property that was first discovered to happen to most propeller-shaped molecules. These fluorophores are non-emissive when dissolved in good solvents or in dilute solution because the intramolecular rotation converts photonic energy to heat and deactivates the excited states non-radiatively. The restrictions of intramolecular rotations (RIR) [32] in J-aggregated (red shift) formation can be predicated in the main cause for the AIEE effect. To date, a variety of compounds with AIEE characteristics have been developed for applications in chemical sensors, biological imaging, and optoelectronic devices.

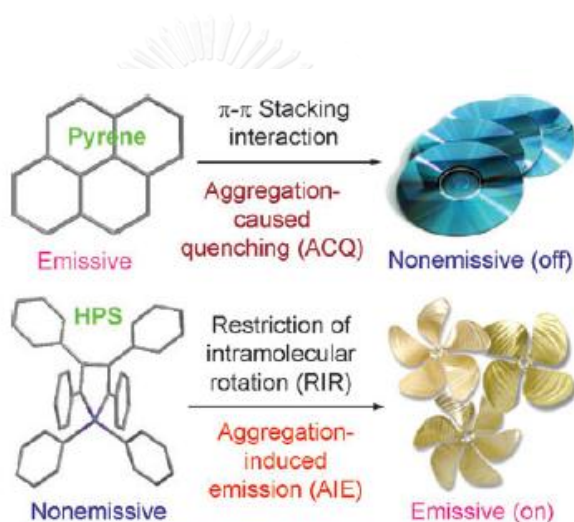


Figure 1.8 Planar molecules such as pyrene tend to aggregate just as discs pile up due to strong π - π stacking interactions, which commonly turn “off” light emission, whereas nonplanar propeller-shaped luminogens such as hexaphenylsilole (HPS) behave oppositely, with their light emissions turned “on” by aggregate formation, due to the restricted intramolecular rotation in the aggregates.

1.3 Naphthalimide derivatives as fluorescent sensors

1,8-Naphthalimide is popularly used as fluorescent signal transducer in sensors because it has high absorption coefficient, strong fluorescence signal, high quantum yield, large Stokes shift, good photo and thermal stability, good solubility in common organic solvents, and simple structural modification. Naphthalimide derivatives have also been widely used as dyes, pigments, optical brighteners, fluorescent markers in

biology, anticancer agents in medicine [33] and materials for organic electronics such as light-emitting devices (OLED) [34]. In addition, a number of naphthalimide derivatives have been used as fluorescent chemosensors [26, 35, 36].

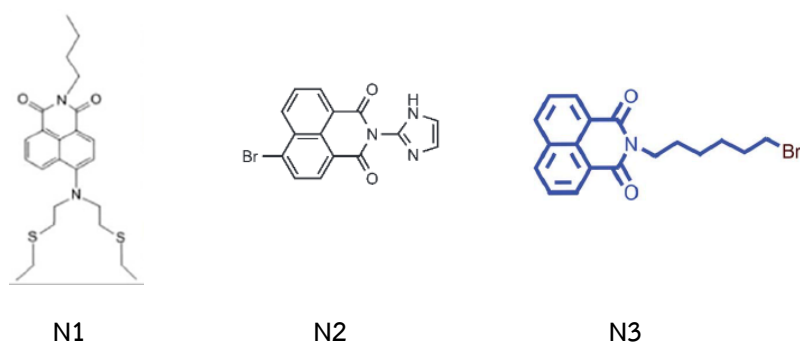


Figure 1.9 Examples of chemosensors derived from 1,8-naphthalimides.

1.4 Chemical sensor for the detection of melamine

In 2014 Li et al. [37] reviewed and summarized the chemical sensors and biosensors for melamine detection developed in the recent 5 years. (Figure 1.10).

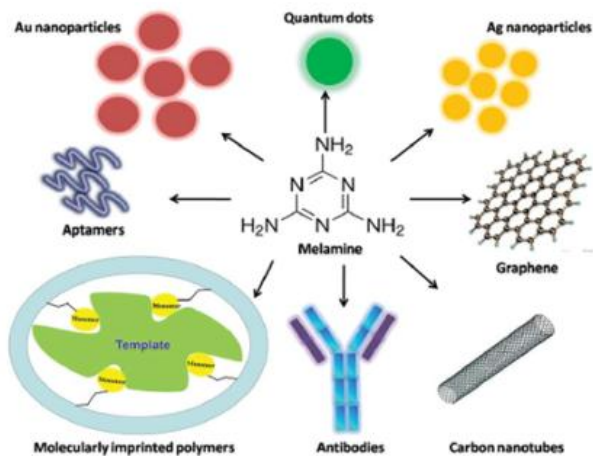


Figure 1.10 Novel recognition and transducer components used for fabrication of sensor for melamine detection sensor.

A favorite method for melamine detection is by fluorescence sensors, which are well known on method of their simplicity, high sensitivity, and easy operation. But different fluorescent material as probes for melamine determination including organic dyes, quantum dots [38-40], metal nanoclusters [41] etc.

In 2010 Zhou et al. [42] developed a novel sensitive cucurbit uril (CB7) sensor [7] of melamine with detection limit of $0.20 \mu\text{g mL}^{-1}$. Fluorescence studies indicate that CB7 forms complex with melamine in a 1:1 mole ratio. The binding constant at various temperatures has been calculated and discussed. CB7 has internal cavity which provides a hydrophobic environment suitable for the complexation with melamine. The H bonding and van der Waals force between melamine and CB7 which promote the formation of melamine-CB7 complex (Figure 1.11)

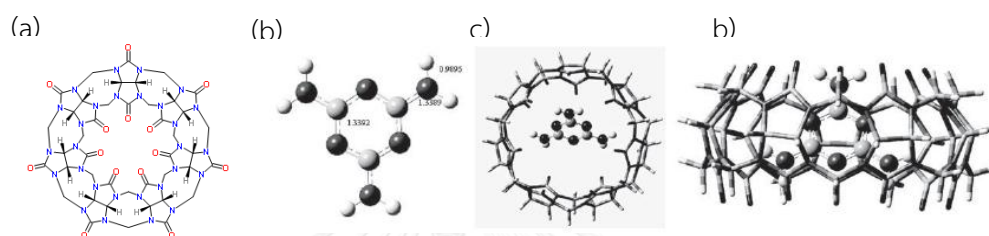


Figure 1.11 a) structure of CB7; Molecular modeling of the CB7-melamine complex. b) conformation of melamine; c) top-view of CB7-melamine complex; d) side-view of CB7-melamine complex.

In 2010 Zhao et al. [43] have reported and detected melamine by molecularly imprinted fluorescence sensors. The sensor was operated on recognition of imprinted sites to guest and have been studied the resultant changes of fluorescence emission when presented of melamine. They have designed and synthesized three fluorescent monomer template, 2-acrylamidoquinoline (2-AAQ), 3-acrylamidoquinoline (3-AAQ) and 8-acrylamidoquinoline (8-AAQ) (Figure 1.12).

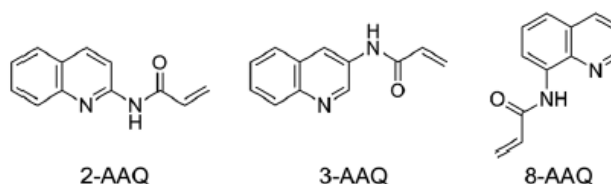


Figure 1.12 Structure formula of florescent functional monomer

The compounds have a core-shell molecular imprinting polymer as a fluorescent chemosensor which was prepared by use of a hydrogen bond-induced enhancement mechanism for the sensing of a non-fluorescent melamine.

The molecule 2-AAQ can free rotation around the C-N bond. In the present of melamine can be restrict intramolecular rotation of 2-AAQ through the formation of tridentate hydrogen bond resulted in the fluorescence enhancement (**Figure 1.13**)

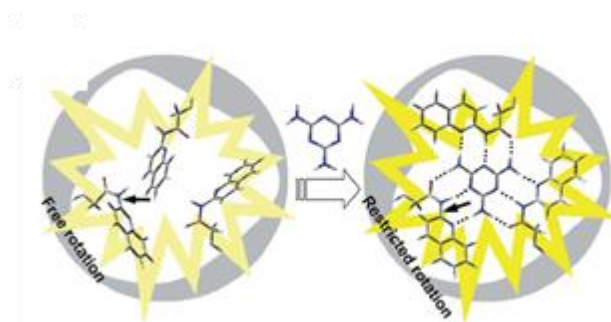


Figure 1.13 Mechanical representation of fluorescence enhancement.

In addition, the detection of melamine using gold nanoparticles (AuNPs) [44-46] or silver nanoparticle (AgNP) [47] via inner filter effect (IFE) principle [48] by fluorescence technique was admired.

In 2011 Guo et al. [49] have reported the detection of melamine based on the high fluorescence quenching ability of gold nanoparticles. The fluorescence was significantly quenched via fluorescence resonance energy transfer (FRET) (**Figure 1.14 (left)**) also the contribution of inner filler effect (IFE). The fluorescein molecules were attached to the surface of gold nanoparticles by electrostatic interaction. In the presence to melamine, less fluorescein could be adsorbed on the surface of gold nanoparticles due to the competitive adsorption of AuNPs between melamine and fluorescein, resulting the fluorescence enhanced (**Figure 1.14 (right)**).

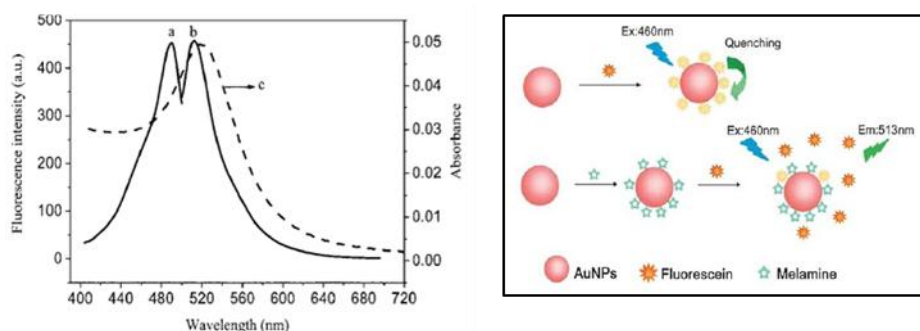


Figure 1.14 (left) excitation spectrum (a) and emission spectrum (b) of fluorescein and absorption spectrum of AuNPs; **(right)** Mechanism for the detection of melamine based on FRET.

In 2012 Sanji et al. [50] designed and synthesized molecule **1** as “turn-on” fluorescence which is AIE-active tetraphenylethene (TPE) with cyanuric acid moieties for the fluorescence sensing of melamine (**Figure 1.15 a**). The molecule **1** is seen to display an intense emission because melamine/cyanuric acid are combine together to form a stable adduct through hydrogen-bonding interactions [51] (**Figure 1.15 b**). Therefore, when it recognizes melamine and then forms aggregates. It was examined by fluorescence spectral changed upon addition of melamine and the naked eye can see less to blue color shown in (**Figure 1.15 c**) in acetonitrile solution. This behavior can demonstrate base on AIE-active molecules show, first reported by Tang and co-worker[52] less emission in solution, but an intense emission when aggregated or in the solid state because of restriction of intramolecular rotations. From graph in the figure 1.15 concentration of melamine can detect 5 μM (0.6 ppm). The emission started to appear within a few hours and the intensity increased as a function of melamine concentration.

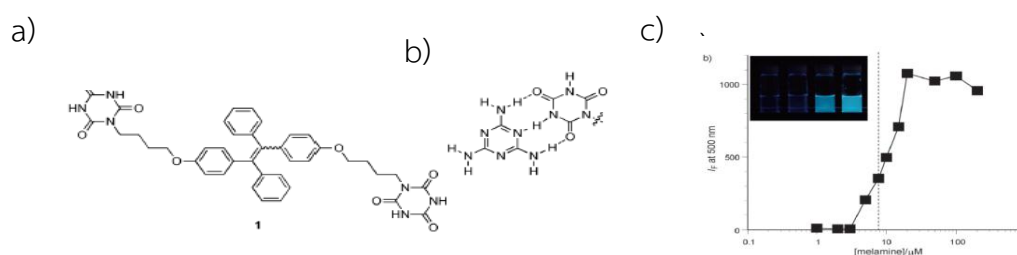
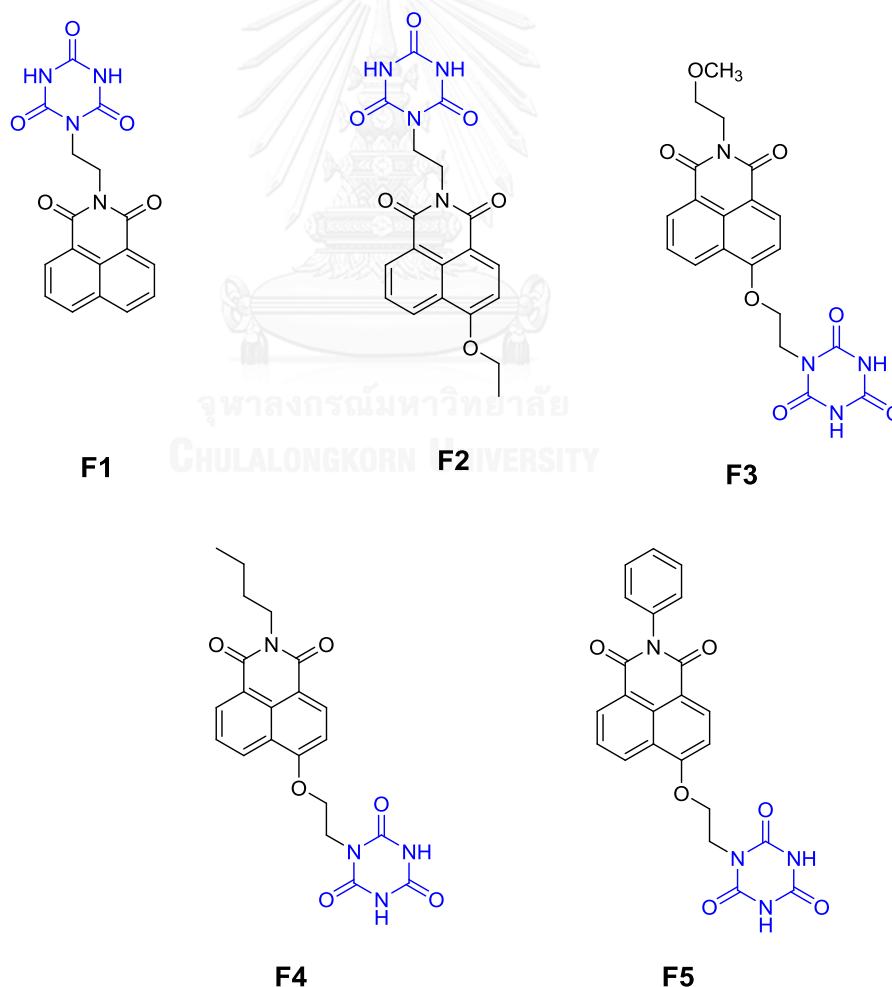


Figure 1.15 a) Structure of **1**; b) Melamine-cyanuric acid adduct formed through multivalent hydrogen bonding; c) Concentration of melamine detected by the molecule **1**.

1.5 Objective of the this research

From the literature review, there has been a little research on melamine detection by fluorescence technique, especially in aqueous media. Therefore, we are interested in the development of a new melamine sensor from 1,8-naphthalimide fluorophore and cyanuric acid receptor (**F1-F5**). The selectivity and sensitivity of these sensors towards melamine were studied, along with the investigation of sensing mechanism.



CHAPTER II

EXPERIMENTAL

2.1 Chemical and Materials

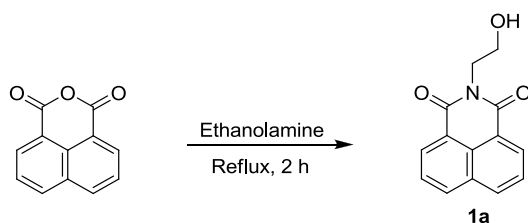
1,8-naphthalic anhydride, 4-bromo 1,8-naphthalic anhydride, 4-phenyl 1,8-naphthalimide, ethanolamine, 2-methoxyethylamine, ethylene glycol, methanesulfonyl chloride, n-butylamine, cyanuric acid, phosphorus tribromide, trimethylamine, 1,8-diazabicyclo[5.4.0]undec-7-ene, potassium hydroxide, magnesium sulphate were commercially available chemicals purchased from Sigma-Aldrich. Solvents such as ethanol and 1,4-dioxane were reagent grade stored over molecular sieve. In anhydrous reactions, solvents such as dichloromethane N,N-dimethylformamide, dimethyl sulfoxide, were dried and distilled before use according to the standard procedure. All column chromatography was operated using Merck silica gel 60 (70-230 mesh). Thin layer chromatography was performed on silica gel plate (Merck F245). Organic solvents used for extraction and chromatography such as dichloromethane, n-hexane, ethyl acetate, methanol were commercial grade and distilled prior to use. The most reactions were carried out under positive pressure of N₂ filled in rubber ballons.

2.2 Analytical Instruments

The ¹H NMR was measured by using 400 MHz ¹H NMR spectrophotometer (Varian, USA). The ¹³C NMR was measured by using 100 MHz Bruker Mercury NMR spectrophotometer (Bruker, Germany), which reported a chemical shifts as ppm in CDCl₃ and DMSO-d₆. A UV-2550 UV visible spectrophotometer (SHIMADZU, Japan) was used for the absorption studies. Emission spectra were acquired on a Carry Eclipse Fluorescence Spectrophotometer (Agilent Technologies).

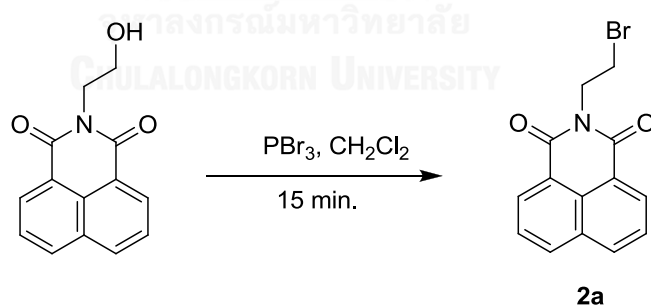
2.3 Synthesis and Characterizations

2.3.1 Synthesis of **1a**



According to literature review [53] 1,8-naphthalic anhydride (2.0 g, 10 mmol) and 3 mL ethanolamine were added into a round bottom flask, the mixture was heated at 170 °C for 2 h under reflux conditions. After the reaction was completed it was left to cool down to room temperature. The mixture was poured into 100 mL of cool water to obtain the solid precipitate. The precipitate will be collected by vacuum filtration, washed with cool water, and dried. After vacuum drying, compound **1a** was obtained as brown solid in 91% yield; $^1\text{H NMR}$ (400 MHz, CDCl_3) δ (ppm): 8.64 (d, $J = 7.3$ Hz, 2H), 8.26 (d, $J = 8.3$ Hz, 2H), 7.79 (t, $J = 7.8$ Hz, 2H), 4.54 (m, 2H), 4.02 (t, $J = 5.3$ Hz, 2H). This data was in good agreement with the literature report.

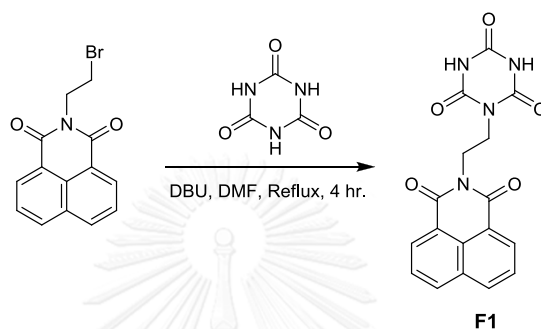
2.3.2 Synthesis of **2a**



Compound **1a** (0.15 g, 0.62 mmol) was dissolved in 20 mL of dichloromethane and then phosphorus tribromide (0.5 eq) was added drop wise. The reaction was stirred in an ice bath for 15 min. After the reaction was completed, it was diluted with water and extracted with CH_2Cl_2 . The combined organic phase was dried over anhydrous MgSO_4 , filtered, and concentrated under reduced pressure. The crude product was purified by column chromatography using CH_2Cl_2 : Hexane (50:50)

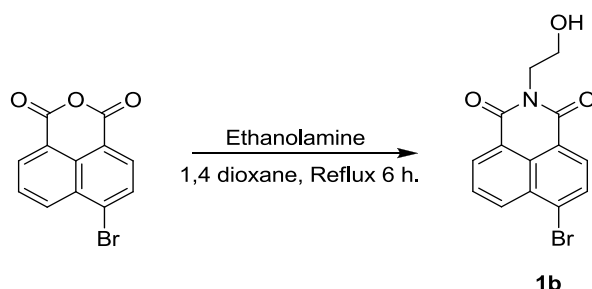
as the eluent to obtain compound **2a** as white solid in 35% yield. ^1H NMR (400 MHz, CDCl_3) δ (ppm): 8.62 (dd, $J = 7.3$ and 1.0 Hz, 2H), 8.23 (dd, $J = 8.3$ and 0.9 Hz, 2H), 7.77 (dd, $J = 8.1$ and 7.4 Hz, 2H), 4.61 (dd, $J = 9.2$ and 5.1 Hz, 2H), 3.67 (t, $J = 7.2$ Hz, 2H). ^{13}C NMR (100 MHz, CDCl_3) δ 163.9, 134.2, 131.6, 131.4, 128.3, 126.9, 122.3, 40.9, 27.6.

2.3.3 Synthesis of **F1**



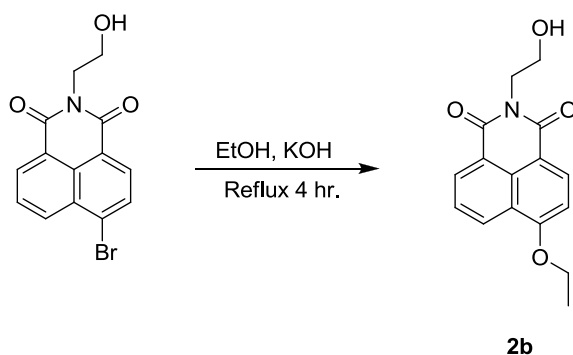
Cyanuric acid (0.35 g, 2.7 mmol) and 1,8-Diazabicyclo[5.4.0]undec-7-ene (DBU, 0.08 ml, 0.5 mmol) were dissolved in DMF (4 mL) at room temperature. The mixture was stirred at $100\text{ }^\circ\text{C}$. Then the compound **2a** (80 mg, 0.27 mmol) was added into the reaction and stirred for 4 h. The mixture was poured into water and extracted with EtOAc. The combined organic phase was dried over anhydrous MgSO_4 , filtered, and concentrated under reduced pressure. The crude substance was dissolved in DMSO and poured into 100 mL of cool water. The white solid was collected by vacuum filtration and dried overnight at room temperature in a vacuum oven to obtain **F1** as white solid in 45% yield. ^1H NMR (400 MHz, DMSO-d_6) δ (ppm): 11.35 (s, 2NH), 8.49 (d, $J = 7.2$ Hz, 2H), 8.45 (d, $J = 8.3$ Hz, 2H), 7.86 (t, $J = 7.8$ Hz, 2H), 4.31 (br, 2H), 4.06 (br, 2H). ^{13}C NMR (100 MHz, DMSO-d_6) δ (ppm): 163.9, 150.0, 148.4, 134.4, 131.3, 130.8, 127.5, 127.2, 121.8, 39.1, 38.0. Elemental analysis : Calculated for $\text{C}_{17}\text{H}_{12}\text{N}_4\text{O}_5$ (MW.352.30) C 57.96, H 3.4, N 15.90%; Found C 58.22, H 3.22, N 15.52%.

2.3.4 Synthesis of **1b**



4-bromo-1,8-naphthalic anhydride (5.01 g, 18.11 mmol) in 1,4 dioxane (25 mL) and 3 mL ethanolamine were added into a round bottom flask, the mixture was heated at 105 °C under reflux conditions for 6 h. After cooling it down to room temperature, the mixture was poured into 100 mL of cool water. The solid precipitate was filtered by vacuum filtration, washed with cool water, and dried overnight at room temperature in a vacuum oven to give **1b** as yellow solid in 95% yield. $^1\text{H NMR}$ (400 MHz, CDCl_3) δ (ppm): 8.67 (d, $J = 7.3$ Hz, 1H), 8.59 (d, $J = 8.5$ Hz, 1H), 8.43 (d, $J = 7.8$ Hz, 1H), 8.05 (d, $J = 7.8$ Hz, 1H), 7.89 (m, 1H), 4.45 (t, $J = 5.3$ Hz, 2H), 3.99 (t, $J = 5.3$ Hz, 2H) This data was in good agreement with the literature report [54].

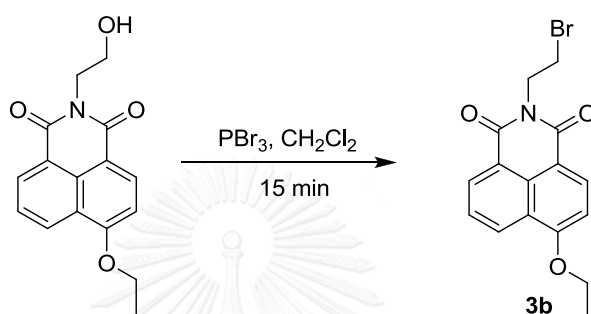
2.3.5 Synthesis of **2b**



Compound **1b** (1.01g, 3.16 mmol) was added into 30 mL of KOH (0.17g, 3.1 mmol) in EtOH and reflux for 4 h. Pour the mixture into 50 mL of water and filtrate

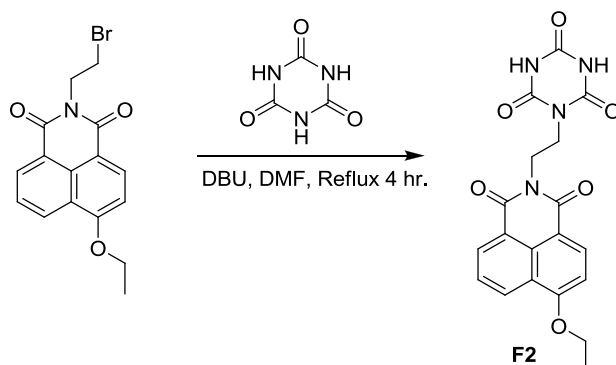
to collect the precipitant. The precipitant was washed with 30 mL of cool water and dried overnight at room temperature to afford **2b** as dark yellow solid in 73% yield. ^1H NMR (400 MHz, CDCl_3) δ (ppm) : 8.61 (d, $J = 7.9$ Hz, 2H), 8.55 (d, $J = 8.3$ Hz, 1H), 7.71 (t, $J = 7.8$ Hz, 1H), 7.03 (d, $J = 8.3$ Hz, 1H), 4.48 (m, 2H), 4.36 (q, $J = 7.0$ Hz, 2H), 4.00 (m, 2H), 1.62 (t, $J = 7.0$ Hz, 3H).

2.3.6 Synthesis of **3b**



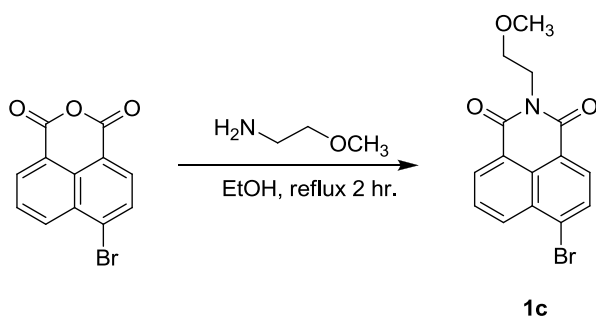
Compound **2b** (0.1 g, 0.36 mmol) was dissolved in 30 ml dichloromethane and then phosphorus tribromide (0.5 eq) was added drop wise. The mixture was stirred in an ice bath for 15 min. After the reaction was completed, the mixture was diluted with water and extracted with CH_2Cl_2 . The combined organic phase was dried over anhydrous MgSO_4 , filtered, and concentrated under reduced pressure. The crude product was purified by column chromatography using EtOAc : Hexane (50:50) as the eluent to give **3b** as pale yellow solid in 42% yield. ^1H NMR (400 MHz, CDCl_3) δ (ppm): 8.60 (d, $J = 7.7$ Hz, 2H), 8.54 (d, $J = 8.3$ Hz, 1H), 7.70 (t, $J = 7.8$ Hz, 1H), 7.02 (d, $J = 8.4$ Hz, 1H), 4.58 (t, $J = 7.2$ Hz, 2H), 4.33 (q, $J = 6.8$ Hz, 2H), 3.64 (t, $J = 7.2$ Hz, 2H), 1.60 (t, $J = 7.0$ Hz, 3H). ^{13}C NMR (100 MHz, CDCl_3) δ 164.3, 163.5, 160.5, 133.8, 131.7, 129.6, 129.0, 125.8, 123.6, 121.9, 114.4, 105.8, 64.5, 40.9, 27.5, 14.2.

2.3.7 Synthesis of F2



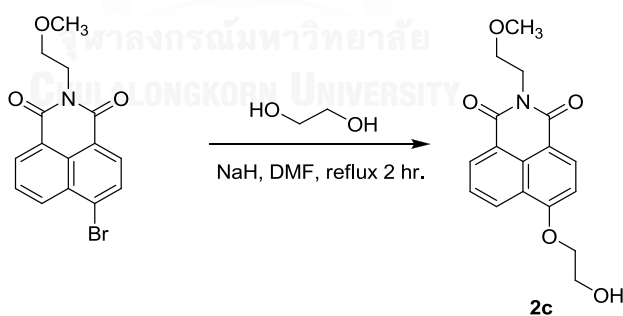
Cyanuric acid (0.33 g, 2.6 mmol) and 1,8-Diazabicyclo[5.4.0]undec-7-ene (DBU) (0.08 ml, 0.5 mmol) in DMF (4 mL) was mixed at room temperature and stirred at 100 °C. The solid compound **3b** (90 mg, 0.26 mmol) was added in the reaction. The reaction took place for 4h. After the reaction was completed, it was diluted with water and extracted with EtOAc. The combined organic phase was dried over anhydrous MgSO_4 , filtered, and concentrated under reduced pressure. The crude substance was dissolved with DMSO and poured into 100 mL of cool water; the white solid was collected by vacuum filtration and then dried overnight at room temperature in a vacuum oven to provide **F2** as pale yellow solid in 68% yield. ^1H NMR (400 MHz, DMSO-d_6) δ (ppm): 11.37 (s, 2NH), 8.55 (d, $J = 8.3$ Hz, 1H), 8.50 (d, $J = 7.2$ Hz, 1H), 8.44 (d, $J = 8.3$ Hz, 1H), 7.82 (t, $J = 7.8$ Hz, 1H), 7.31 (d, $J = 8.4$ Hz, 1H), 4.43 (m, 2H), 4.30 (br, 2H), 4.05 (br, 2H), 1.51 (t, $J = 6.9$ Hz, 3H). ^{13}C NMR (100 MHz, DMSO-d_6) δ (ppm): 164.1, 163.4, 159.7, 149.9, 148.4, 133.4, 131.1, 128.8, 128.5, 126.3, 122.9, 121.7, 113.8, 106.9, 64.8, 37.8, 14.3. Elemental analysis : Calculated for $\text{C}_{19}\text{H}_{16}\text{N}_4\text{O}_6$ (MW. 396.35) C 57.58, H 4.07, N 14.14%; Found C 58.01, H 3.66, N 13.80%.

2.3.8 Synthesis of **1c**



4-Bromo-1,8-naphthalic anhydride (2 g, 7.3 mmol) and ethanol 20 mL were added into a round bottom flask and then drop wise 2-methoxyethylamine about 3 ml. The mixture was heated at 85 °C under the reflux conditions for 2 h. After the reaction was completed, it was left to cool down to room temperature. The mixture was poured into 100 ml of cool water and the solid precipitate was filtered by vacuum filtration, and washed with cool water. After vacuum drying, compound **1c** was obtained as pale brown solid in 99 % yield. ^1H NMR (400 MHz, CDCl_3) δ (ppm): 8.62 (d, 1H), 8.52 (d, 1H), 8.37 (d, 1H), 7.99 (d, 1H), 7.81 (t, 1H), 4.40 (t, 2H), 3.68 (t, 2H), 3.34 (s, 3H). This data was in good agreement with the literature report. [55].

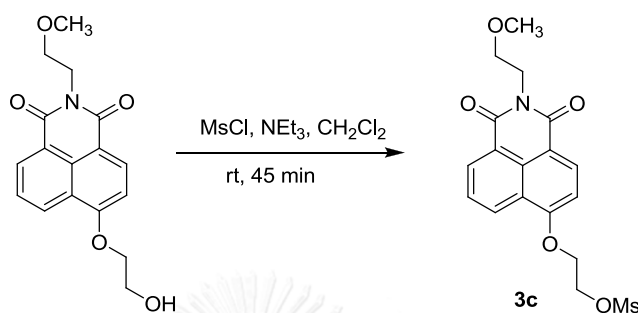
2.3.9 Synthesis of **2c**



Compound **1c** (0.5 g, 1.5mmol) was added into 5 mL of DMF with NaH (0.1g, 1.5 mmol) and reflux for 2 h. After the reaction was completed, it was diluted with water and extracted with EtOAc. The combined organic phase was dried over anhydrous Na_2SO_4 . The crude product was purified by column chromatography using EtOAc : Hexane (80:20) compound **2c** was obtained as yellow solid in 96 %yield. ^1H NMR (400 MHz, CDCl_3) δ (ppm) : 8.61 (d, $J = 7.9$ Hz, 2H), 8.55 (d, $J = 8.3$ Hz, 1H), 7.71 (t, $J =$

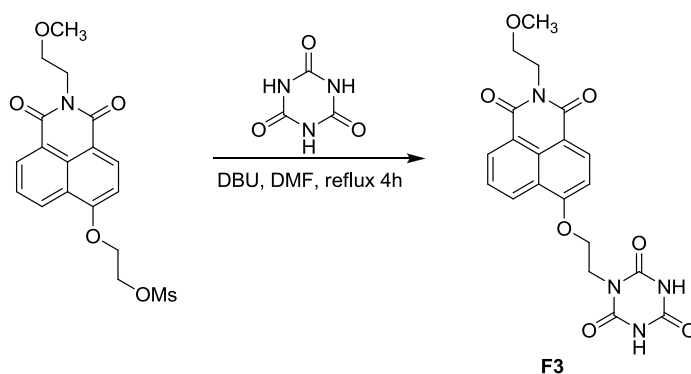
7.8 Hz, 1H), 7.03 (d, $J = 8.3$ Hz, 1H), 4.48 (m, 2H), 4.36 (q, $J = 7.0$ Hz, 2H), 4.00 (m, 2H), 1.62 (t, $J = 7.0$ Hz, 3H). ^{13}C NMR (100 MHz, CDCl_3) δ 164.5, 163.9, 159.7, 133.4, 131.6, 129.3, 128.4, 125.9, 123.3, 122.2, 115.1, 105.9, 70.4, 69.7, 61.2, 58.7, 39.1.

2.3.10 Synthesis of **3c**



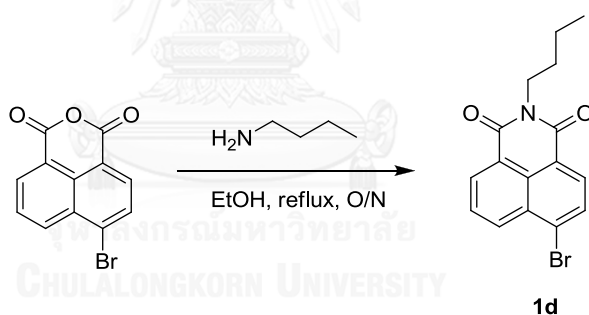
The compound **2c** (0.2 g, 0.63 mmol) was dissolved in 15 mL dichloromethane and then triethylamine (TEA) (0.4 mL, 0.32 mmol) and methanesulfonylchloride (MsCl) (0.3 mL, 0.36 mmol) were added drop wise. The reaction was stirred in an ice bath for 45 min. When the reaction was completed, it was diluted with water and extracted with CH_2Cl_2 . The combined organic phase was dried over anhydrous MgSO_4 , filtered, and concentrated under reduced pressure. The crude product was purified by column chromatography using 100% in EtOAc as the eluent to give **3c** as pale yellow solid in 92 %yield. ^1H NMR (400 MHz, CDCl_3) δ 8.55 (m, 2H), 8.47 (d, $J = 8.2$ Hz, 1H), 7.69 (t, $J = 7.8$ Hz, 1H), 6.99 (d, $J = 8.3$ Hz, 1H), 4.75 (m, 2H), 4.53 (m, 2H), 4.40 (t, $J = 5.9$ Hz, 2H), 3.71 (t, $J = 5.9$ Hz, 2H), 3.37 (s, 3H), 3.12 (s, 3H). ^{13}C NMR (100 Hz, CDCl_3) δ 164.4, 163.8, 158.8, 133.1, 131.9, 129.4, 128.5, 126.3, 123.3, 122.4, 115.8, 105.9, 69.7, 66.8, 66.6, 58.7, 39.1, 37.9.

2.3.11 Synthesis of **F3**

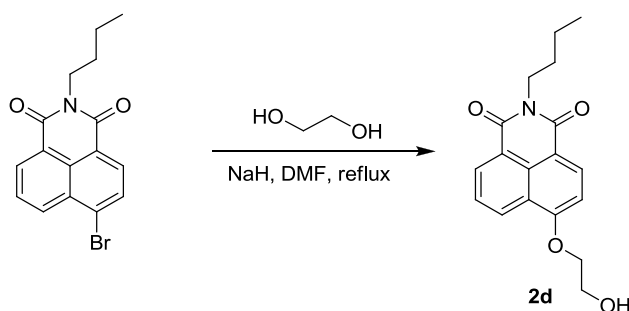


Cyanuric acid (0.32 g, 2.5 mmol) and 1,8-Diazabicyclo[5.4.0]undec-7-ene (DBU) (0.1 ml, 0.5 mmol) in DMF (5 mL) at room temperature. The mixture was stirred at 100 °C. The solid compound **3c** (0.1 g, 0.25 mmol) was added in the reaction and reflux for 4 h. After the reaction was completed, it was diluted with water and extracted with EtOAc. The combined organic phase was dried over anhydrous MgSO₄, filtered, and concentrated under reduced pressure. The crude product was purified by column chromatography using CH₂Cl₂: MeOH (96:4) as the eluent to afford **F3** as pale yellow solid in 89% yield. ¹H NMR (400 MHz, DMSO-d₆) δ 8.54 – 8.47 (m, 2H), 8.44 (d, *J* = 8.1 Hz, 1H), 7.80 (t, *J* = 7.9 Hz, 1H), 7.31 (d, *J* = 8.4 Hz, 1H), 4.48 (s, 2H), 4.24 (d, *J* = 6.3 Hz, 4H), 3.57 (t, *J* = 6.1 Hz, 2H), 3.25 (s, 3H). ¹³C NMR (100 MHz, DMSO) δ 163.5, 162.9, 159.5, 149.9, 148.6, 133.3, 131.1, 128.6, 128.55, 126.3, 122.9, 121.8, 114.3, 106.8, 68.7, 66.2, 58.1, 38.4. Elemental analysis : Calculated for C₂₀H₁₈N₄O₇: C 56.34, H 4.26, N 13.14% Found C 56.93, H 4.52, N 11.98%.

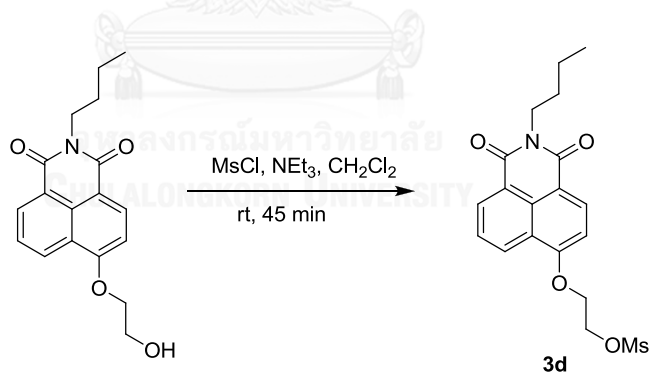
2.3.12 Synthesis of **1d**



Added 4-bromo 1,8 naphthalic anhydride (1 g, 3.7 mmol) in ethanol 20 ml and dropwise N-butylamine (0.7ml, 7.5 mmol). The mixture was reflux for overnight. When the reaction complete, it was recrystallized by cool ethanol to obtain **1d** as brown bound in 94 %yield. ¹H NMR (400 MHz, CDCl₃) δ 8.63 (d, *J* = 7.3 Hz, 1H), 8.53 (d, *J* = 8.5 Hz, 1H), 8.39 (d, *J* = 7.9 Hz, 1H), 8.01 (d, *J* = 7.9 Hz, 1H), 7.82 (m, 1H), 4.14 (m, 2H), 1.69 (dd, *J* = 15.3, 7.9 Hz, 2H), 1.43 (m, 2H), 0.95 (t, *J* = 7.3 Hz, 3H). This data was in good agreement with the literature report [56].

2.3.13 Synthesis of **2d**

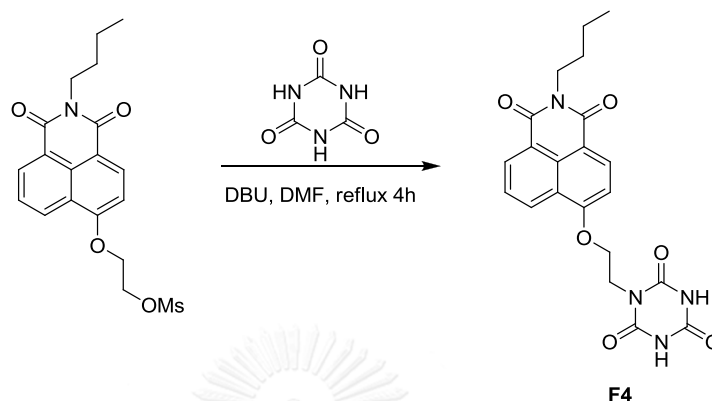
The compound **2d** was synthesized following the procedure described for **2c**. After a purification by column chromatography using CH_2Cl_2 : EtOAc (90:10) as the eluent, compound **2d** was obtained as a yellow solid in 94 % yield. ^1H NMR (400 MHz, CDCl_3) δ 8.50 (m, 2H), 8.45 (d, $J = 8.3$ Hz, 1H), 7.62 (t, $J = 7.8$ Hz, 1H), 7.00 (d, $J = 8.3$ Hz, 1H), 4.39 (m, 2H), 4.18 (dd, $J = 7.8$ and 3.5 Hz, 2H), 4.14 (m, 2H), 1.70 (m, 2H), 1.43 (dt, $J = 14.8$ and 7.4 Hz, 2H), 0.97 (t, $J = 7.3$ Hz, 3H). ^{13}C NMR (100 MHz, CDCl_3) δ 164.3, 163.6, 159.7, 133.1, 131.5, 129.3, 128.3, 125.8, 123.4, 122.4, 115.3, 105.9, 70.3, 61.2, 40.0, 29.9, 20.1, 13.8.

2.3.14 Synthesis of **3d**

The compound **3d** was synthesized following the procedure described for **3c**. After a purification by column chromatography using CH_2Cl_2 : EtOAc (90:10) as the eluent, compound **3d** was obtained as a yellow solid in 93 % yield. ^1H NMR (400 MHz, CDCl_3) δ 8.57 (m, 2H), 8.49 (d, $J = 8.2$ Hz, 1H), 7.71 (t, $J = 7.8$ Hz, 1H), 6.99 (d, $J = 8.3$ Hz, 1H), 4.76 (m, 2H), 4.53 (m, 2H), 4.15 (m, 2H), 3.12 (s, 3H), 1.68 (m, 2H), 1.43 (dt, $J = 14.8$ and 7.4 Hz, 2H), 0.97 (t, $J = 7.3$ Hz, 3H). ^{13}C NMR (100 MHz, CDCl_3) δ 164.3, 163.7,

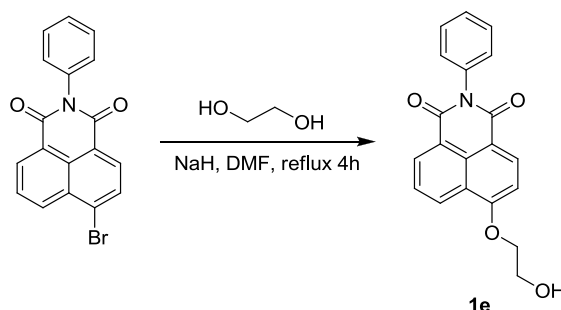
158.8, 132.8, 131.7, 129.4, 128.4, 126.3, 123.3, 122.9, 115.9, 105.8, 66.8, 66.7, 40.1, 37.9, 30.3, 20.4, 13.9.

2.3.15 Synthesis of **F4**



The compound **F4** was synthesized follow the procedure described for **F3**. After a purification by column chromatography using CH_2Cl_2 : MeOH (96:4) as the eluent to provide **F4**, a pale yellow solid was obtained in 85 %yield ^1H NMR (400 MHz, DMSO) δ 11.52 (s, 2NH), 8.47 (t, $J = 6.8$ Hz, 2H), 8.40 (d, $J = 8.3$ Hz, 1H), 7.77 (t, $J = 7.8$ Hz, 1H), 7.28 (d, $J = 8.4$ Hz, 1H), 4.48 (t, $J = 5.0$ Hz, 2H), 4.25 (t, $J = 4.8$ Hz, 2H), 4.01 (t, $J = 7.3$ Hz, 2H), 1.59 (dt, $J = 15.0$ and 7.5 Hz, 2H), 1.34 (dq, $J = 14.6$ and 7.4 Hz, 2H), 0.92 (t, $J = 7.3$ Hz, 3H). ^{13}C NMR (100 MHz, DMSO- d_6) δ 163.5, 162.9, 159.3, 150.1, 148.7, 133.1, 130.9, 128.5, 128.4, 126.2, 122.9, 121.8, 114.3, 106.7, 66.2, 39.2, 29.7, 19.7, 13.6. HRMS m/z Calcd for $\text{C}_{21}\text{H}_{20}\text{N}_4\text{NaO}_6$ $[\text{M}+\text{Na}]^+$: 447.1281 Found: 447.1299.

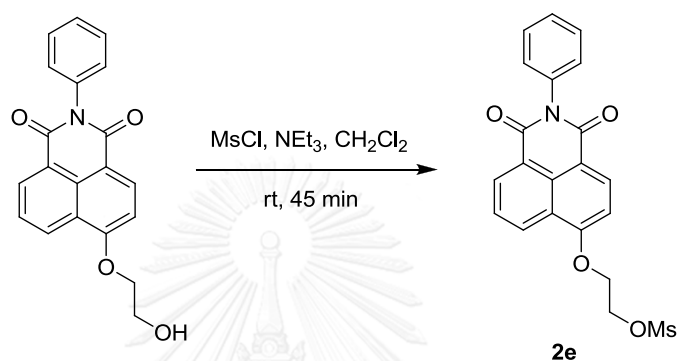
2.3.16 Synthesis of **1e**



The compound **1e** was synthesized follow the procedure described for **2d**. After a purification by column chromatography using CH_2Cl_2 : EtOAc (90:10) as the eluent to provide **1e**, a yellow solid was obtained in 92 %yield ^1H NMR (400 MHz, CDCl_3) δ

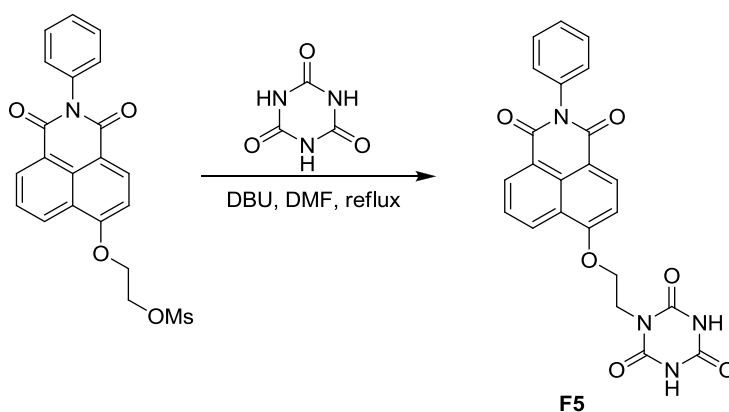
8.69 – 8.61 (m, 2H), 8.58 (d, $J = 8.3$ Hz, 1H), 7.74 (t, $J = 7.8$ Hz, 1H), 7.55 (t, $J = 7.5$ Hz, 2H), 7.47 (t, $J = 7.4$ Hz, 1H), 7.32 (d, $J = 7.4$ Hz, 2H), 7.09 (d, $J = 8.3$ Hz, 1H), 4.46 – 4.41 (m, 2H), 4.21 – 4.16 (m, 2H). ^{13}C NMR (100 MHz, CDCl_3) δ 164.8, 164.2, 160.2, 135.8, 133.9, 132.2, 130.0, 129.5, 128.9, 128.7, 128.7, 126.3, 123.8, 122.8, 115.7, 106.4, 70.6, 61.4.

2.3.17 Synthesis of **2e**



The compound **2e** was synthesized follow the procedure described for **3d**. After a purification by column chromatography using CH_2Cl_2 : EtOAc (90:10) as the eluent to provide **2e**, a yellow solid was obtained in 91 %yield ^1H NMR (400 MHz, CDCl_3) δ 8.68 (d, $J = 8.4$ Hz, 2H), 8.61 (d, $J = 8.4$ Hz, 1H), 7.79 (t, $J = 7.8$ Hz, 1H), 7.55 (d, $J = 7.0$ Hz, 2H), 7.49 (d, $J = 6.6$ Hz, 1H), 7.32 (d, $J = 7.1$ Hz, 2H), 7.08 (d, $J = 7.9$ Hz, 1H), 4.79 (s, 2H), 4.59 (s, 2H), 3.14 (s, 3H). ^{13}C NMR (100 MHz, CDCl_3) δ 133.6, 132.4, 129.5, 129.0, 128.9, 128.8, 126.7, 106.2, 66.9, 66.8, 38.2.

2.3.18 Synthesis of **F5**



The compound **F5** was synthesized follow the procedure described for **F3** After a purification by column chromatography using CH₂Cl₂ : MeOH (96:4) as the eluent to provide **F5**, a pale yellow solid was obtained in 83 %yield ¹H NMR (400 MHz, DMSO) δ 11.55 (s, 2NH), 8.56 (d, *J* = 8.2 Hz, 1H), 8.50 (d, *J* = 7.2 Hz, 1H), 8.45 (d, *J* = 8.2 Hz, 1H), 7.83 (t, *J* = 7.8 Hz, 1H), 7.52 (t, *J* = 7.4 Hz, 2H), 7.45 (t, *J* = 7.2 Hz, 1H), 7.39 – 7.31 (m, 3H), 4.51 (d, *J* = 4.9 Hz, 2H), 4.28 (d, *J* = 4.8 Hz, 2H). ¹³C NMR (100 MHz, DMSO-d₆) δ 163.8, 163.1, 159.4, 150.0, 148.6, 136.1, 133.2, 131.1, 129.1, 128.7, 128.6, 127.9, 126.3, 123.1, 122.4, 114.8, 106.7, 66.2. HRMS m/z Calcd for C₂₃H₁₆N₄NaO₆ [M+Na]⁺: 467.0968 Found: 467.0985.

2.4 Photophysical properties

The stock solutions of **F1** and **F2** (1mM) were prepared by dissolving in 10 mL acetonitrile (CH₃CN) 10 ml. The 10 mM stock solution of **F3**, **F4** and **F5** were prepared by dissolving in dimethyl sulfoxide (DMSO).

2.4.1 UV-Visible spectroscopy

The stock solutions of fluorophores were dilute to 100 μ M. The UV-Visible absorption spectra of the stock solution of fluorophore were recorded in the range of 250-600 nm at room temperature.

2.4.1.1 Molar extinction coefficient (ϵ)

The molar extinction coefficient (ϵ) of **F1** to **F5** were calculated from the UV-Visible absorption spectra at various concentrations. The maximum intensity of all samples had better not be more than value of 1. The absorption intensity of maximum wavelengths (λ) of each compound was plotted versus the concentrations (C) at the respective excitation wavelengths. The molar extinction coefficient (ϵ) represented into the following equation:

$$A = \epsilon bC$$

2.4.2 Fluorescence spectroscopy

The stock solutions of fluorophore **F1** and **F2** were dilute to 100 μM . The emission spectra of fluorophores were recorded in the range of 350-650 nm at room temperature. An excitation wavelength was observed at 334 nm (**F1**), 366 nm (**F2**), 367 nm (**F3, F4**), 365 nm and (**F5**).

2.4.2.1 Fluorescence quantum yield

The fluorescence quantum yield of **F1** and **F2** were performed in CH_3CN and **F3** to **F5** were performed in DMSO. The 2-aminopyridine ($\Phi = 0.60$) in 0.1 M H_2SO_4 was used as the reference for **F1** and quinine sulphate ($\Phi = 0.54$) in 0.1 M H_2SO_4 were used as the references for **F2** to **F5**. The UV-visible absorption spectra of fluorophores should not exceed 0.1. The fluorescent emission spectra of the same concentration using appropriate excitation wavelengths selected were recorded based on the absorption maximum wavelength (λ_{max}) of each compound. The integrated fluorescent intensities were plotted versus the absorbance at the respective excitation wavelengths. Each plot should be linear relation and were shown y-interception and gradient m . In addition, the fluorescent quantum yield (Φ_F) was obtained from graph of integrated fluorescence intensity versus absorbance represented into the following equation:

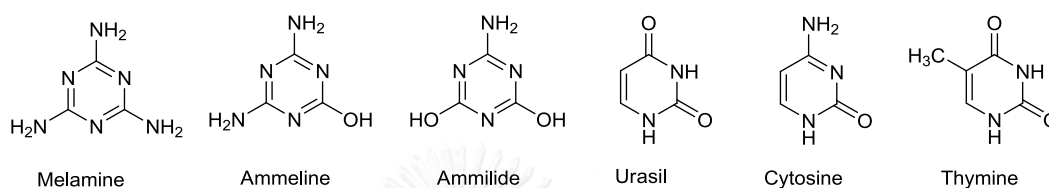
$$\Phi_X = \Phi_{ST} \left(\frac{\text{Grad}_X}{\text{Grad}_{ST}} \right) \left(\frac{\eta_X^2}{\eta_{ST}^2} \right)$$

The subscripts Φ_{ST} is the fluorescence quantum yield of a standard reference which are 2-Aminopyridine ($\Phi = 0.60$), quinine sulfate ($\Phi=0.54$) and Φ_X is the fluorescence quantum yield of sample and η is the refractive index of solvent.

2.5 Fluorescence sensor study

2.5.1 Melamine sensors

The concentrations of **F1** and **F2** were adjusted to 0.1 mM in CH₃CN and **F3**, **F4** and **F5** were adjusted to 0.5 mM, 0.1 mM, 0.01 mM in DMSO, respectively. Stock solutions of melamine, thymine, urasil, ammelide, ammeline, and cytosine were prepared in water at concentrations of 10 mM.



2.5.2 Interference behaviors from relative structure of melamine

Under the same measurement conditions, competitive signaling behavior of **F3** to **F5** toward melamine in the presence of coexistence relative structure as background was studied. The concentration of fluorophore, melamine and relative structure is 1:1:10 equivalent in DMSO: H₂O ((1:9), v/v).

2.5.3 Effect of water content

Under the same measurement conditions by varied water content between 10% - 90% water in DMSO, the UV-Visible absorption spectra were recorded from 250 nm to 600 nm at room temperature and the emission spectra of fluorophores were recorded from 350 nm to 650 nm at room temperature using an excitation wavelength at 366 nm (**F3**, **F4**) and 365 nm (**F5**).

2.5.4 Time-dependent effect

The emission intensity of **F3**, **F4** and **F5** has concentrations were 0.5 mM, 0.1 mM, 0.01 mM, respectively. In condition, DMSO: H₂O (1:9) and melamine 1 mM was continuously monitored for a period of 60 minutes.

2.5.5 Surfactant study

The stock solution of **F5** was diluted in 0.01 mM. The fluorophore was excited at 365 nm. The photophysical properties were studied in three types of surfactant; anion (SDC and SDBS), cation (DTAB and TTAB), non-ionic (Tween-20 and Triton X-100). The stock solutions of surfactants of 1mM were prepared in Milli-Q water. All of surfactant stock solutions were diluted in 50 μM . The final volumes of the mixture were adjusted to 1000 μL .

2.5.6 pH effect

The emission intensity of **F3**, **F4** and **F5** have concentrations were 0.5 mM, 0.1 mM, 0.01 mM in DMSO, respectively. The pH effect on fluorescence signaling of **F3** to **F5** was investigated by measuring of emission spectra in the series of buffer between pH 5.0-8.0. The pH of the solution was fixed by using HEPES buffer (pH 5.0-7.0), phosphate (pH 8.0) and each buffer solution were 10 mM of concentrate. The buffer solutions were used diluent.

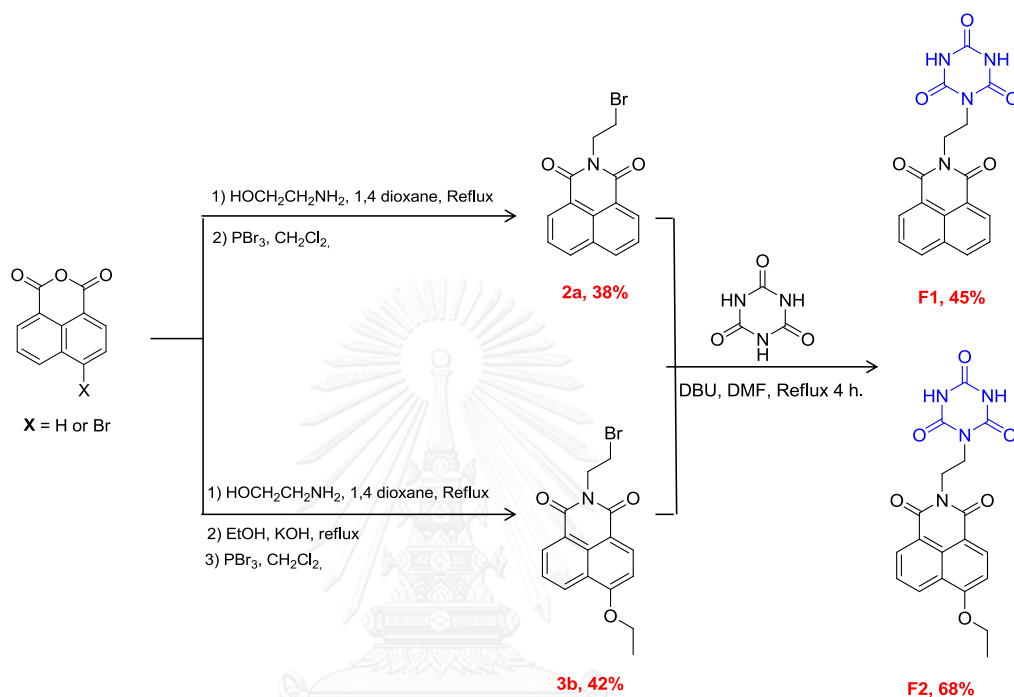
2.5.7 Limit of detection

The limit of detection of fluorophore was estimate by plotting of fluorescence change of fluorophore (**F4** and **F5**) in the presence of melamine by very concentrations in DMSO: H₂O (1:9). Also, the minimum concentration of melamine that gives the fluorescence intensity was determined with a signal-to-background ratio of three.

CHAPTER III

RESULTS AND DISCUSSION

3.1 Synthesis and characterization



Scheme 3.1 Synthesis of **F1** and **F2**.

The synthesis of **F1** and **F2** began by a known synthesis with a condensation reaction gave **1a** and **1b** in excellent yield. Only the **1b** synthesis via a nucleophilic aromatic substitution of the bromine by ethoxy in refluxing ethanol provided **2b**. The substitution reaction with PBr₃ in CH₂Cl₂ obtained **2a** and **3b**, respectively. Finally the nucleophilic substitution reaction of bromide in **2a** and **3b** by cyanuric acid in the presence of DBU and reflux in DMF afforded **F1** as white solid in 45 % yield while, the **F2** as yellow solid in 68 % yield (**Scheme 3.1**). Both of the molecule **F1** and **F2** was characterized by ¹H NMR spectroscopy in DMSO-d₆ (**Figure 3.1**) the amide proton of cyanuric acid appeared as singlet at 11.4 ppm indicating the reaction complete which was confirmed by elemental analysis. Meanwhile, the appearance the signal of proton at h and i (H_h = 4.48 ppm, H_i = 1.62 ppm) in spectrum of **F2** is part of ethoxy moiety (**Figure 3.2**). The ¹³C-NMR and elemental analysis of target

compound **F1** and **F2** and ^1H NMR and ^{13}C -NMR spectroscopy of **1a**, **2a**, **1b**, **2b** and **3b** are shown in appendix.

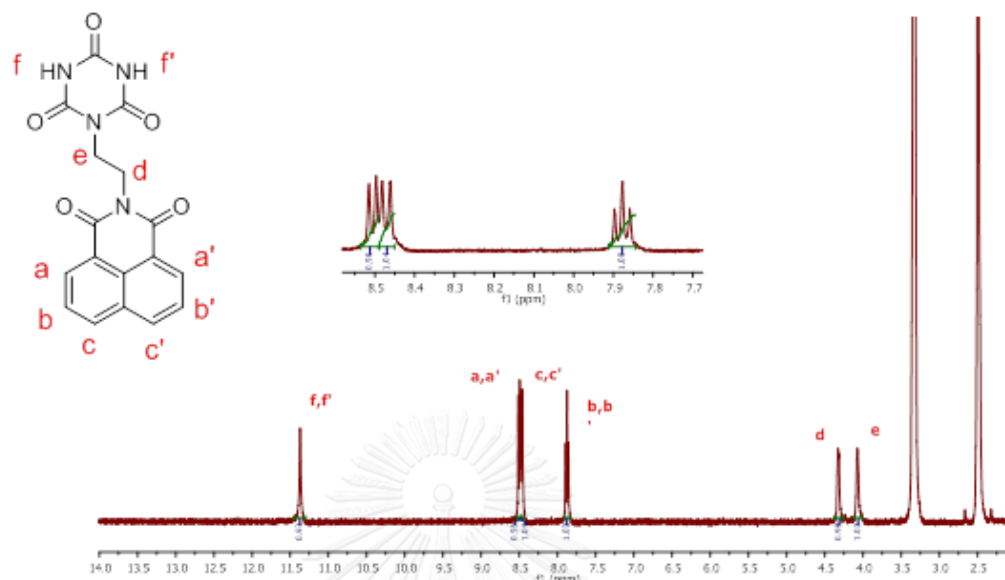


Figure 3.1 ^1H NMR spectroscopy (400 MHz, DMSO-d_6) of **F1**.

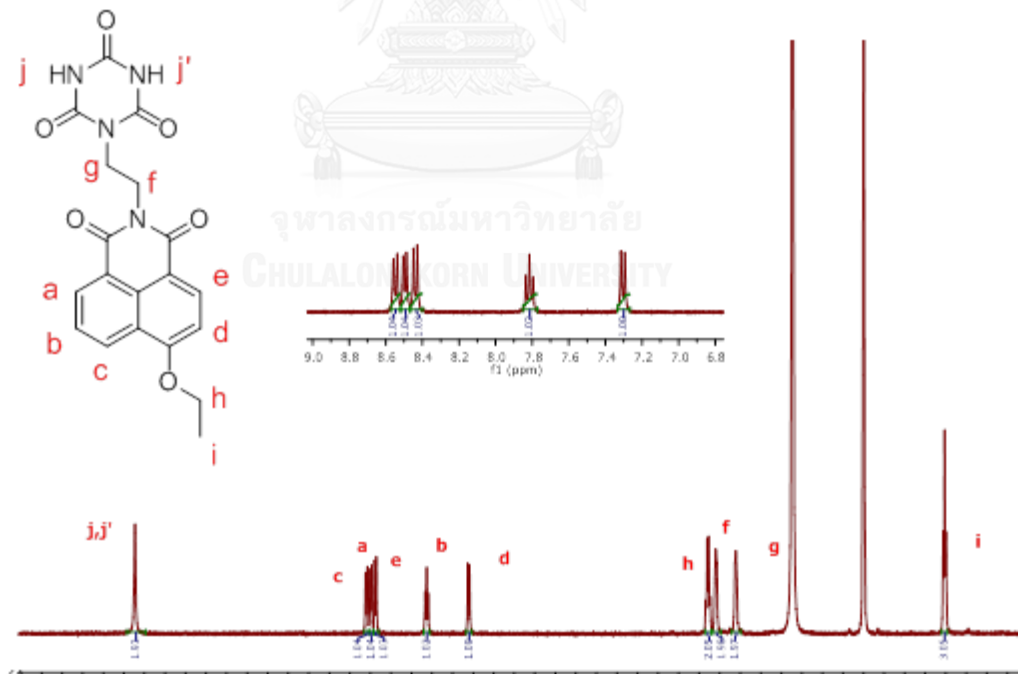
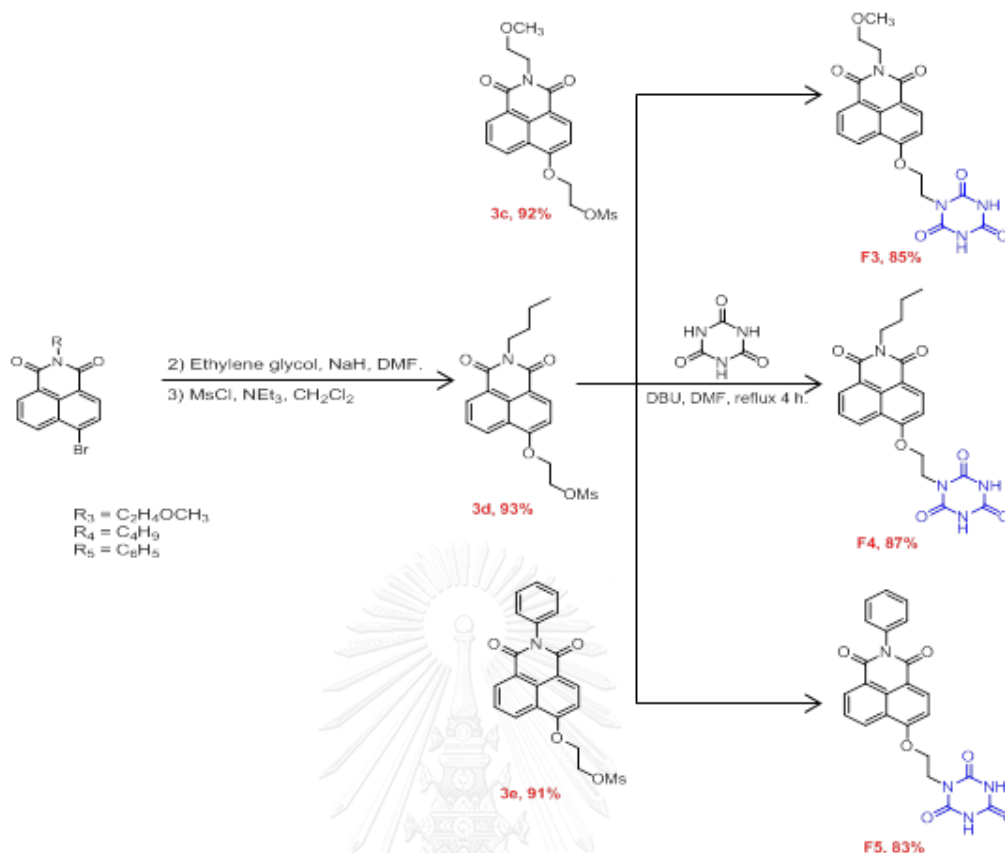


Figure 3.2 ^1H NMR spectroscopy (400 MHz, DMSO-d_6) of **F2**.



Scheme 3.2 Synthesis of **F3**, **F4** and **F5**.

The fluorophore **F3** and **F4** was started a known synthesis a condensation reaction of 1,8 naphthalic anhydride with 2-methoxyethylamine and n-buthylamine, respectively, gave **1c** and **1b** in excellent yield. Meanwhile, a nucleophilic aromatic substitution of the bromine in 4-bromo 1,8-naphthalimide derivatives by ethylene glycol in refluxing DMF provided **2c**, **2d** and **1e** in excellent yield. Then mesylate reaction by methanesulfonyl chloride and NEt₃ in CH₂Cl₂ obtained **3c**, **3d** and **2e** in excellent yield. Finally, the nucleophilic substitution reaction with cyanuric acid in the presence of DBU and reflux in DMF afforded **F3**, **F4** as pale yellow solid while, **F5** as yellow solid in excellent yield of 85, 87, 83 % yield, respectively (**scheme 3.2**). All the target molecule was characterized by ¹H NMR spectroscopy in DMSO-d₆ the amide proton of cyanuric acid appeared as singlet at 11.5 ppm indicating the reaction complete which was confirmed by elemental analysis or high mass resolution spectrometry (HRMS). In addition, ¹H NMR spectrum of the molecule **F3** are shown in **Figure 3.3** appeared proton signals of 2-methoxyethylamine corresponding at 4.40

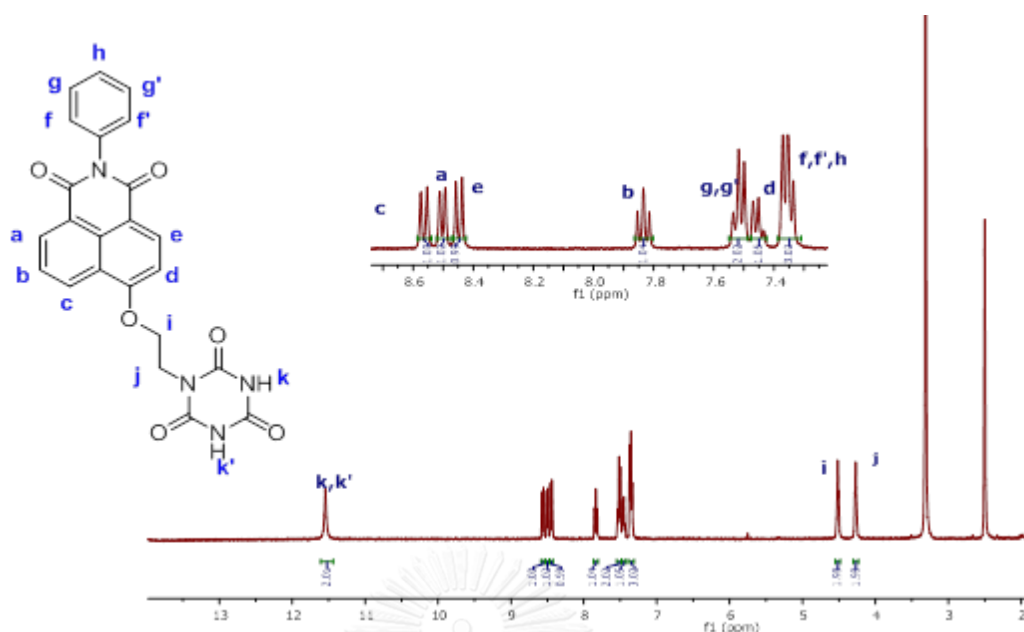


Figure 3.5 ^1H NMR spectroscopy (400 MHz, DMSO-d_6) of F5.

3.2 Photophysical properties of F1 to F5

The absorption and emission properties of F1 to F5 in their good solvents were investigated and summarized in table 3.1. The normalized absorption and emission spectra are shown in Figure 3.6 and 3.7.

Table 3.1 Photophysical properties of F1 to F5

| Compound | Solvent | Absorption | | Emission | |
|----------|------------------------|-----------------------------|---|-----------------------------|-------------------|
| | | λ_{max} (nm) | ϵ ($\text{M}^{-1} \text{cm}^{-1}$) | λ_{max} (nm) | Φ_{F} |
| F1 | CH_3CN | 332 | 5243 | 378 | 0.06 ^a |
| F2 | CH_3CN | 366 | 11958 | 435 | 0.49 ^b |
| F3 | DMSO | 367 | 4654 | 448 | 0.49 ^b |
| F4 | DMSO | 367 | 4272 | 450 | 0.53 ^b |
| F5 | DMSO | 365 | 4987 | 450 | 0.49 ^b |

^a 2-aminopyridine in 0.1 M H_2SO_4 ($\Phi = 0.60$) was the reference.

^b quinine sulfate in 0.1 M H_2SO_4 ($\Phi = 0.54$) was the reference.

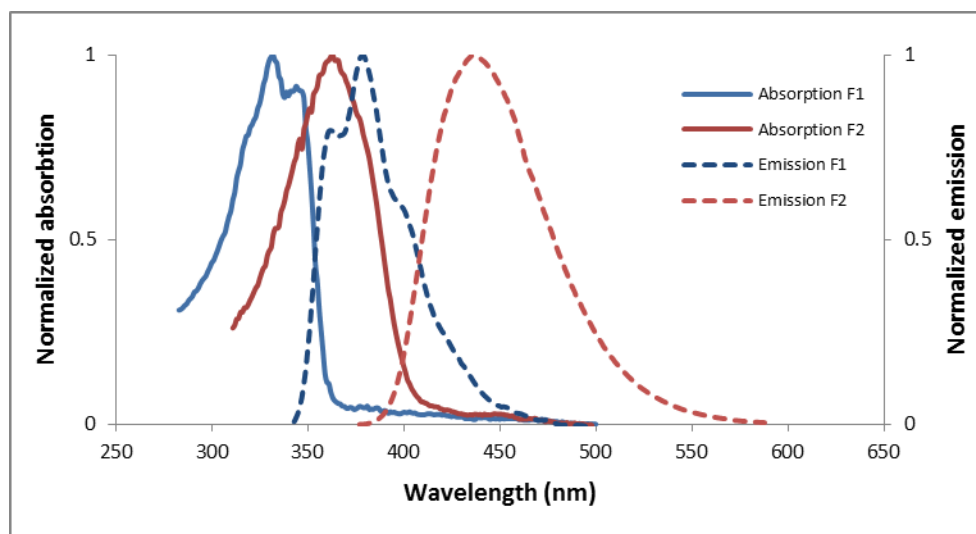


Figure 3.6 Normalized absorption and emission spectra of **F1** and **F2** in CH_3CN .

The photophysical properties of **F1** and **F2** in CH_3CN were shown (**Figure 3.6**). The **F1** exhibited maximum wavelength of absorption at 332 nm and maximum wavelength of emission at 378 nm. From the results were shown that the substitution in C-4 position of **F2** gave a maximum wavelength of absorption at 366 nm and maximum wavelength of emission at 435 nm. For the quantum yield, **F2** shows a higher value than **F1** due to ethoxy ($-\text{OCH}_3$) in the C4-position of naphthalimide. As a result, the **F2** exhibited fluorescence intensity in the blue region which is generally characteristic electron transition in the naphthalimide derivatives with good electron-donating alkoxy group at C-4 position leads to a narrower HOMO-LUMO gap. Nevertheless, the absorption and emission of **F2** exhibited in the red-shift.

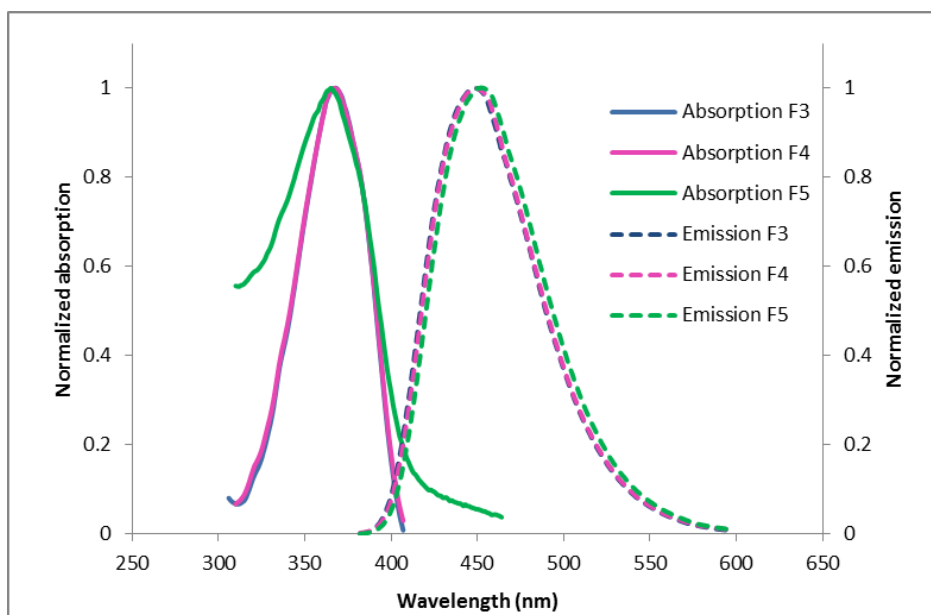


Figure 3.7 Normalized absorption and emission spectra of **F3** and **F5** in DMSO.

The sensor **F3** to **F5** contain cyanuric acid pendant in C-4 position. Their UV-vis absorption spectrum showed a broad absorption band with λ_{\max} around 365-367 nm associated with the π - π^* electronic transition of the substituted by a heteroatom at the C-4 position. The similar λ_{\max} values of these molecules indicated their comparable electronic energy band gap. The emission spectra of sensor **F3** to **F5** appeared at lower energy indicating a larger Stokes shifts than comparing with that of **F1**. These results may be the sensor **F3** to **F5** containing both electron donor (alkoxy group) and electron acceptor in the structure causing an ICT process.

3.3 Screening of F1 to F3 toward melamine

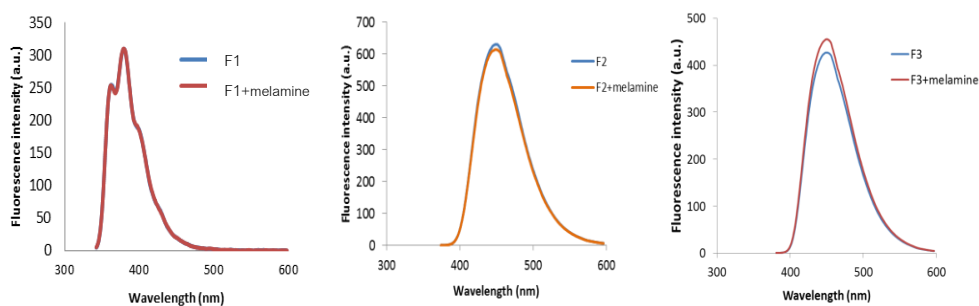


Figure 3.8 Screening of **F1** to **F3** in organic solvent.

The **F1** and **F2** are well soluble in CH_3CN , while the **F3** dissolve in DMSO. The responses of these fluorophore toward melamine were investigated by monitoring their fluorescent signal changes in the presence of melamine. When **F1-F3** are dissolved in pure organic solvents, fluorescence signal change was not observed as shown in **Figure 3.8**. However, when dissolved in aqueous-organic mixture, the fluorescence signal changes of **F3** can be observed upon addition of melamine. On the other hand, the fluorescent signals of **F1** and **F2** were not significantly changed (**Figure 3.9**).

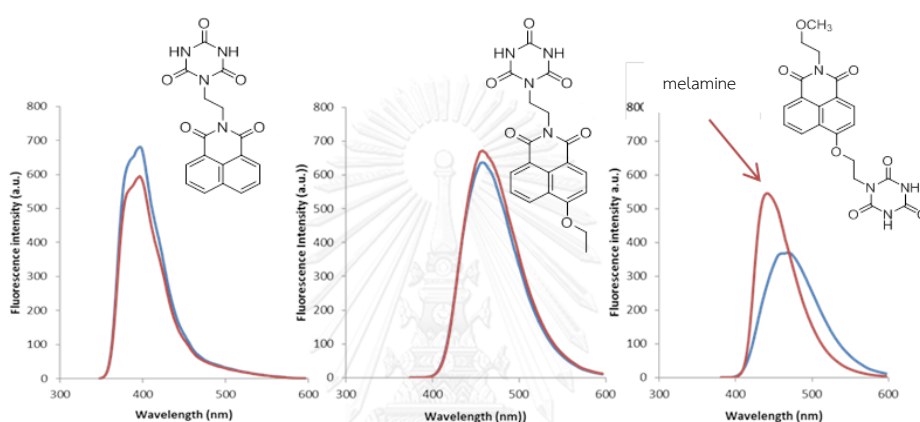


Figure 3.9 Screening of **F1** to **F3** in aqueous media.

The effect of water content on fluorescent intensity of **F3** was then examined using a various ratio of water: DMSO as solvents. **Figure 3.10** (left) shows that there is a sharp decrease in fluorescent intensity of **F3** when the water content reaches 90%. This may result from the aggregation of **F3** which can be witnessed by the decrease of absorbance as shown in **Figure 3.10** (right). The sensing mechanism might then involve the de-aggregation of **F3** by addition of melamine.

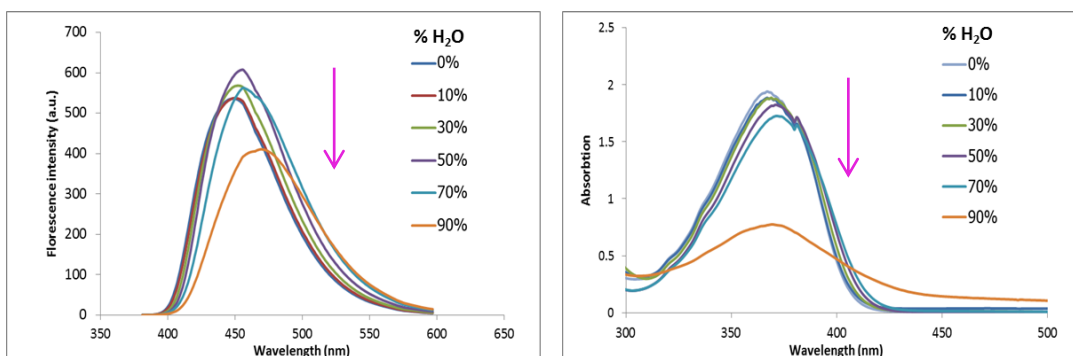


Figure 3.10 Fluorescent spectra (left) and absorption spectra (right) of fluorophore **F3** (500 μM) in DMSO and various water contents.

The selectivity of **F3** towards melamine was then studied using melamine and other compounds with similar structure. **Figure 3.11** shows that **F3** has good selectivity towards melamine with a fair sensitivity ($I/I_0 = 1.5$).

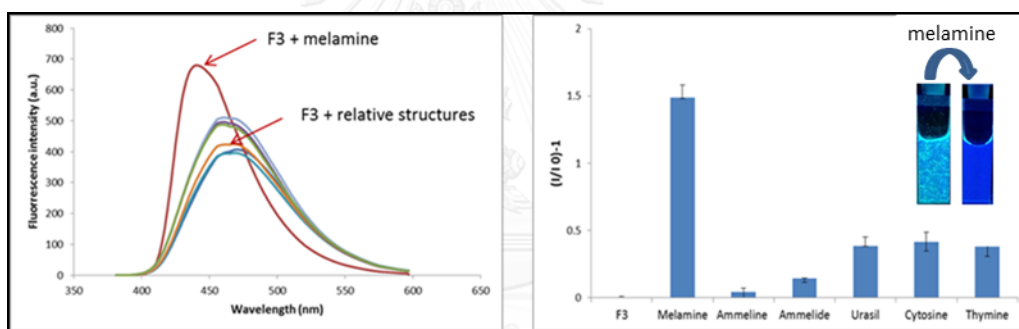


Figure 3.11 Selectivity screening of **F3** in aqueous media.

By the assumption that the hydrophobicity of fluorophore can cause aggregation-caused quenching (ACQ) and melamine can then deaggregate the fluorophore, we then design the more hydrophobic compound **F4** and **F5** to compare with **F3**.

3.4 Screening of **F4** and **F5** towards melamine

When **F4** and **F5** were dissolved in aqueous DMSO, it was found that their fluorescent signals can be altered by addition of melamine. The signal of **F4** increased upon addition of melamine, whereas the signal of **F5** was quenched (**Figure 3.12**).

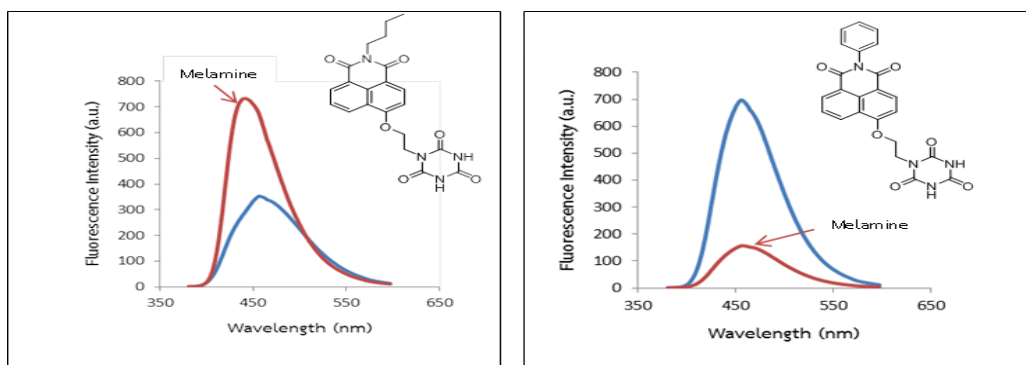


Figure 3.12 Screening of **F4** and **F5** in aqueous media.

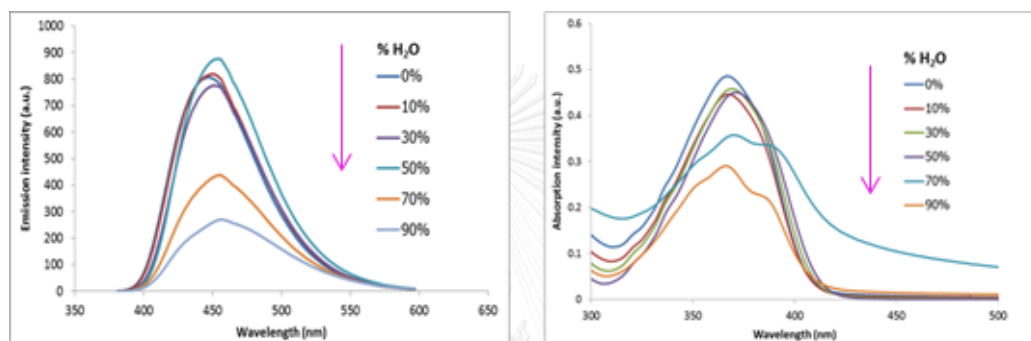


Figure 3.13 Fluorescent spectra (left) and absorption spectra (right) of **F4** (100 μ M) in DMSO and various water contents.

According to fluorescent signals of the **F4** in DMSO of different water contents their emissions are weakened when water is added (Figure 3.13 (left)). The increasing of water results the solvating power of the 90% water in DMSO to the sensor becomes so poor that most of the molecules become aggregated. As a result of the aggregate formation, the light emission of **F4** is quenched associating with ACQ. Moreover, high polarity of solvent can stabilize the excited state leading to red shift in the fluorescent and absorption spectra as shown in (Figure 3.13 (right)). As expected, the designed molecule **F4** with hydrophobic N-butyl chain showed low emission ($I_0 \sim 280$) in 90% water in DMSO comparing with **F3** ($I_0 \sim 400$).

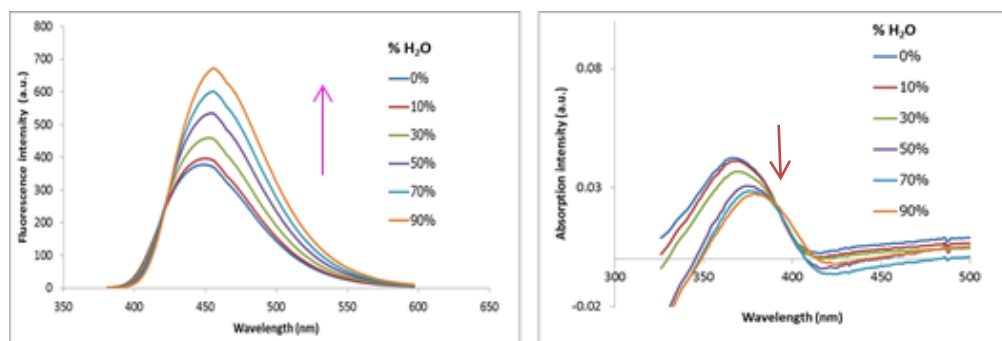


Figure 3.14 Fluorescent spectra (left) and absorption spectra (right) of **F5** (10 μM) in DMSO and various water contents.

On the other hand, the fluorophore **F5** exhibited aggregation-induced emission (AIE) characteristics. The fluorescent signal of the **F5** was enhanced in the increasing of water. The fluorescence enhancement because in aqueous media intramolecular rotations are restricted by the formation of aggregates that block the nonradiative channels and populate the radiative excitons, thereby making the molecule emissive in the aggregate state. The appearance of a red-shifted, sharp emission band suggests the formation of aggregates (**Figure 3.14 (left)**). This is in aggregation with observation of level-off long wavelength tail in the absorption spectra **Figure 3.14 (right)**.

3.5 selectivity study of **F4** and **F5** toward melamine

To investigate the selectivity of **F4** and **F5** toward melamine, ammeline, ammelide, uracil, cytosine, and thymine were tested. In **Figure 3.15** and **3.16** shown the **F4** and **F5** displayed high selectivity, only melamine caused a significant fluorescence enhancement effect. Showed a fluorescence response in the presence of melamine No fluorescence signal increases were observed in the presence of similar structure.

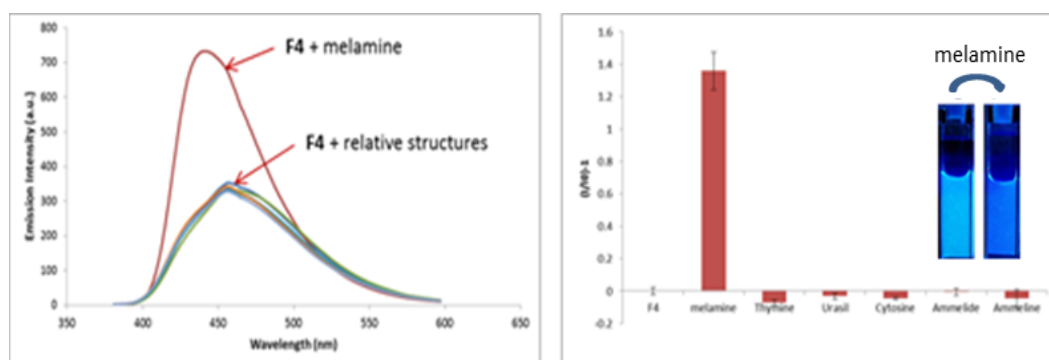


Figure 3.15 Selectivity screening of F4 in aqueous media.

On the other hand, the F5 exhibited high selectivity toward melamine resulting a significant fluorescence quenching as shown in the Figure 3.16

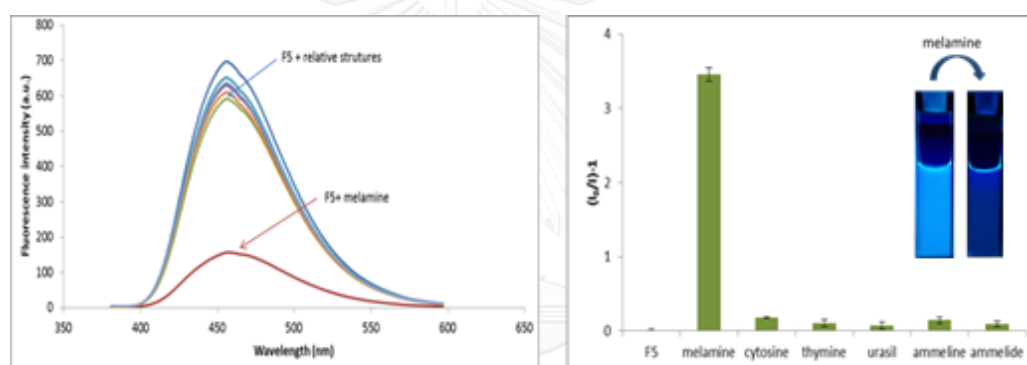


Figure 3.16 Selectivity screening of F5 in aqueous media.

3.6 Proposed mechanism of F4 toward melamine

From the result above, the emission of F4 is weakened in 90% water in DMSO resulting from π - π stacking causing the aggregation confirmed by absorption and emission spectra as mention in Figure 3.14. The fluorescence intensity enhanced after addition of melamine could be due to the de-aggregation through multivalent hydrogen-bonding interactions between cyanuric and melamine (Figure 3.17). The de-aggregation can be proved by UV-visible spectroscopy. The absorption intensity increased when melamine increased (Figure 3.18).

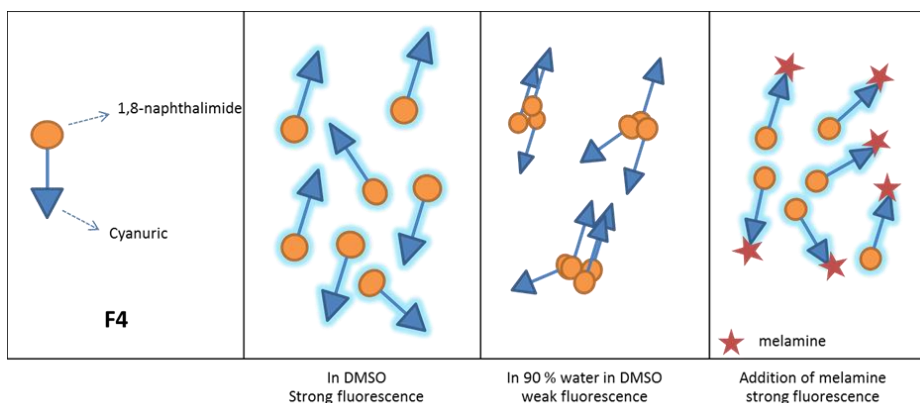


Figure 3.17 Proposed behaviors of **F4** after addition of melamine.

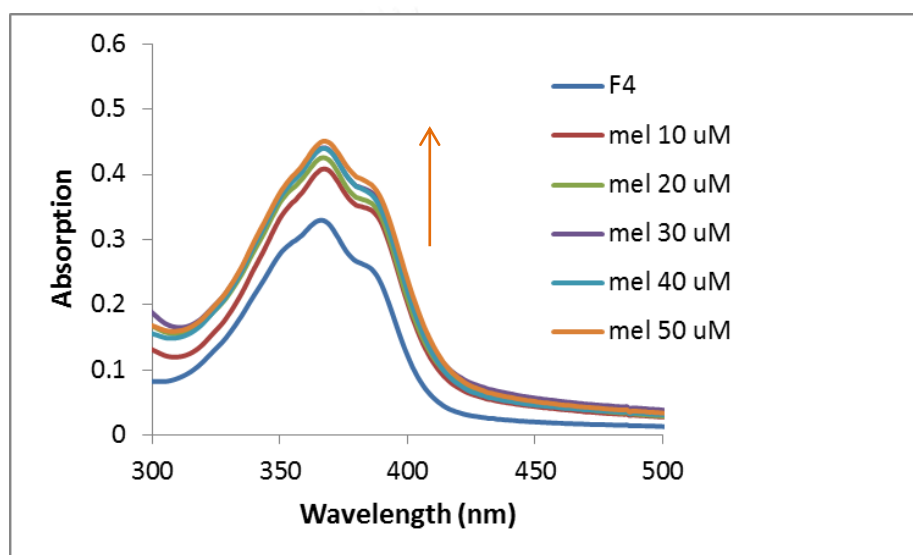


Figure 3.18 Absorption spectra of fluorophore **F4** ($100 \mu\text{M}$) in 90% water in DMSO in the various melamine contents.

On the other hand, the aggregation form of **F5** in aqueous DMSO exhibited the AIE characteristic. Thus, the addition of melamine facilitated the de-aggregation of **F5** and, therefore, resulting in the fluorescence quenching is shown in **Figure 3.19**.

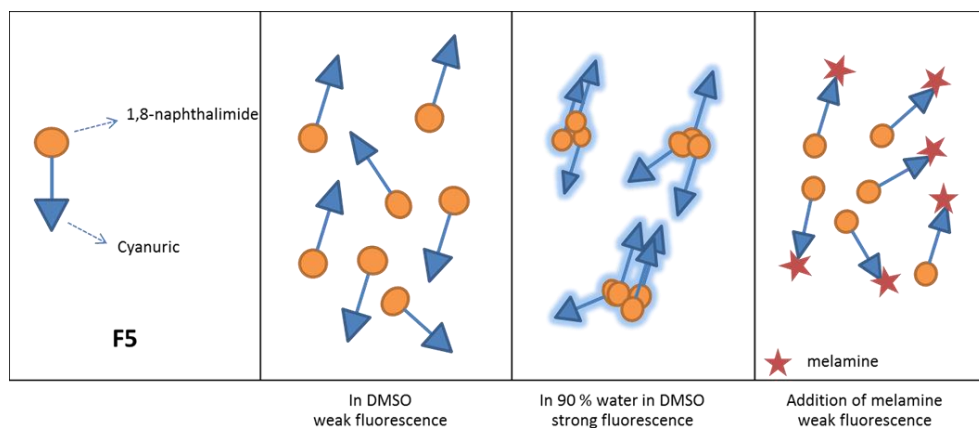


Figure 3.19 Proposed behaviors of **F4** after addition of melamine.

3.7 Melamine detection optimization

3.7.1 pH effect study

To investigate pH effect of **F3** to **F5** toward the fluorescence intensity in the absence of melamine (Figure 3.18) at high pH value, the fluorescence intensity of **F3** and **F4** increased because deprotonation of N-H amide proton result in increasing water solubility. However, it can be seen that I/I_0 value of **F4** in buffer pH 8, pH 9 and milli Q water was no significantly different. This might be implied that pH range: pH 5-9 had no effect on the sensing behavior of **F3** to melamine shown in Figure 3.19.

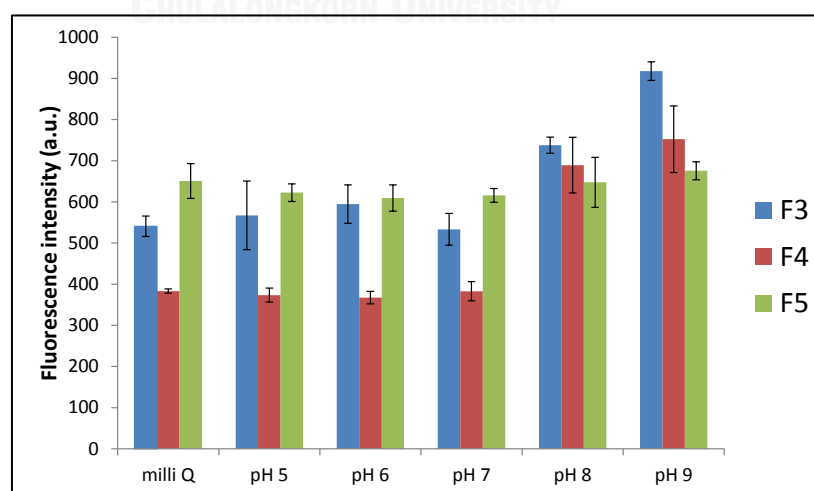


Figure 3.20 The fluorescence intensity of **F3** (500 μM), **F4** (100 μM) and **F5** (10 μM) in 10% DMSO/ buffer pH 5-9.

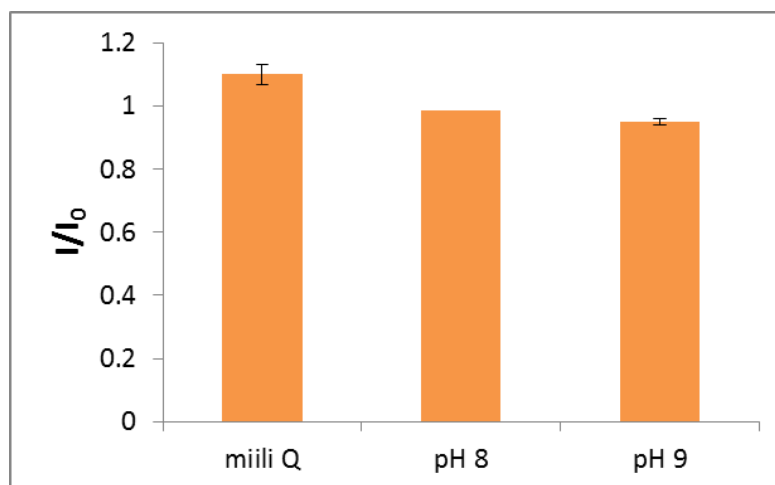


Figure 3.21 The fluorescence intensity **F3** (100 μM) upon addition of melamine 10 equivalent in 10% DMSO/aqueous solution.

3.7.2 Water content for detection of melamine

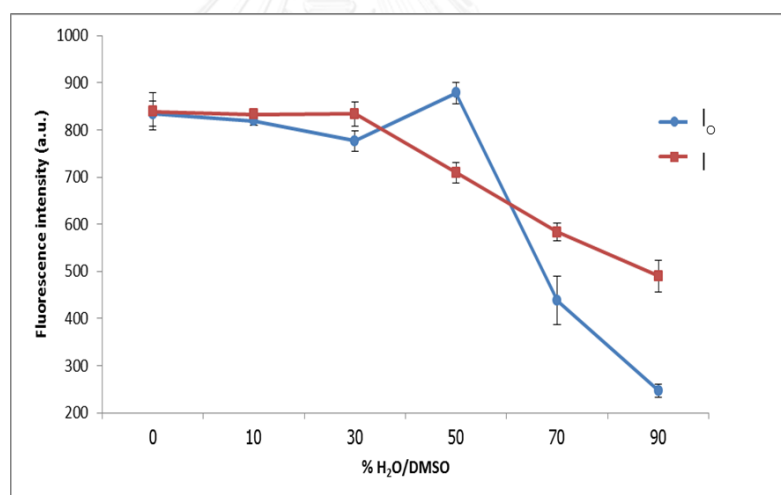


Figure 3.22 Fluorescence intensity in the absent of melamine (I_0) and in the presence of (I).

To optimization condition for detection of melamine in content of water was shown in **Figure 3.20**, the fluorescence intensity in the absence of melamine (I_0) and the present of melamine (I). The results indicated the fluorescence intensity of **F4** in the presence of melamine (I/I_0) was reached a maximum point at 90% of water in DMSO. Therefore, this mixture of solvents at 90% of water in DMSO was selected for further optimization study.

3.7.3 Time-dependent study

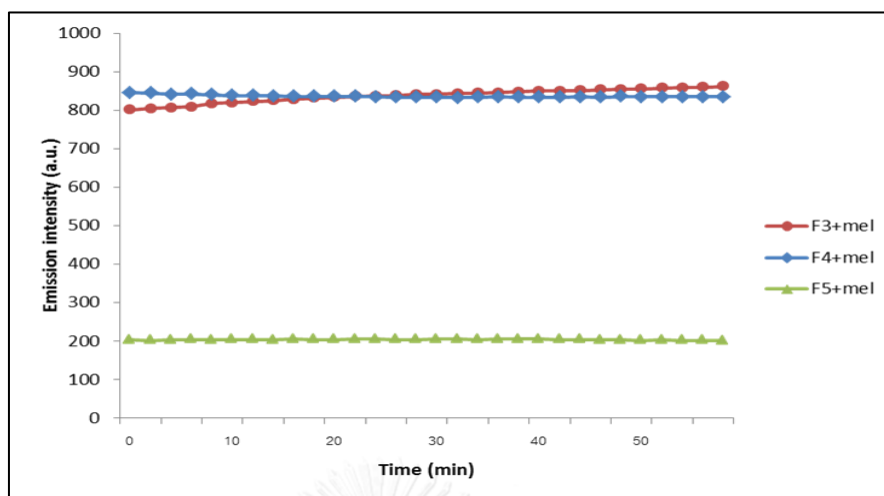


Figure 3.23 Time dependent change in fluorescence intensity of **F3**, **F4** and **F5** upon addition of melamine 10 equivalent in 90% water in DMSO.

The time dependent studies of **F3**, **F4**, and **F5** in the presence of melamine were performed. Upon the addition of 10 equivalents of relative structures of melamine as shown in **Figure 3.21**, the fluorescence intensity was unchanged. This suggested that time progress had no effect on the measurements which was beneficial in fluorescent sensing because the analyte could be detected immediately.

3.7.4 Surfactant study

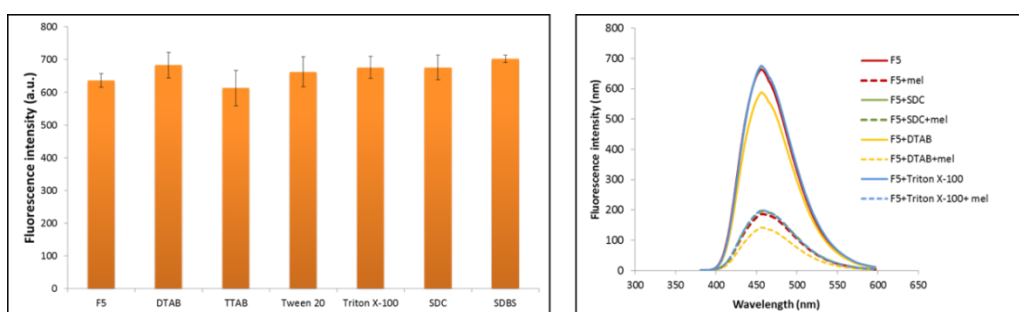


Figure 3.24 Surfactant study of fluorescence intensity of **F5** (10 μM) toward various 100 μM surfactant (left), the fluorescence intensity of **F5** in the presence of melamine 100 μM in SDC, DTAB and Triton X-100 (100 μM) (right).

Several studies have reported that surfactant compound can enhance fluorescent signal that is an advantage for the quenching mode. Therefore, the effect of surfactants was investigated due to improve sensing efficiency. The various surfactant were used such as anionic (SDC and SDBS), cationic (DTAB and TTAB), non-ionic (Tween-20 and Triton X-100). In the presence of surfactants 100 μM , The initial fluorescent intensity of sensor (I_0) did not show any change compared with without surfactant. Moreover, the surfactant did not effect on quenching efficiency.

3.8 Interferences test

The results from selectivity test showed that **F3**, **F4** and **F5** could respond to melamine. The interference test was completed by adding melamine and relative structures. The fluorescence response (I/I_0) or (I_0/I) were shown in **Figure 3.23**, **3.24**, and **3.25** in the presence of mixture melamine/relative structures in 1:10 equivalent. As a result, it was observed that the relative structures did not interfere to the detection of melamine.

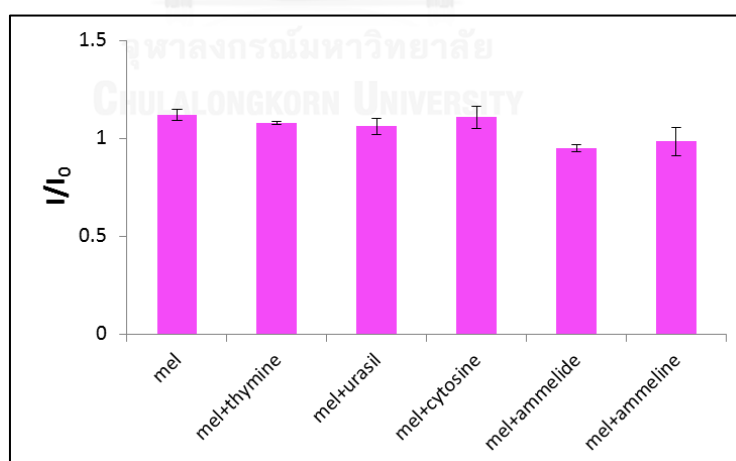


Figure 3.25 The bar represent the fluorescence enhancement ratio (I/I_0) of **F3** upon addition of melamine in the present of relative structures ($\lambda_{\text{ex}}=366$ nm; Medium = 90% water in DMSO; $[\text{F3}] = 0.5$ mM; $[\text{mel}] = 0.5$ mM; $[\text{relative structures}] = 5$ mM).

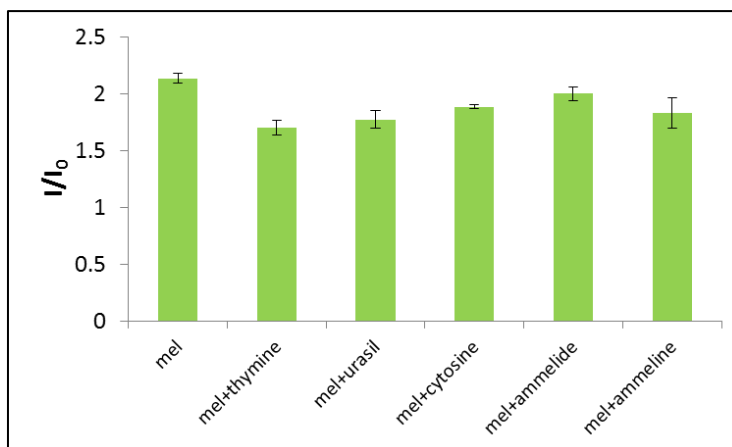


Figure 3.26 The bar represent the fluorescence enhancement ratio (I/I_0) of **F4** upon addition of melamine in the present of relative structures ($\lambda_{ex}=366$ nm; Medium = 90% water in DMSO; $[F4]=0.1$ mM; $[mel]=0.1$ mM; $[relative\ structures]=1$ mM).

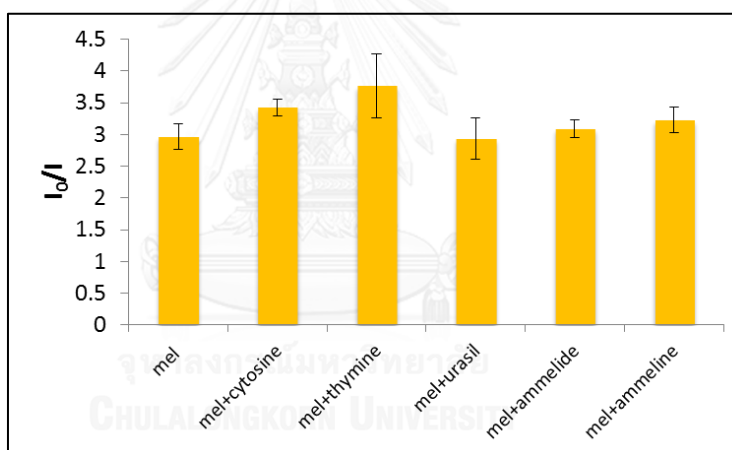


Figure 3.27 The bar represent the fluorescence enhancement ratio (I/I_0) of **F5** upon addition of melamine in the present of relative structures ($\lambda_{ex}=365$ nm; Medium = 90% water in DMSO; $[F5]=0.01$ mM; $[mel]=0.5$ mM; $[relative\ structures]=5$ mM).

3.9 Detection limit of F4 and F5 toward melamine

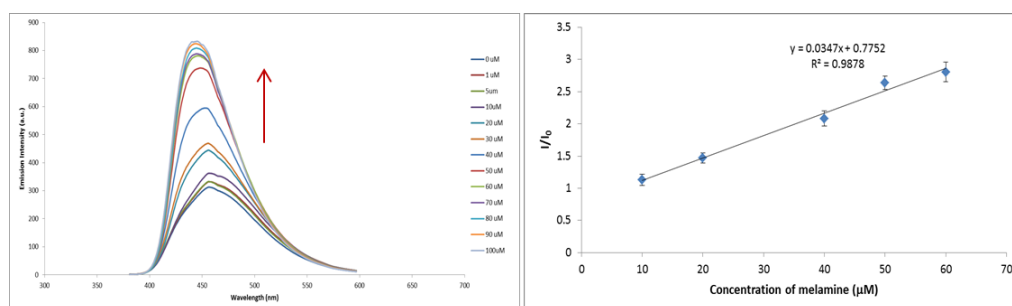


Figure 3.28 The fluorescence spectra (left), the fluorescence intensity change (I/I_0) of [F4] = 100 μM, versus [melamine] in condition = 90% water in DMSO.

The fluorescence spectra of sensor F4 in the presence of various concentration of melamine are shown in **Figure 3.26 (left)**. It can be observed that the fluorescence intensity was increase gradually with increasing the concentration of melamine. The **figure 3.26 (right)** exhibits the good linear relationship between fluorescence intensity at 444 nm and concentration of melamine ($R^2 = 0.9878$) providing the detection limit of 6.7 μM (0.8 ppm) at a signal-to noise. Therefore, the fluorophore F4 are able to use for melamine detection in aqueous system.

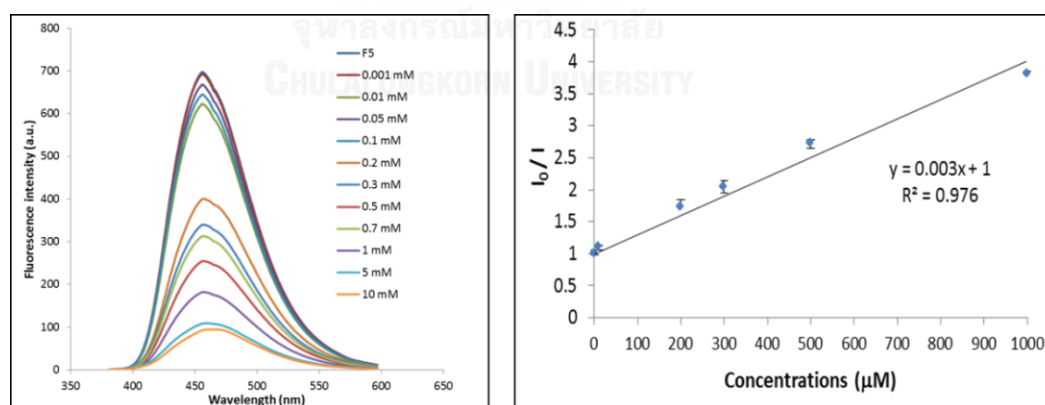


Figure 3.29 The fluorescence spectra (left), the fluorescence intensity change (I/I_0) of [F4] = 100 μM, versus [melamine] in condition = 90% water in DMSO.

The fluorescence quenching of sensor F5 contained different concentrations of melamine. Where I_0 and I are the fluorescent intensity of fluorophore in the absence

and presence of melamine, respectively. [analyte] is the concentration of the melamine. A diagram which indicated the relationship between I_0/I and the concentration of melamine was shown in **Figure 3.27 (right)** and the quenching constant (K_{sv}) was calculated according to the Stern–Volmer equation:

$$I_0/I - 1 = K_{sv}[\text{analyte}]$$

The detection limits of **F5** as fluorescent sensors for melamine are found to be 25 μM (3.2 ppm). This finding demonstrates the utility of aggregates in the detection of melamine. The Stern–Volmer plots of aggregates **F5** are linear (**Figure 3.27 (right)**) and give quenching constants (K_{sv}) 3000 M^{-1} . The quenching of fluorescence in compound **F5** upon the addition of melamine can also be observed by the naked eye.

3.10 ^1H NMR experiment

In an attempt to monitor the interaction of fluorophore **F4** and melamine, a series of NMR spectra were recorded at ambient temperature using **F4** and melamine (1: 10 eq). No significant change could be observed on the spectra, which might be due to the fast hydrogen-deuterium exchange when a solution of melamine in D_2O are added to a solution of **F4** in DMSO-d_6 .

CHAPTER IV

CONCLUSION

4.1 Conclusion

In conclusion, five novel fluorescent sensors (**F1-F5**) were successfully synthesized in good yields with an aim to use as sensors for melamine. The sensors compose of 1,8-naphthalimide as a fluorophore and cyanuric unit as a selective receptor for melamine. The structure of all fluorescent sensors were characterized and confirmed by NMR spectroscopy, UV-Vis and fluorescence spectrophotometry, elemental analysis and high resolution mass spectrometry.

The selectivity investigation of melamine indicated that **F3**, **F4**, and **F5** show selective fluorogenic responses towards melamine. The fluorescence sensing mechanism involves the fluorophore de-aggregation by multivalent hydrogen-bonding interactions between melamine and cyanuric moieties. When dissolved in aqueous DMSO (90% water), sensor **F3** and **F4** showed ACQ behavior resulting in weak fluorescent emission. After the addition of melamine which can form strong hydrogen bonds with the cyanuric pendants, the fluorescent intensities were enhanced as resulting from the de-aggregation. The turn-on sensor **F4** provided the detection limit for melamine at 0.8 ppm. On the other hand, the aggregation form of **F5** in aqueous DMSO exhibited the AIE characteristic. Thus, the addition of melamine facilitated the de-aggregation of **F5** and, therefore, resulting in the fluorescence quenching. The Stern-Volmer constant (K_{sv}) was determined to be $3 \times 10^3 \text{ M}^{-1}$ with the detection limit of 3.2 ppm. This research has established a new concept in molecular design for easy-to-use and selective melamine sensors which are compatible with aqueous application.

4.2 Suggestion for future works

The present data suggested that the modification of substituent on the 1,8-naphthalimide nitrogen from 2-methoxyethyl to n-butyl could provide a melamine sensor with higher sensitivity. Therefore, it is likely that the substitution on that

nitrogen with more hydrophobic groups such as n-hexyl, n-octyl, or larger aliphatic chains may result in sensors that could aggregate well in aqueous DMSO, which lead to the lower fluorescent intensity prior to the addition of melamine. If these aggregated fluorophores are de-aggregated by melamine, a strong signal enhancement and high sensitivity could be observed. However, it is also possible that the hydrophilicity of melamine may not be sufficient to de-aggregate the fluorophores with high hydrophobicity. Therefore, this structure modification must be carefully fine-tuned.



REFERENCES

- [1] Sun, F., Ma, W., Xu, L., Zhu, Y., Liu, L., Peng, C., Wang, L., Kuang, H., and Xu, C. Analytical methods and recent developments in the detection of melamine. TrAC Trends in Analytical Chemistry **29**(11) (2010): 1239-1249.
- [2] Liu, Y., Todd, E.E.D., Zhang, Q., Shi, J.-r., and Liu, X.-j. Recent developments in the detection of melamine. Journal of Zhejiang University. Science. B **13**(7) (2012): 525-532.
- [3] Update: Interim Safety and Risk Assessment of Melamine and its Analogues in Food for Humans [Online]. 2008. Available from: <http://www.fda.gov/Food/FoodborneIllnessContaminants/ChemicalContaminants/ucm164520.htm> [03/10/2008]
- [4] Melamine and Cyanuric acid: Toxicity, Preliminary Risk Assessment and Guidance on Levels in Food [Online]. 2008. Available from: <http://www.who.int/topics/melamine/en/> [25/09/2008]
- [5] Venkatasami, G. and Sowa Jr, J.R. A rapid, acetonitrile-free, HPLC method for determination of melamine in infant formula. Analytica Chimica Acta **665**(2) (2010): 227-230.
- [6] Chou, S.S., Hwang, D.F., and Lee, H.F. High performance liquid chromatographic determination of cyromazine and its derivative melamine in poultry meats and eggs. Journal of Food and Drug Analysis **11**(4) (2003): 290-295.
- [7] Hao, X.-j., Zhou, X.-h., Zhang, Y., Liu, L.-h., Long, F., Song, L., and Shi, H.-c. Melamine detection in dairy products by using a reusable evanescent wave fiber-optic biosensor. Sensors and Actuators B: Chemical **204** (2014): 682-687.
- [8] Chen, L., Zeng, Q., Du, X., Sun, X., Zhang, X., Xu, Y., Yu, A., Zhang, H., and Ding, L. Determination of melamine in animal feed based on liquid chromatography tandem mass spectrometry analysis and dynamic microwave-assisted extraction coupled on-line with strong cation-exchange

- resin clean-up. Analytical and Bioanalytical Chemistry **395**(5) (2009): 1533-1542.
- [9] Sun, F., Liu, L., Kuang, H., and Xu, C. Development of ELISA for melamine detection in milk powder. Food and Agricultural Immunology **24**(1) (2013): 79-86.
- [10] Liao, C.W., Chen, Y.R., Chang, J.L., and Zen, J.M. Single-run electrochemical determination of melamine in dairy products and pet foods. Journal of Agricultural and Food Chemistry **59**(18) (2011): 9782-7.
- [11] Paul, I.E., Rajeshwari, A., Prathna, T.C., Raichur, A.M., Chandrasekaran, N., and Mukherjee, A. Colorimetric detection of melamine based on the size effect of AuNPs. Analytical Methods **7**(4) (2015): 1453-1462.
- [12] Lachenmeier, D.W., Eberhard, H., Fang, F., Birk, S., Peter, D., Constanze, S., and Manfred, S. NMR-spectroscopy for nontargeted screening and simultaneous quantification of health-relevant compounds in foods: The example of melamine. Journal of Agricultural and Food Chemistry **57**(16) (2009): 7194-7199.
- [13] Huang, H.Y., Lin, C.L., Jiang, S.H., Singco, B., and Cheng, Y.J. Capillary electrochromatography-mass spectrometry determination of melamine and related triazine by-products using poly(divinyl benzene-alkene-vinylbenzyl trimethylammonium chloride) monolithic stationary phases. Analytica Chimica Acta **719** (2012): 96-103.
- [14] Lakowicz, J.R. Principles of Fluorescence Spectroscopy. 3 ed.: Springer US, 2006.
- [15] Quenching of Fluorescence. in Lakowicz, J. Principles of Fluorescence Spectroscopy, pp. 277-330: Springer US, 2006.
- [16] Tian, H., Xu, T., Zhao, Y., and Chen, K. Two-path photo-induced electron transfer in naphthalimide-based model compound. Journal of the Chemical Society, Perkin Transactions 2 (3) (1999): 545-550.
- [17] Wei, T., Wang, J., Chen, Y., and Han, Y. Combining the PeT and ICT mechanisms into one chemosensor for the highly sensitive and selective detection of zinc. RSC Advances **5**(70) (2015): 57141-57146.

- [18] Marinova, N.V., Georgiev, N.I., and Bojinov, V.B. Design, synthesis and pH sensing properties of novel 1,8-naphthalimide-based bichromophoric system. Journal of Photochemistry and Photobiology A: Chemistry **222**(1) (2011): 132-140.
- [19] Liu, S., Bai, H., Sun, Q., Zhang, W., and Qian, J. Naphthalimide-based fluorescent photoinduced electron transfer sensors for saccharides. RSC Advances **5**(4) (2015): 2837-2843.
- [20] de Silva, A.P., Moody, T.S., and Wright, G.D. Fluorescent PET (Photoinduced Electron Transfer) sensors as potent analytical tools. Analyst **134**(12) (2009): 2385-2393.
- [21] Daly, B., Ling, J., and de Silva, A.P. Current developments in fluorescent PET (photoinduced electron transfer) sensors and switches. Chemical Society Reviews **44**(13) (2015): 4203-4211.
- [22] Jia, X., Yang, Y., Xu, Y., and Qian, X. Naphthalimides for labeling and sensing applications. Pure and Applied Chemistry **86**(7) (2014).
- [23] Georgiev, N.I., Bojinov, V.B., and Nikolov, P.S. The design, synthesis and photophysical properties of two novel 1,8-naphthalimide fluorescent pH sensors based on PET and ICT. Dyes and Pigments **88**(3) (2011): 350-357.
- [24] Dash, N., Malakar, A., Kumar, M., Mandal, B.B., and Krishnamoorthy, G. Metal ion dependent "ON" intramolecular charge transfer (ICT) and "OFF" normal switching of the fluorescence: Sensing of Zn^{2+} by ICT emission in living cells. Sensors and Actuators B: Chemical **202** (2014): 1154-1163.
- [25] Hong, Y., Lam, J.W.Y., and Tang, B.Z. Aggregation-induced emission: phenomenon, mechanism and applications. Chemical Communications (29) (2009): 4332-4353.
- [26] Chen, Z., Wu, D., Han, X., Nie, Y., Yin, J., Yu, G.-A., and Liu, S.H. 1,8-Naphthalimide-based highly blue-emissive fluorophore induced by a bromine atom: reversible thermochromism and vapochromism characteristics. RSC Advances **4**(109) (2014): 63985-63988.
- [27] Shen, X.Y., Wang, Y.J., Zhao, E., Yuan, W.Z., Liu, Y., Lu, P., Qin, A., Ma, Y., Sun, J.Z., and Tang, B.Z. Effects of substitution with donor-acceptor groups on the

- properties of tetraphenylethene trimer: aggregation-induced emission, solvatochromism, and mechanochromism. The Journal of Physical Chemistry C **117**(14) (2013): 7334-7347.
- [28] Hong, Y., Lam, J.W.Y., and Tang, B.Z. Aggregation-induced emission. Chemical Society Reviews **40**(11) (2011): 5361-5388.
- [29] Wang, E., Lam, J.W.Y., Hu, R., Zhang, C., Zhao, Y.S., and Tang, B.Z. Twisted intramolecular charge transfer, aggregation-induced emission, supramolecular self-assembly and the optical waveguide of barbituric acid-functionalized tetraphenylethene. Journal of Materials Chemistry C **2**(10) (2014): 1801-1807.
- [30] Chen, Y., Wang, Y., Yuan, Y., Jiao, Y., Pu, X., and Lu, Z. Deactivation mechanism of a novel AIE-active naphthalimide derivative in more polar solutions. Physical Chemistry Chemical Physics **17**(2) (2015): 1309-1316.
- [31] Kassl, C.J. and Christopher Pigge, F. Anion detection by aggregation-induced enhanced emission (AIEE) of urea-functionalized tetraphenylethylenes. Tetrahedron Letters **55**(34) (2014): 4810-4813.
- [32] Wang, J., Mei, J., Shen, X., Qin, A., Sun, J.Z., and Tang, B.Z. Effect of pH on the detection of explosive in aqueous solution using a hyperbranched polytriazole with aggregation-induced emission characteristics. Journal of Molecular and Engineering Materials **01**(03) (2013): 1340004.
- [33] Jin, W., Jiang, J., Wang, X., Zhu, X., Wang, G., Song, Y., and Bai, C. Continuous intra-arterial blood pH monitoring in rabbits with acid–base disorders. Respiratory Physiology & Neurobiology **177**(2) (2011): 183-188.
- [34] Triboni, E.R., Fernandes, M.R., Garcia, J.R., Carreira, M.C., Berlinck, R.G.S., Filho, P.B., Roman, L.S., Hümmelgen, I.A., Reyes, R., and Cremona, M. Naphthalimide-derivative with blue electroluminescence for OLED applications. Journal of Taibah University for Science **9**(4) (2015): 579-585.
- [35] Zhang, Z., Chen, Y., Xu, D., Yang, L., and Liu, A. A new 1,8-naphthalimide-based colorimetric and “turn-on” fluorescent Hg²⁺ sensor. Spectrochimica Acta Part A: Molecular and Biomolecular Spectroscopy **105** (2013): 8-13.

- [36] Wang, J., Yang, L., Hou, C., and Cao, H. A new n-imidazolyl-1,8-naphthalimide based fluorescence sensor for fluoride detection. Organic & Biomolecular Chemistry **10**(31) (2012): 6271-6274.
- [37] Li, Y., Xu, J., and Sun, C. Chemical sensors and biosensors for the detection of melamine. RSC Advances **5**(2) (2015): 1125-1147.
- [38] Cao, X., Shen, F., Zhang, M., Guo, J., Luo, Y., Li, X., Liu, H., Sun, C., and Liu, J. Efficient inner filter effect of gold nanoparticles on the fluorescence of CdS quantum dots for sensitive detection of melamine in raw milk. Food Control **34**(1) (2013): 221-229.
- [39] Zhang, M., Cao, X., Li, H., Guan, F., Guo, J., Shen, F., Luo, Y., Sun, C., and Zhang, L. Sensitive fluorescent detection of melamine in raw milk based on the inner filter effect of Au nanoparticles on the fluorescence of CdTe quantum dots. Food Chemistry **135**(3) (2012): 1894-900.
- [40] Gong, Y., Wu, H., and Fan, Z. Water-soluble Eu(iii)-doped ZnS quantum dots for the room-temperature phosphorescence detection of melamine in milk products. Analytical Methods **5**(21) (2013): 6114-6119.
- [41] Roy, B., Saha, A., and Nandi, A.K. Melamine sensing through riboflavin stabilized gold nanoparticles. Analyst **136**(1) (2011): 67-70.
- [42] Zhou, Y.-Y., Yang, J., Liu, M., Wang, S.-F., and Lu, Q. A novel fluorometric determination of melamine using cucurbit[7]uril. Journal of Luminescence **130**(5) (2010): 817-820.
- [43] Zhao, J., Nie, L., Zhang, L., Jin, Y., Peng, Y., Du, S., and Jiang, N. Molecularly imprinted layer-coated silica nanoparticle sensors with guest-induced fluorescence enhancement: theoretical prediction and experimental observation. Analytical Methods **5**(12) (2013): 3009-3015.
- [44] Li, L., Li, B., Cheng, D., and Mao, L. Visual detection of melamine in raw milk using gold nanoparticles as colorimetric probe. Food Chemistry **122**(3) (2010): 895-900.
- [45] Niu, C., Liu, Q., Shang, Z., Zhao, L., and Ouyang, J. Dual-emission fluorescent sensor based on AIE organic nanoparticles and Au nanoclusters for the detection of mercury and melamine. Nanoscale **7**(18) (2015): 8457-8465.

- [46] Chen, Z., Zhang, C., and Wang, C. A colorimetric assay of dopamine utilizing melamine modified gold nanoparticle probes. Analytical Methods **7**(3) (2015): 838-841.
- [47] Ping, H., Zhang, M., Li, H., Li, S., Chen, Q., Sun, C., and Zhang, T. Visual detection of melamine in raw milk by label-free silver nanoparticles. Food Control **23**(1) (2012): 191-197.
- [48] Ameer, F.S., Ansar, S.M., Hu, W., Zou, S., and Zhang, D. Inner filter effect on surface enhanced raman spectroscopic measurement. Analytical Chemistry **84**(20) (2012): 8437-8441.
- [49] Guo, L., Zhong, J., Wu, J., Fu, F., Chen, G., Chen, Y., Zheng, X., and Lin, S. Sensitive turn-on fluorescent detection of melamine based on fluorescence resonance energy transfer. Analyst **136**(8) (2011): 1659-1663.
- [50] Sanji, T., Nakamura, M., Kawamata, S., Tanaka, M., Itagaki, S., and Gunji, T. Fluorescence "turn-on" detection of melamine with aggregation-Induced-emission-active tetraphenylethene. Chemistry – A European Journal **18**(48) (2012): 15254-15257.
- [51] Zhang, J., Ou, C., Shi, Y., Wang, L., Chen, M., and Yang, Z. Visualized detection of melamine in milk by supramolecular hydrogelations. Chemical Communications **50**(85) (2014): 12873-12876.
- [52] Tong, H., Hong, Y., Dong, Y., Hau, Lam, J.W.Y., Li, Z., Guo, Z., Guo, Z., and Tang, B.Z. Fluorescent "light-up" bioprobes based on tetraphenylethylene derivatives with aggregation-induced emission characteristics. Chemical Communications (35) (2006): 3705-3707.
- [53] Li, H.-T., Jiang, Z.-Q., Zheng, J., Wang, X., Pan, Y., Wang, F., and Yu, S.-Q. A novel 1,8-naphthalimide probe: synthesis and interactions with nucleic acid and its precursor. Research on Chemical Intermediates **32**(1) (2006): 43-57.
- [54] Wan, X., Liu, T., and Liu, S. Thermoresponsive core cross-linked micelles for selective ratiometric fluorescent detection of Hg²⁺ ions. Langmuir **27**(7) (2011): 4082-4090.

- [55] Montoya, L.A. and Pluth, M.D. Selective turn-on fluorescent probes for imaging hydrogen sulfide in living cells. Chemical Communications **48**(39) (2012): 4767-4769.
- [56] Tian, Z., Liu, Y., Tian, B., and Zhang, J. The synthesis and fluorescence properties of novel 1,8-naphthalimide derivatives. Research on Chemical Intermediates **41**(2) (2015): 1157-1169.





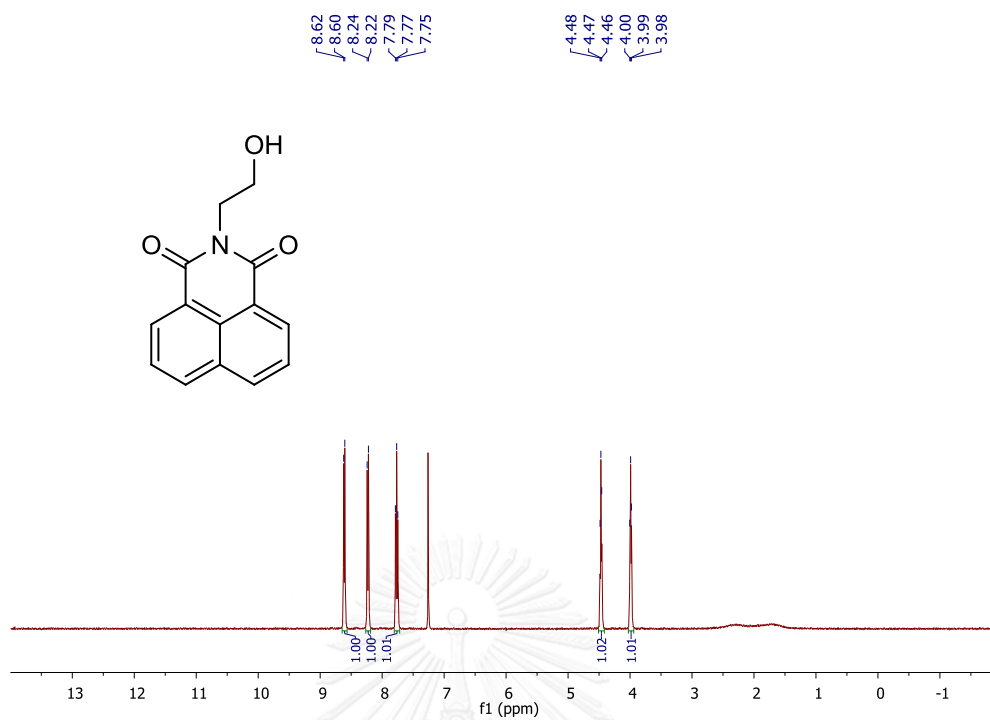


Figure A.1 $^1\text{H-NMR}$ spectrum of **1a** in CDCl_3 .

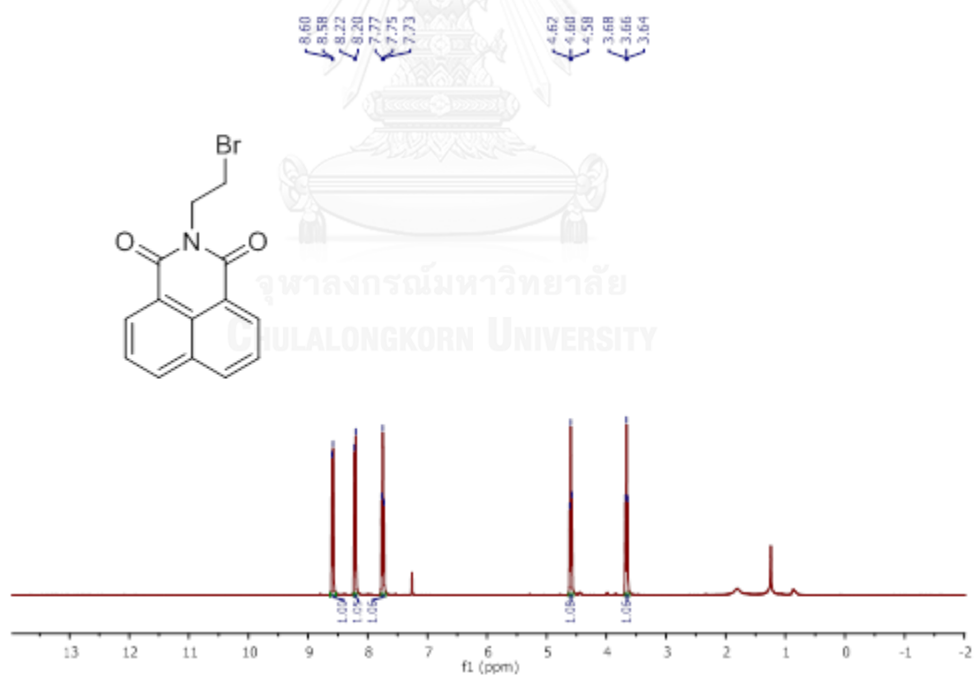


Figure A.2 $^1\text{H-NMR}$ spectrum of **2a** in CDCl_3 .

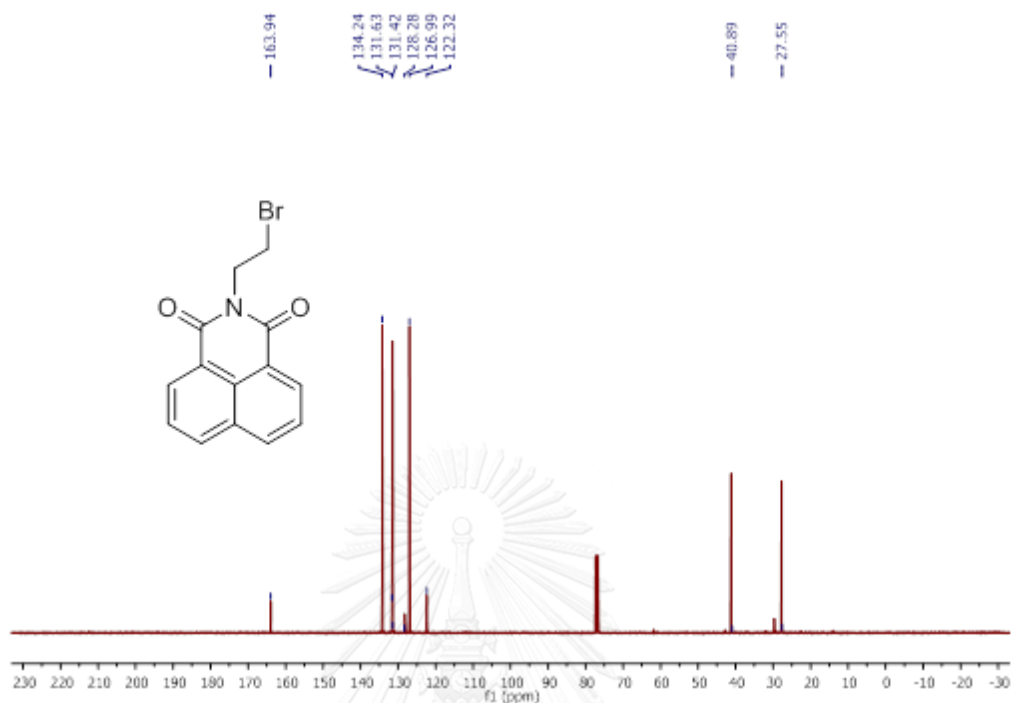


Figure A.3 ^{13}C -NMR spectrum of **2a** in CDCl_3 .

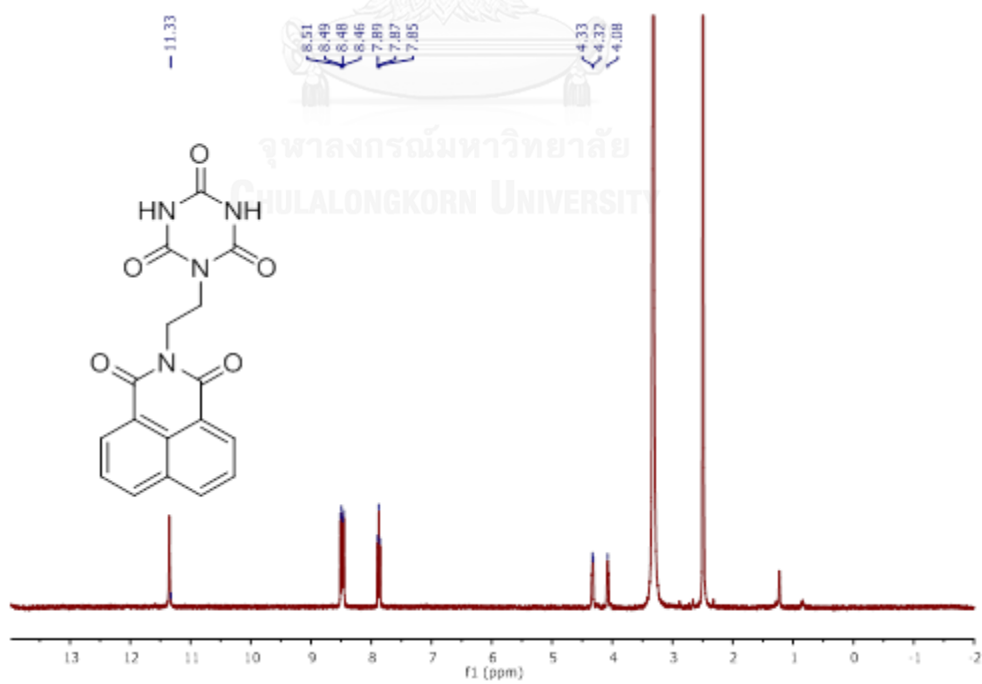


Figure A.4 ^1H -NMR spectrum of **F1** in CDCl_3 .

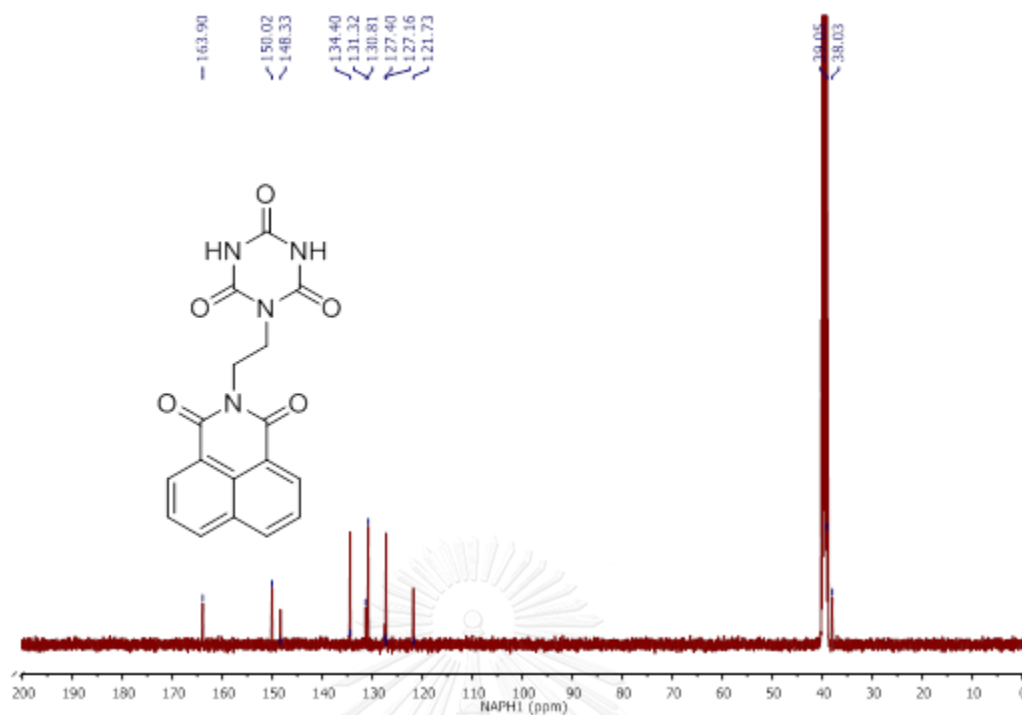


Figure A.5 $^{13}\text{C-NMR}$ spectrum of F1 in DMSO- d_6 .

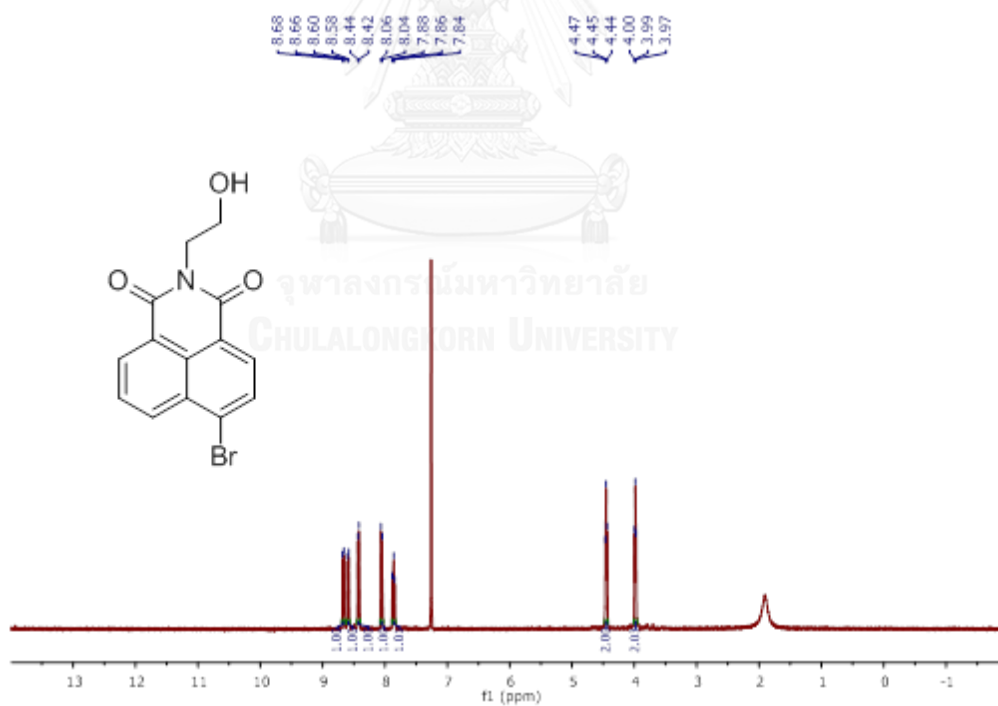


Figure A.6 $^1\text{H-NMR}$ spectrum of 1b in CDCl_3 .

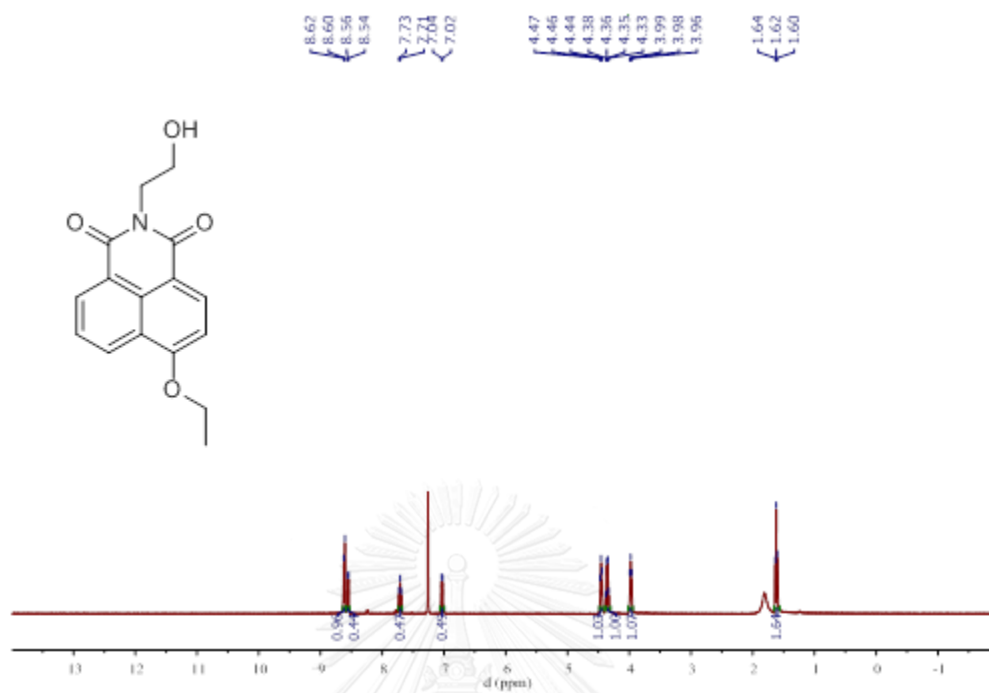


Figure A.7 $^1\text{H-NMR}$ spectrum of **2b** in CDCl_3 .

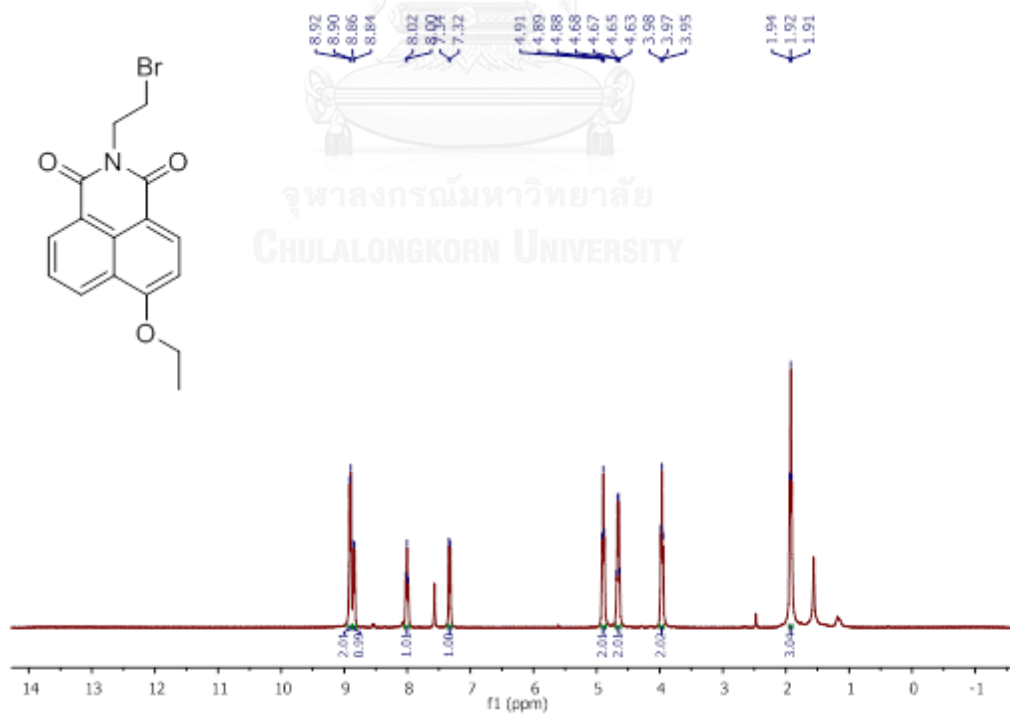


Figure A.8 $^1\text{H-NMR}$ spectrum of **3b** in CDCl_3 .

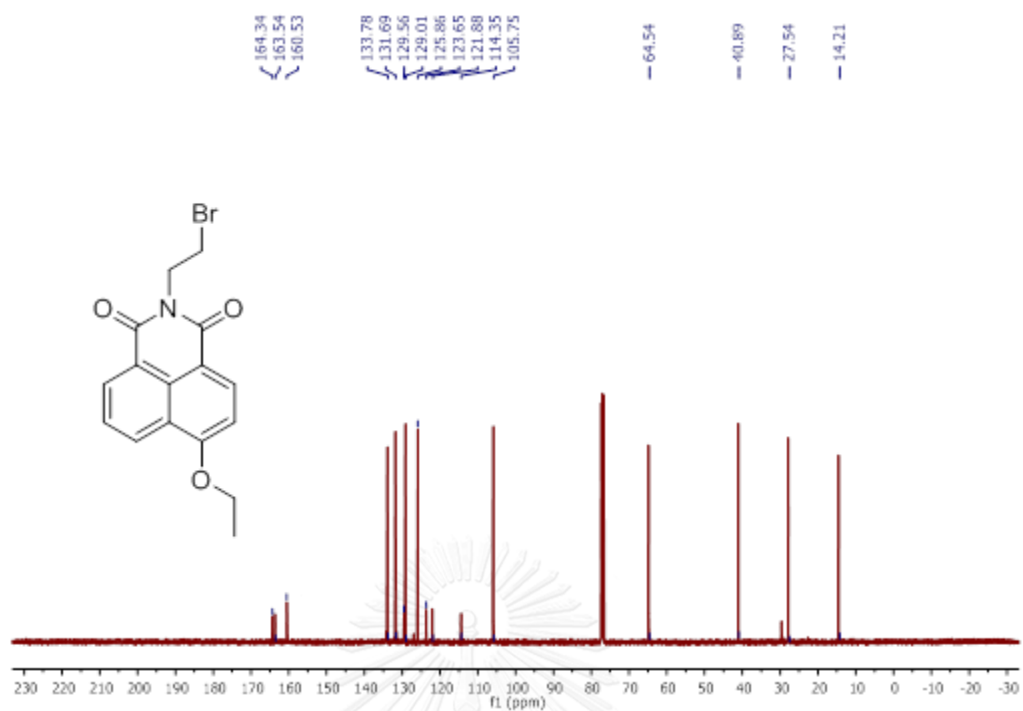


Figure A.9 $^{13}\text{C-NMR}$ spectrum of 3b in CDCl_3 .

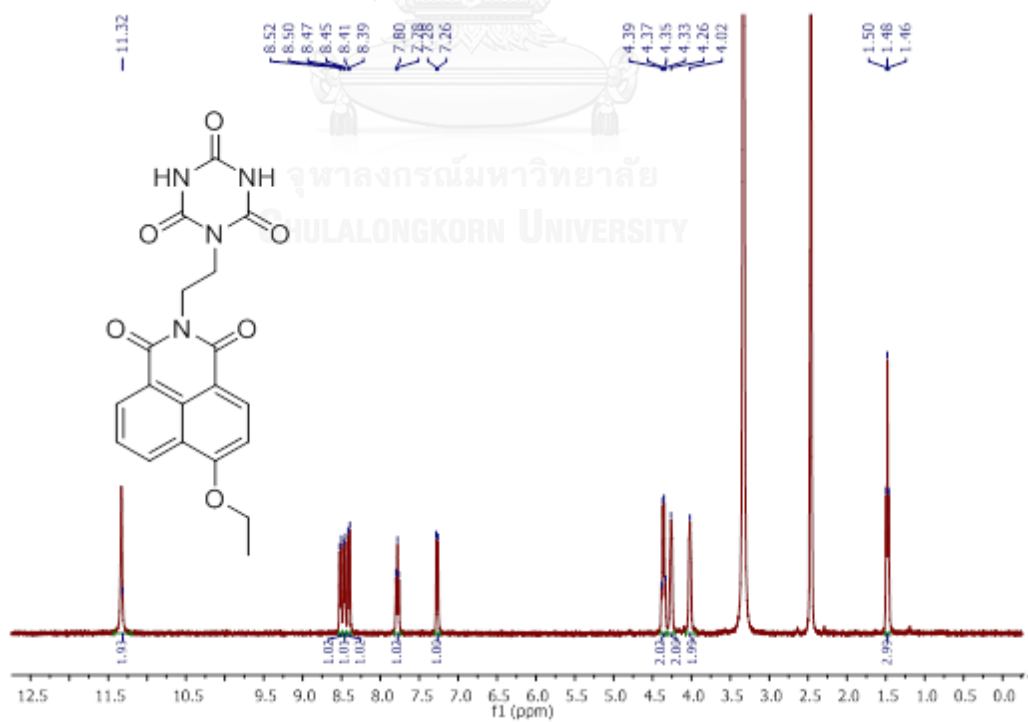


Figure A.10 $^1\text{H-NMR}$ spectrum of F2 in DMSO-d_6 .

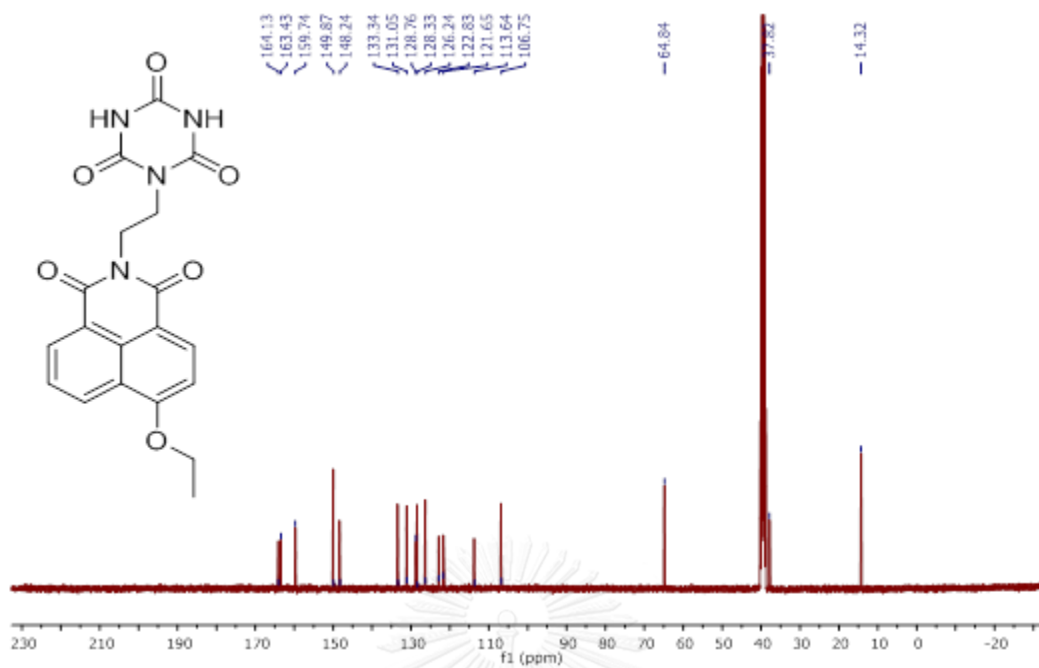


Figure A.11 $^{13}\text{C-NMR}$ spectrum of F2 in DMSO-d_6 .

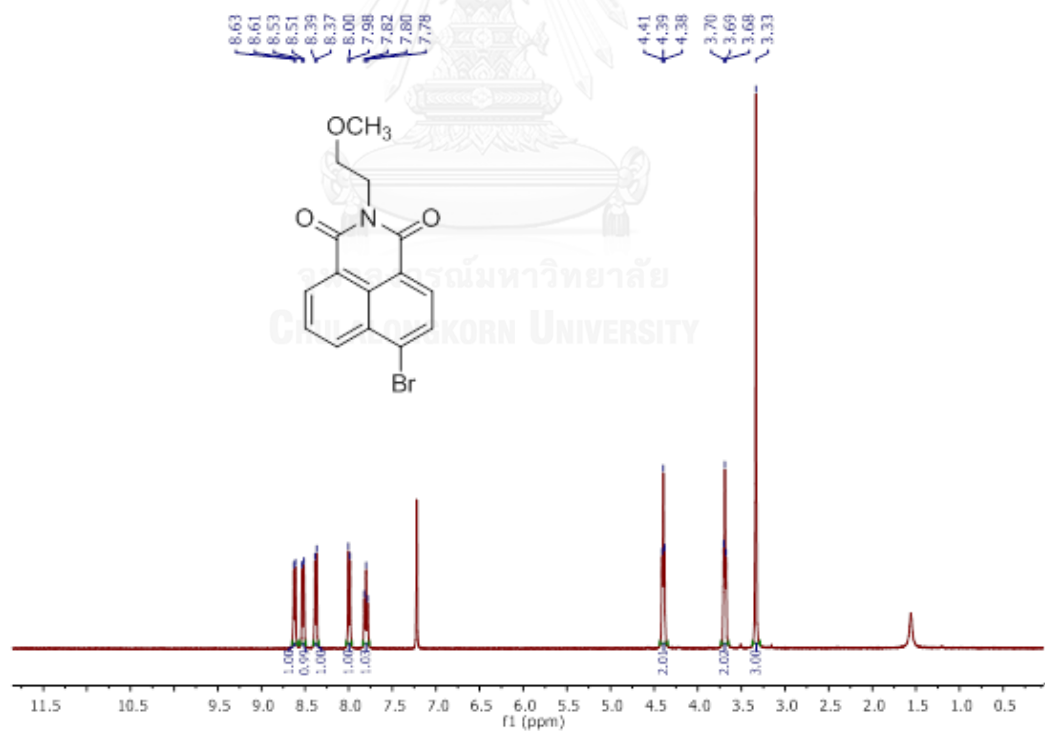


Figure A.12 $^1\text{H-NMR}$ spectrum of 1c in CDCl_3 .

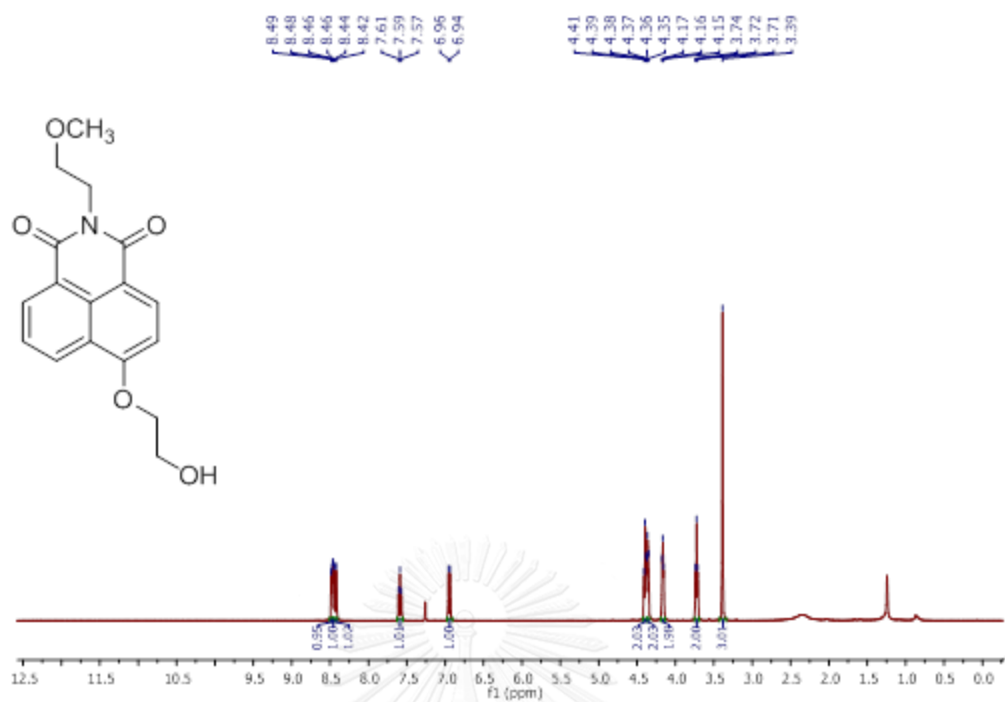


Figure A.13 ¹H-NMR spectrum of **2c** in CDCl₃.

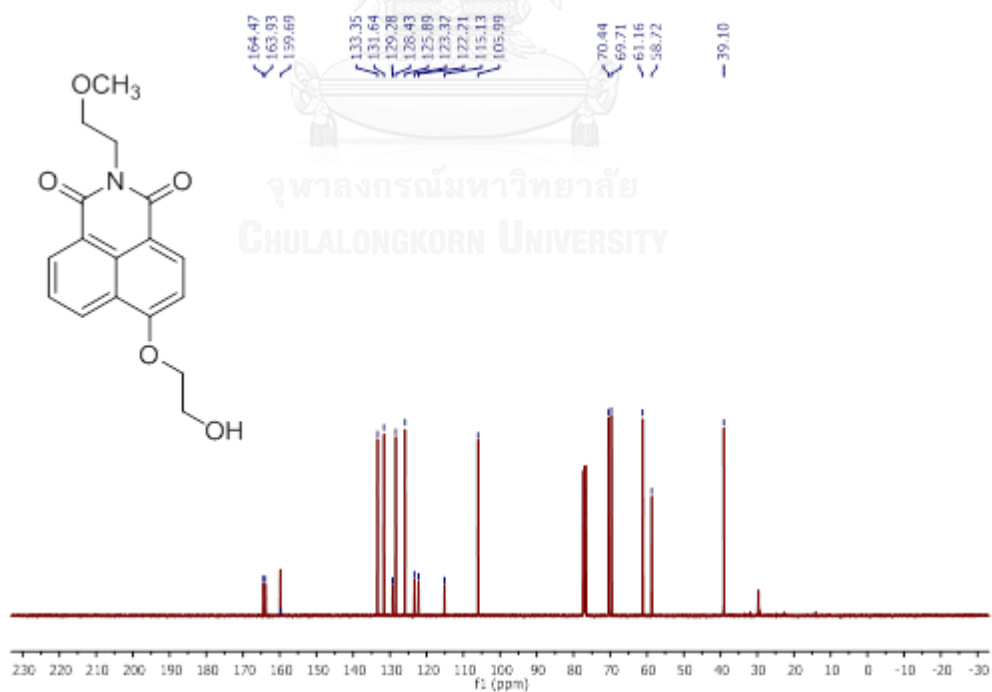


Figure A.14 ¹³C-NMR spectrum of **2c** in CDCl₃.

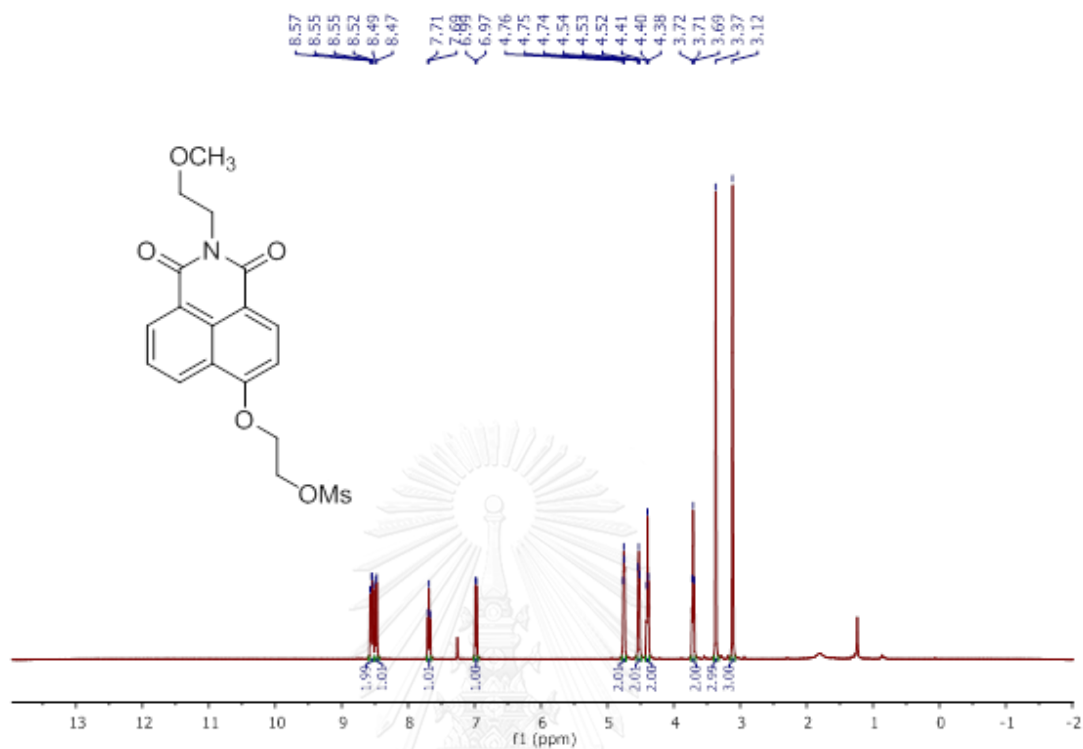


Figure A.15 $^1\text{H-NMR}$ spectrum of **3c** in CDCl_3 .

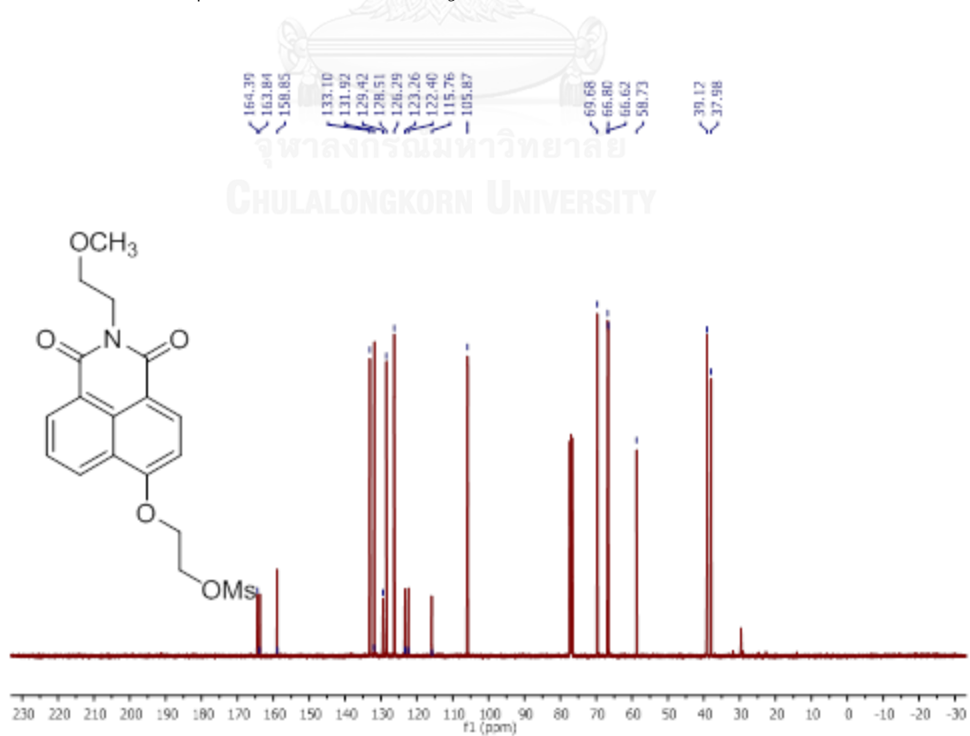


Figure A.16 $^{13}\text{C-NMR}$ spectrum of **3c** in CDCl_3 .

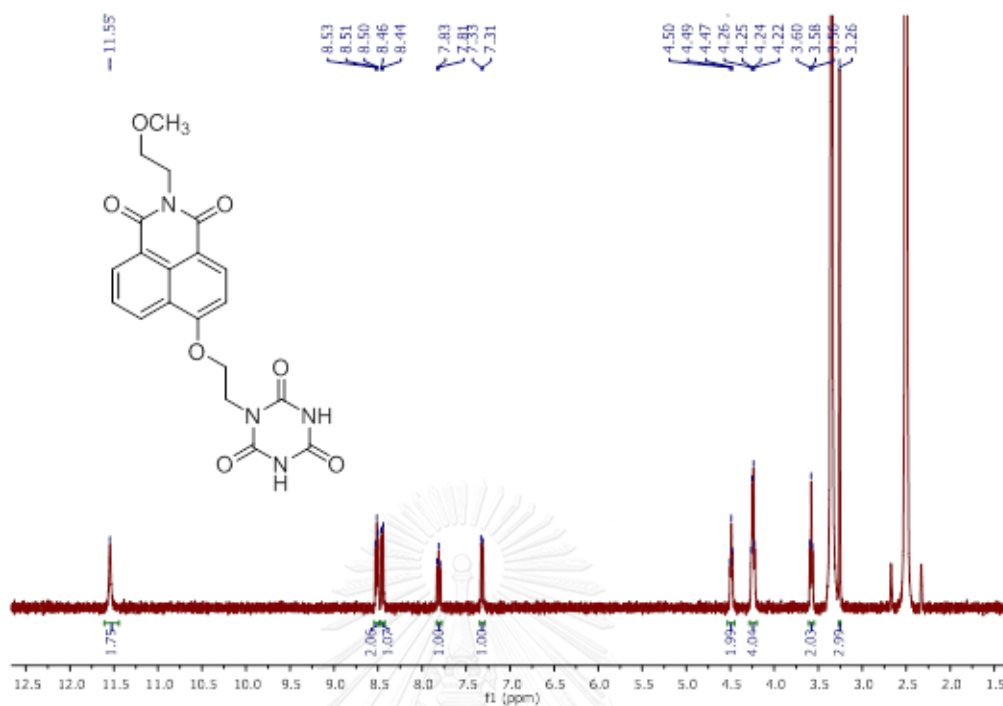


Figure A.17 $^1\text{H-NMR}$ spectrum of F3 in DMSO-d_6 .

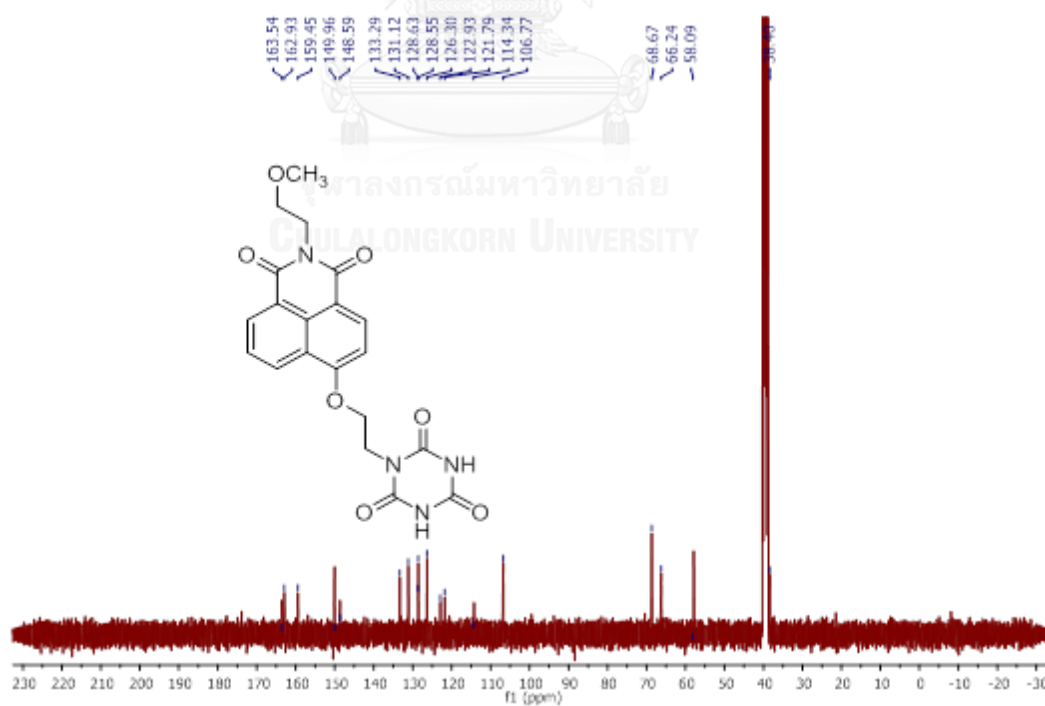
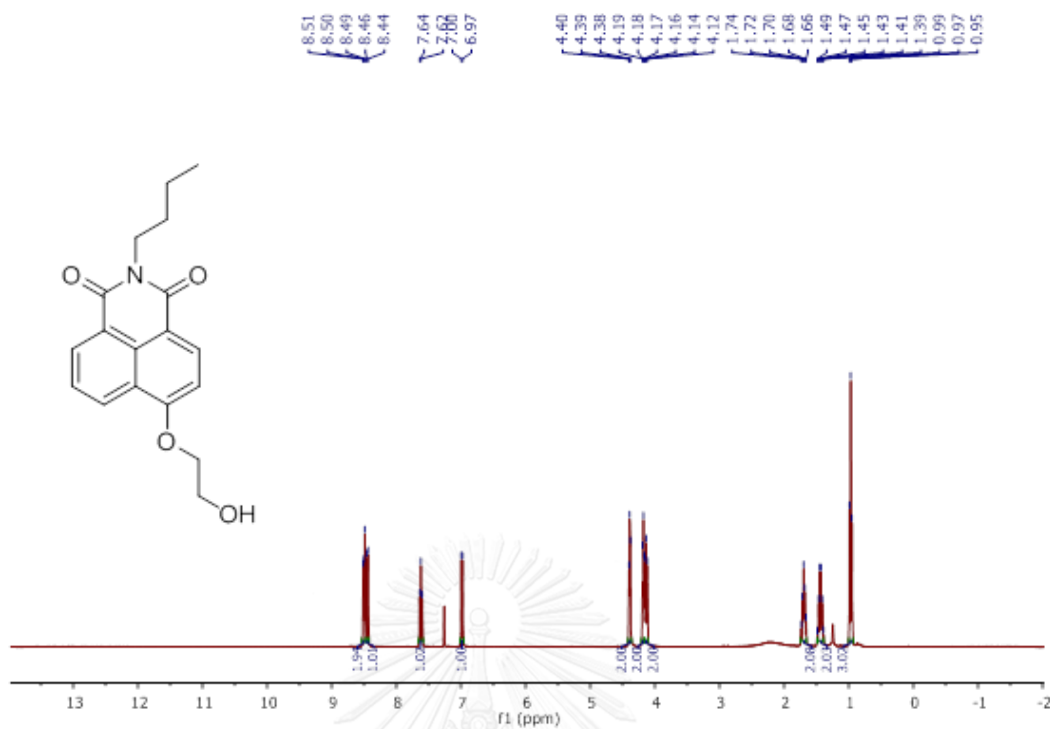
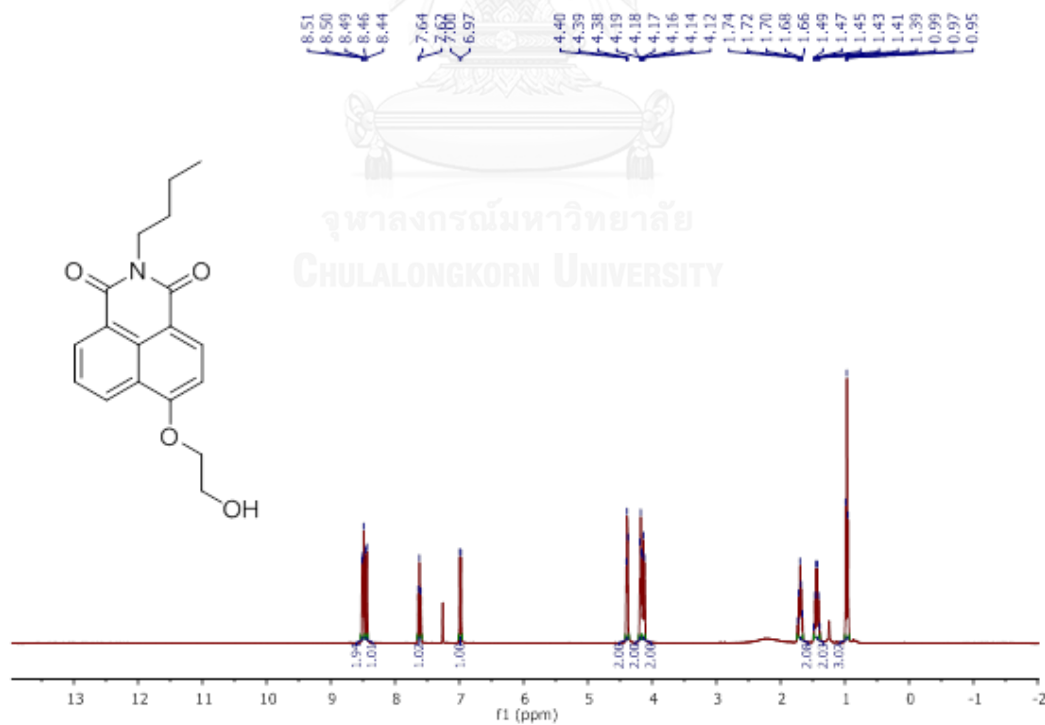


Figure A.18 $^{13}\text{C-NMR}$ spectrum of F3 in DMSO-d_6 .

Figure A.19 $^1\text{H-NMR}$ spectrum of 1d in CDCl_3 .Figure A.20 $^1\text{H-NMR}$ spectrum of 2d in CDCl_3 .

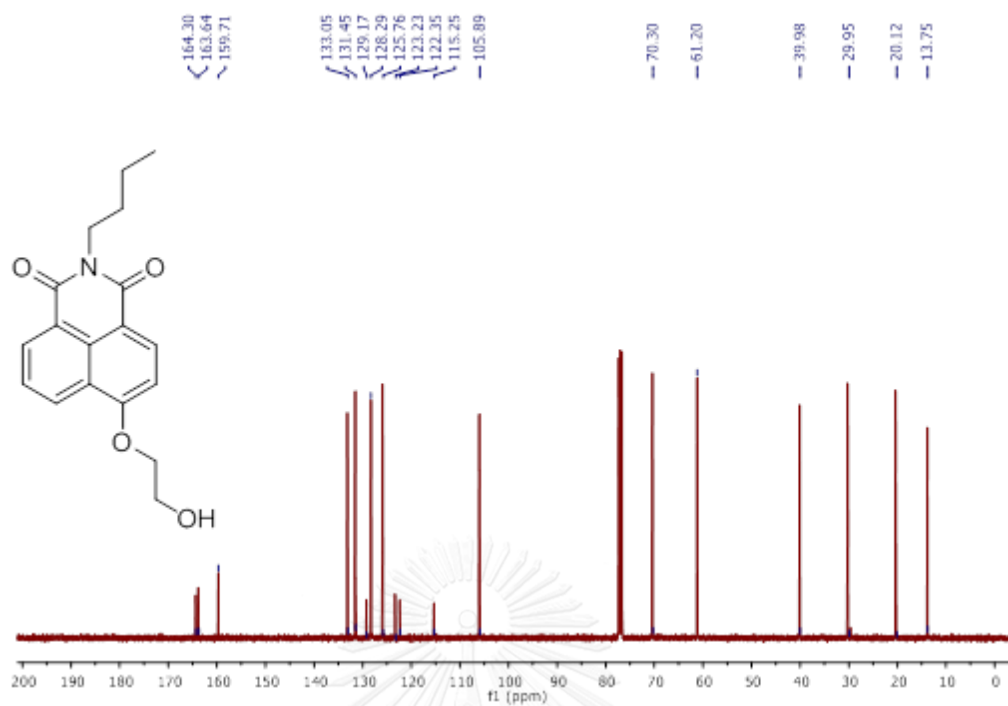


Figure A.21 ^{13}C -NMR spectrum of **2d** in CDCl_3 .

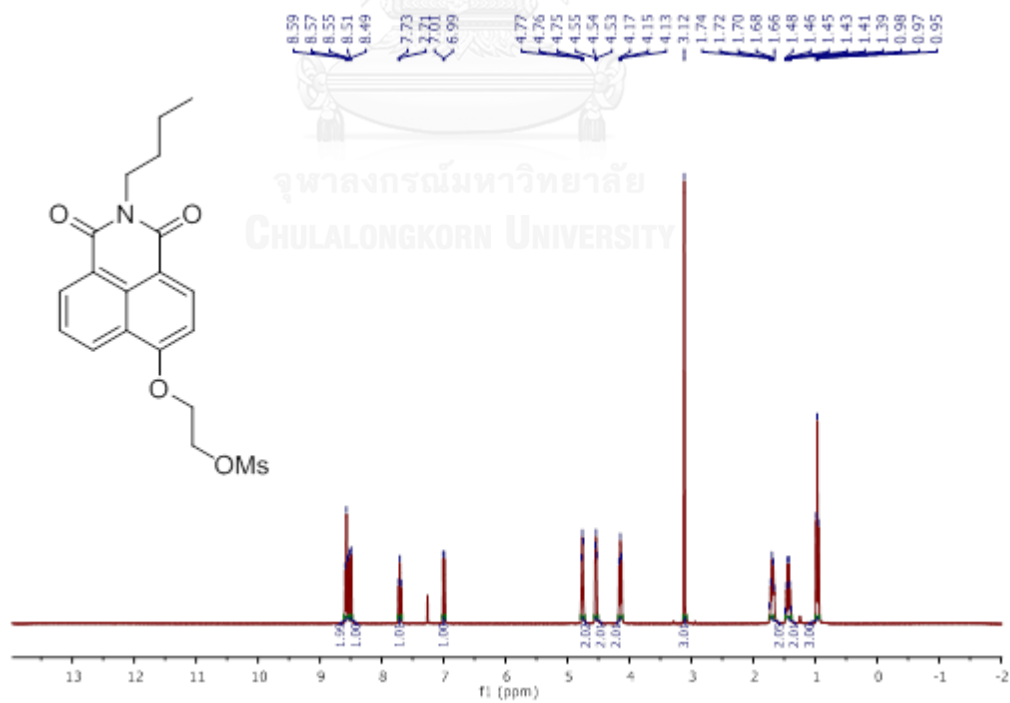


Figure A.22 ^1H -NMR spectrum of **3d** in CDCl_3 .

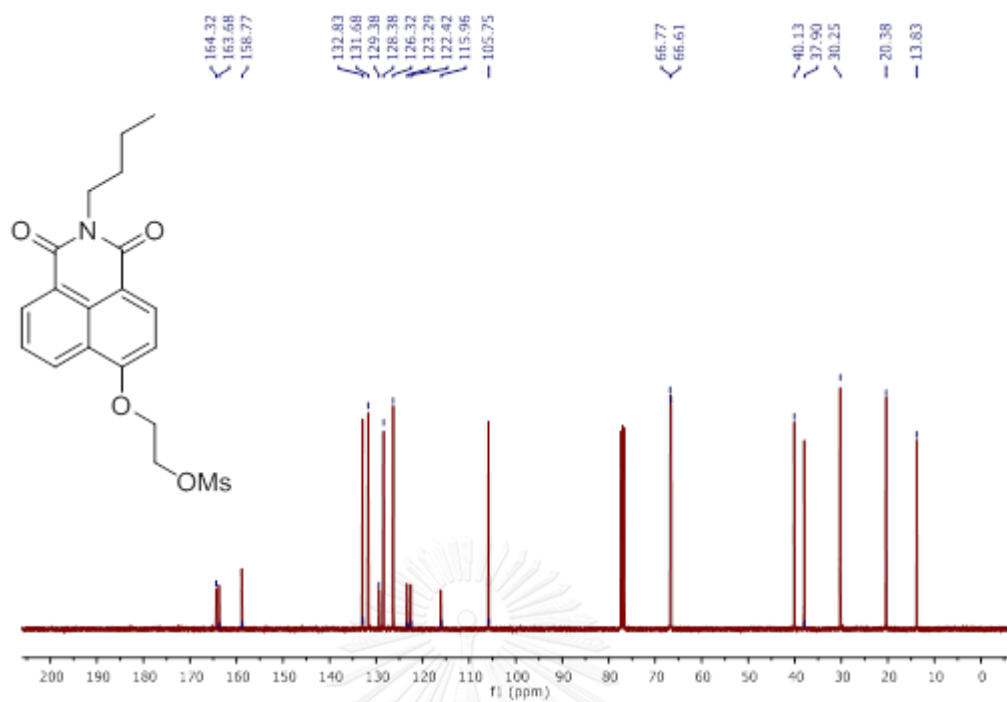


Figure A.23 ¹³C-NMR spectrum of 3d in CDCl₃.

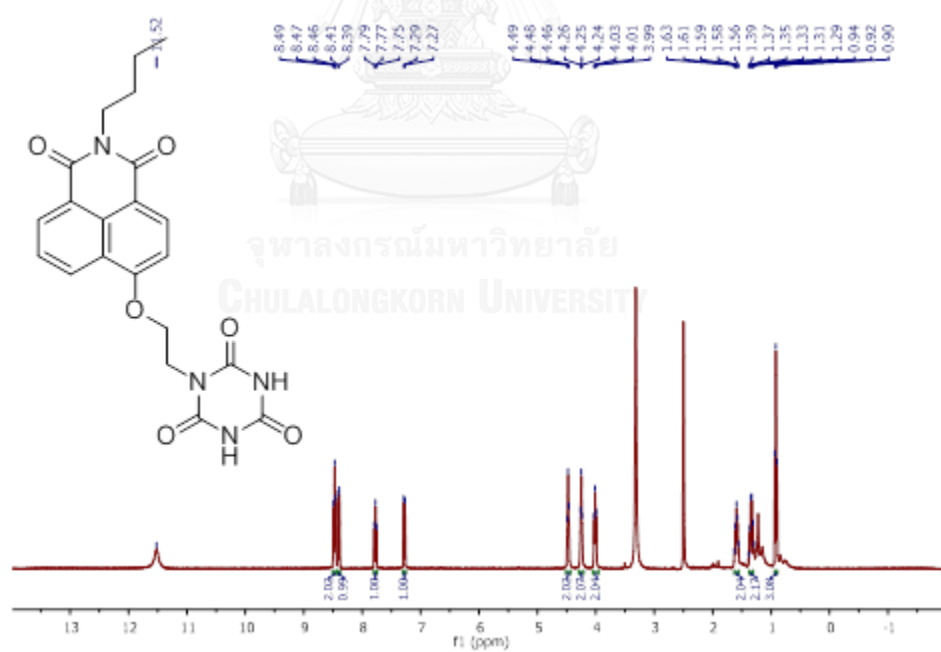


Figure A.24 ¹H-NMR spectrum of F4 in DMSO-d₆.

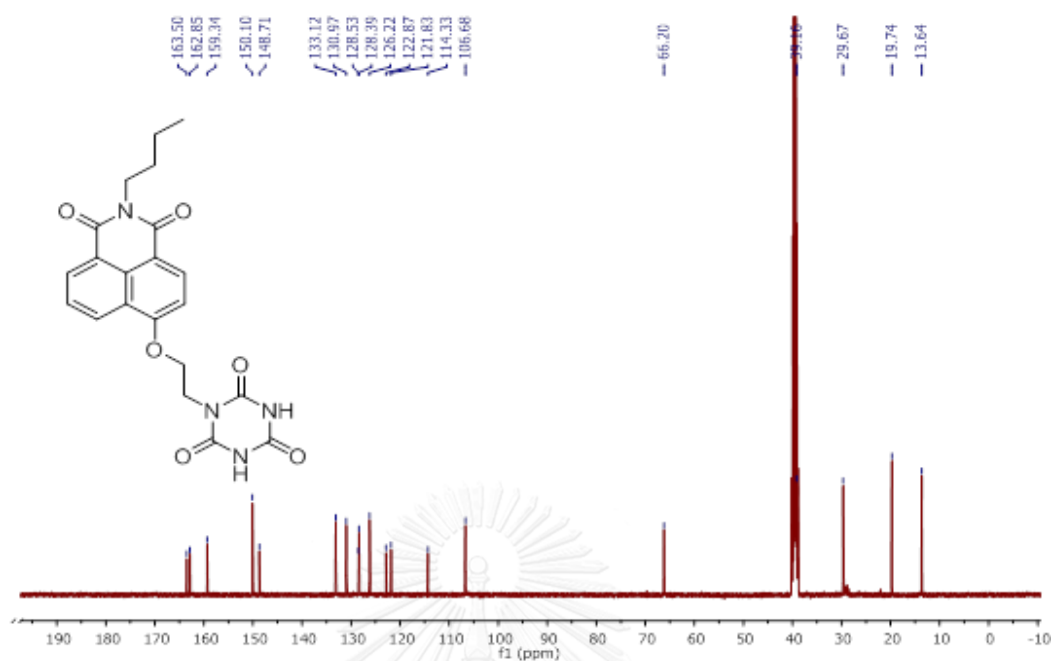


Figure A.25 ¹³C-NMR spectrum of F4 in DMSO-d₆.

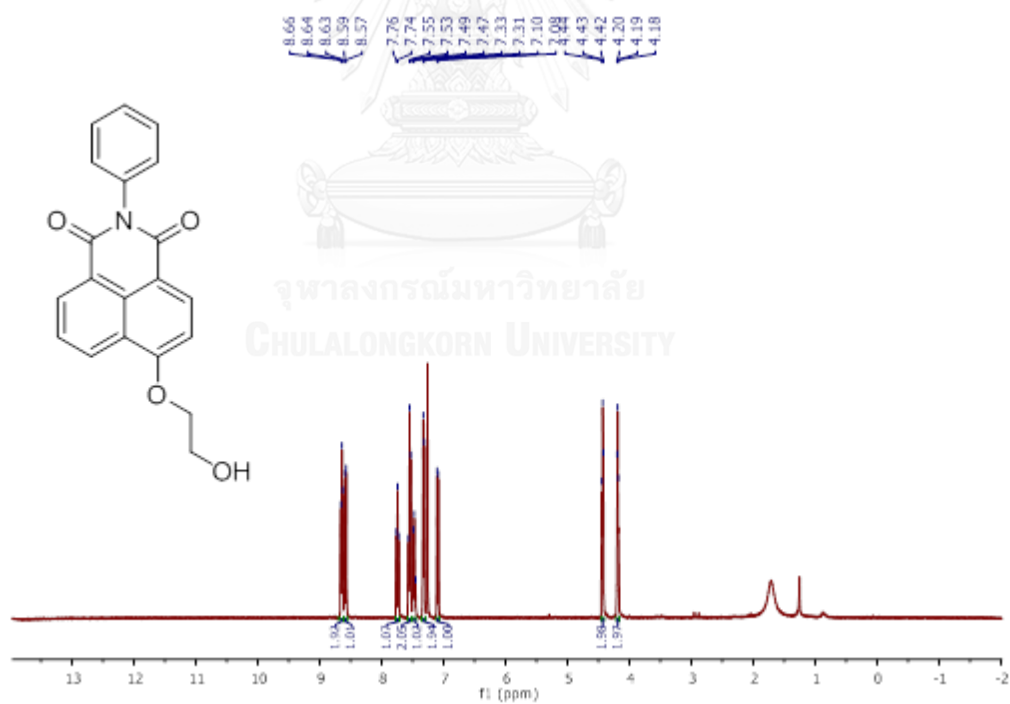


Figure A.26 ¹H-NMR spectrum of 1e in CDCl₃.

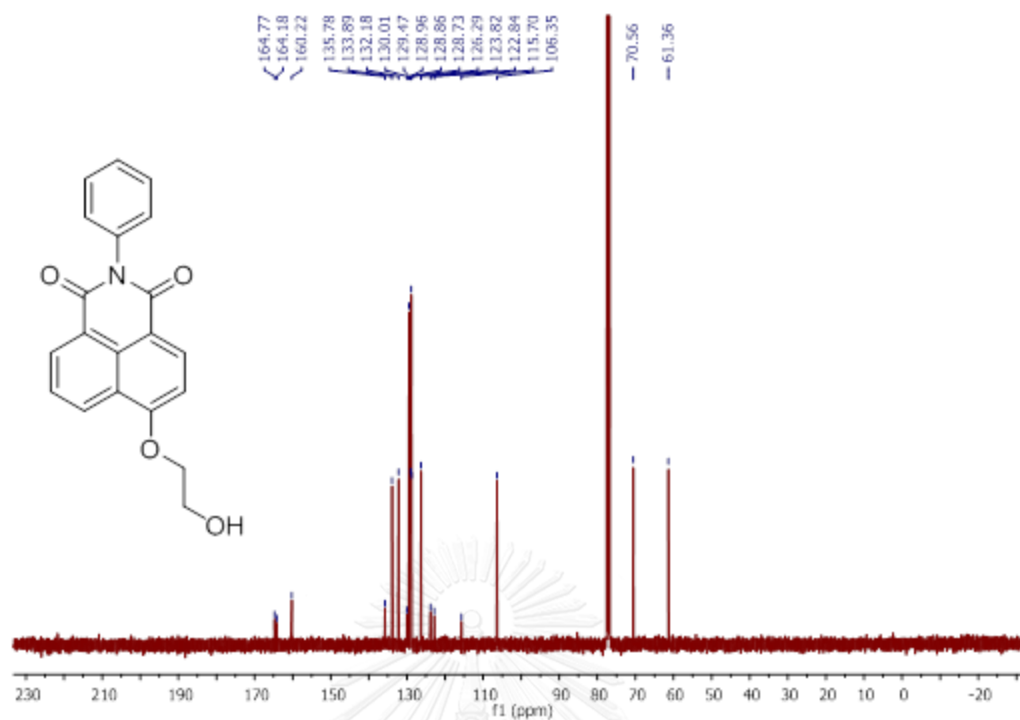


Figure A.27 $^{13}\text{C-NMR}$ spectrum of **1e** in CDCl_3 .

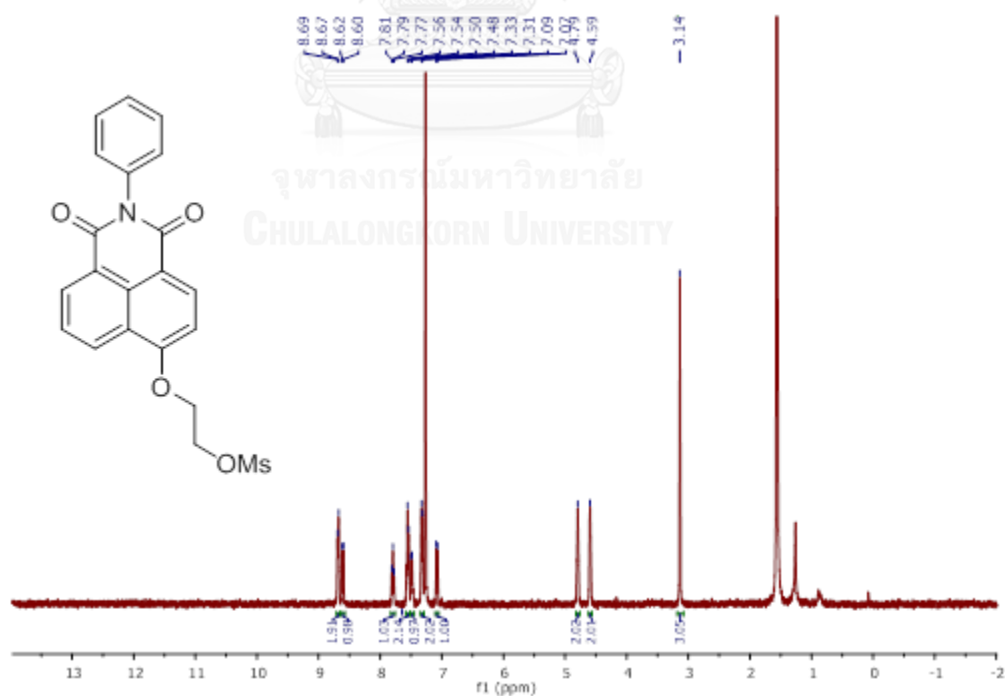


Figure A.28 $^1\text{H-NMR}$ spectrum of **2e** in CDCl_3 .

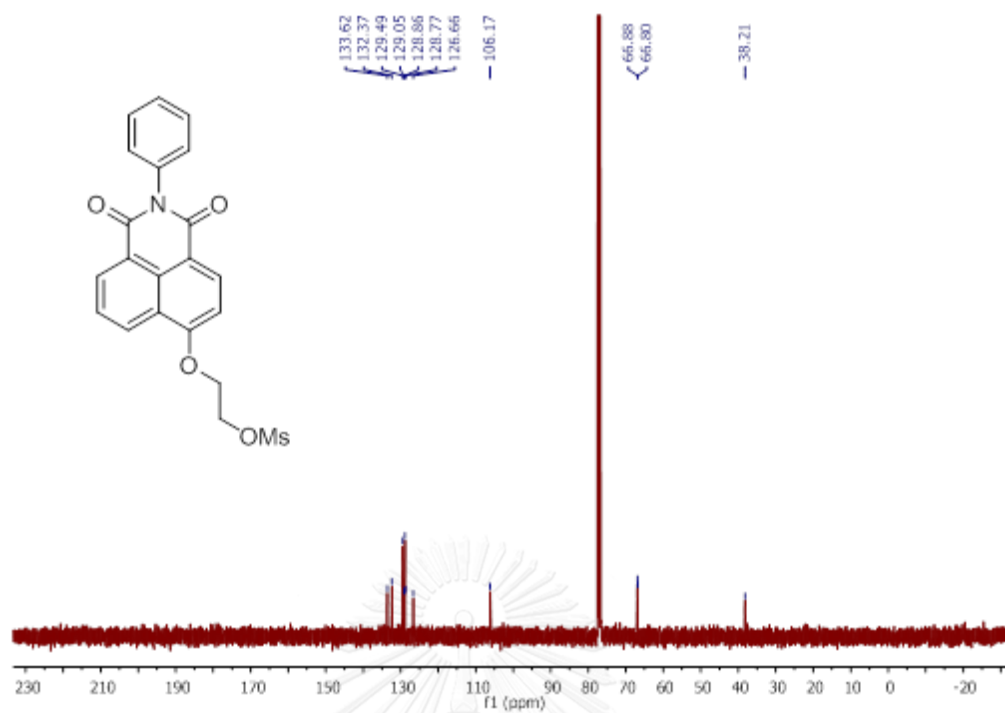


Figure A.29 $^1\text{H-NMR}$ spectrum of **2e** in CDCl_3 .

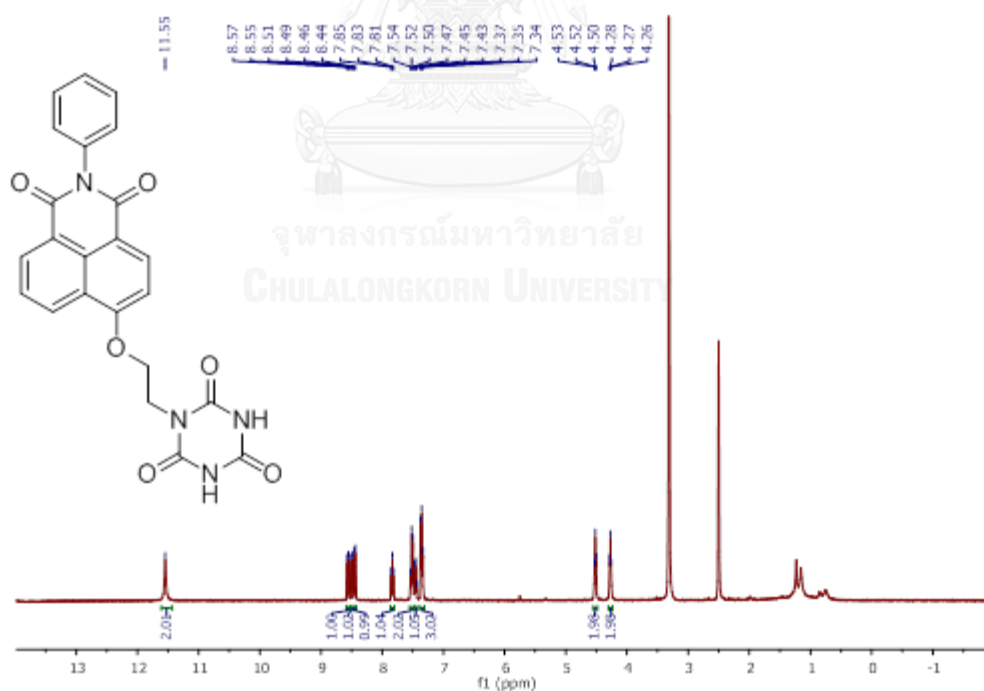


Figure A.30 $^1\text{H-NMR}$ spectrum of **F5** in DMSO-d_6 .

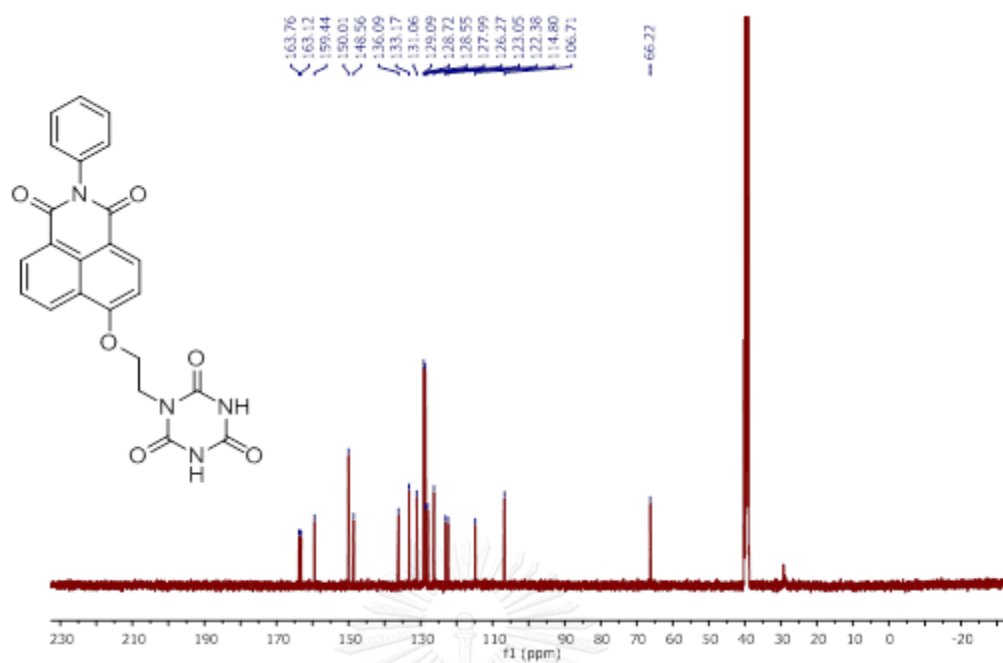


Figure A.31 $^{13}\text{C-NMR}$ spectrum of F5 in DMSO- d_6 .

ใบส่งตัวอย่าง
ศูนย์เครื่องมือวิจัยวิทยาศาสตร์และเทคโนโลยี

รหัส S573404

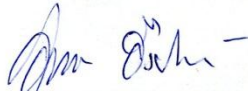
รหัสผู้ขอรับบริการ 0547-2557 (ถ้าทราบรหัสผู้ขอรับบริการให้กรอกข้อมูลตั้งแต่ข้อ 4 ถ้าไม่ทราบให้กรอกตั้งแต่ข้อ 1)

1. ช่างเจ้า / บริษัท (ภาษาไทย) ภรภัทร สำอางค์
2. (ชื่อภาษาจีน/ชื่อภาษาอังกฤษ/ชื่อภาษาไทย) pompat sam-ang
3. ที่อยู่ติดต่อได้สะดวก 47 ใหญ่ลดพาร์ทเมนต์ ห้อง 2-412 เขตราชเทวี พญาไท กทม 10400
4. มหาวิทยาลัย จุฬาลงกรณ์มหาวิทยาลัย ภาควิชา เคมี คณะ วิทยาศาสตร์
5. ชื่อตัวแทน / ผู้ติดต่อได้ จุฬาลงกรณ์มหาวิทยาลัย โทรศัพท์ 0915140056 โทรสาร -
6. ถ้าเป็นเจ้าหน้าที่ประจำหน่วยงาน งานวิจัย วิทยานิพนธ์ โครงการ การเรียนการสอน
7. ต้องการให้ชั่งน้ำหนักเงินในนาม ศูนย์บริการวิชาการแห่งจุฬาลงกรณ์มหาวิทยาลัย (RES500530120-AM)
8. ขอส่งตัวอย่างให้วิเคราะห์ด้วยเครื่อง CHNS/O Analyser จำนวน 2 ตัวอย่าง mode ธาตุ
9. ต้องการวิเคราะห์ C,H,N.
10. ข้อมูลของตัวอย่าง, รหัส NAPH-CYA-1, NAPH-CYA-2
11. ต้องการผลการวิเคราะห์แบบ ข้อมูลดิบ/สเปกตรัมภาพถ่าย CD/DVD รายงานภาษาไทย รายงานภาษาอังกฤษ
12. รับผิดชอบวิเคราะห์โดย รับเอง EMS (50บาท/ครั้ง) FAX (50บาท/ครั้ง) Email
13. ชำระเงินค่าบริการวิเคราะห์โดย เงินสด/เช็ค

ลงชื่อ จิตราพร

ผู้ส่งตัวอย่าง วันที่ 21 พ.ย. 2557

| Sample name | | %Carbon | %Hydrogen | %Nitrogen |
|-------------|---------|---------|-----------|-----------|
| NAPH-CYA-1 | (1) | 58.24 | 3.23 | 15.52 |
| | (2) | 58.19 | 3.20 | 15.52 |
| | Average | 58.22 | 3.22 | 15.52 |
| NAPH-CYA-2 | (1) | 58.11 | 3.65 | 13.85 |
| | (2) | 57.90 | 3.67 | 13.75 |
| | Average | 58.01 | 3.66 | 13.80 |


(นางสาวอัมพร อังปรณแก้ว)
ผู้วิเคราะห์


(นางสุนันท์ รังษิกัญจนส่อง)
หัวหน้าฝ่ายวิเคราะห์

26/11/2014

Figure A.32 Elemental Analysis of F1 and F2.

\\DATA\Template_CHNS - 7 7 58\582722_2682_719R sh

ใบส่งตัวอย่าง
ศูนย์เครื่องมือวิจัยวิทยาศาสตร์และเทคโนโลยี

รหัส S582722

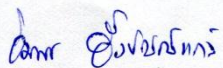
รหัสผู้ขอรับบริการ 0351-2558 (ถ้าทราบรหัสผู้ขอรับบริการให้กรอกข้อมูลตั้งแต่ข้อ 4 ถ้าไม่ทราบให้กรอกตั้งแต่ข้อ 1)

1. ช่างเจ้า / บริษัท (ภาษาไทย) จิตรานูช เพ็งสวัสดิ์
2. ชื่อภาษาอังกฤษเมื่อต้องการรายงานภาษาอังกฤษ CHITTRANUCH PENGSAWAD
3. ที่อยู่ติดต่อได้สะดวก 115/226 หมู่ 7 วิชาลัย 5 สวนผัก คลังชั้น กทม 10170
4. มหาวิทยาลัย จุฬาลงกรณ์มหาวิทยาลัย ภาควิชา เคมี คณะ วิทยาศาสตร์
5. ชื่อตัวแทน / ผู้ติดต่อได้ จุฬาลงกรณ์มหาวิทยาลัย โทรศัพท์ 0876882202 โทรสาร -
6. ถ้าเป็นเจ้าหน้าที่โปรดระบุเป็น งานวิจัย วิทยานิพนธ์ โครงการ การเขียนการสอน
7. ต้องการให้ออกใบเสร็จรับเงินในนาม ภาคเคมี คณะวิทยาศาสตร์
8. ขอส่งตัวอย่างให้วิเคราะห์ด้วยเครื่อง CHNS/O Analyser จำนวน 1 ตัวอย่าง mode ธาตุ
9. ต้องการวิเคราะห์ CHN
10. ข้อมูลของตัวอย่าง, รหัส NAPH CYA3
11. ต้องการผลการวิเคราะห์แบบ ข้อมูลดิบ/สเปกตรัมภาพถ่าย CD/DVD รายงานภาษาไทย รายงานภาษาอังกฤษ
12. รับผลวิเคราะห์โดย รับเอง EMS (50บาท/ครั้ง) FAX (50บาท/ครั้ง) Email
13. ชำระเงินค่าบริการวิเคราะห์โดย เงินสด/เช็ค

ลงชื่อ จิตรานูช ผู้ส่งตัวอย่าง วันที่ 29 ก.ค. 2558

| ค่าที่ระบุมา | | %C | %H | %N |
|--------------|-------|--------------|-------------|--------------|
| NAPH CYA3 | (1)* | 56.44 | 4.26 | 13.14 |
| | (2)* | 56.44 | 4.62 | 12.59 |
| | (3)** | 57.20 | 4.58 | 11.79 |
| | (4)** | 57.69 | 4.37 | 11.18 |
| | (5)** | 56.22 | 4.58 | 12.55 |
| | (6)** | 56.70 | 4.37 | 11.90 |
| | (7)** | 56.51 | 4.56 | 12.35 |
| | (8)** | 56.67 | 4.64 | 12.45 |
| | (9)** | 57.20 | 4.58 | 11.79 |
| | (9)** | 57.69 | 4.37 | 11.18 |
| เฉลี่ย | | <u>56.93</u> | <u>4.52</u> | <u>11.98</u> |

* ผลวิเคราะห์จากการวิเคราะห์ด้วยเครื่องมือ
** ผลวิเคราะห์จากการคำนวณใหม่


(นางสาวอัมพร อึ้งปรกรณ์แก้ว)

ผู้วิเคราะห์


(นางสุนันท์ รังษิกกาญจน์สอง)

หัวหน้าฝ่ายวิเคราะห์

1/8/2015

Figure A.33 Elemental Analysis of F3.

Mass Spectrum List Report

| Analysis Info | | Acquisition Date | |
|-----------------------|----------------------------------|-----------------------|---------------|
| Analysis Name | OSCUJP581109001.d | 11/10/2015 1:39:18 PM | |
| Method | MKE_tune_low_positive_20130204.m | Operator | Administrator |
| Sample Name | F4 | Instrument | micrOTOF 72 |
| Acquisition Parameter | | Set Corrector Fill | 50 V |
| Source Type | ESI | Ion Polarity | Positive |
| Scan Range | n/a | Capillary Exit | 180.0 V |
| Scan Begin | 50 m/z | Hexapole RF | 90.0 V |
| Scan End | 3000 m/z | Skimmer 1 | 45.5 V |
| | | Hexapole 1 | 25.0 V |
| | | Set Pulsar Pull | 337 V |
| | | Set Pulsar Push | 337 V |
| | | Set Reflector | 1300 V |
| | | Set Flight Tube | 9000 V |
| | | Set Detector TOF | 2093 V |

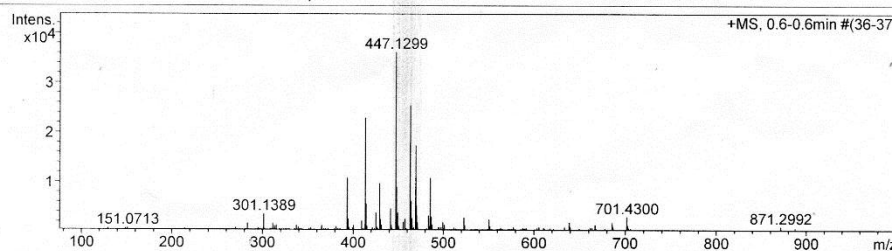


Figure A.34 HRMS spectrum of F4.

Mass Spectrum List Report

| Analysis Info | | Acquisition Date | |
|-----------------------|----------------------------------|-----------------------|---------------|
| Analysis Name | OSCUJP581109002.d | 11/10/2015 1:42:49 PM | |
| Method | MKE_tune_low_positive_20130204.m | Operator | Administrator |
| Sample Name | F5 | Instrument | micrOTOF 72 |
| | F5 | | |
| Acquisition Parameter | | Set Corrector Fill | 50 V |
| Source Type | ESI | Ion Polarity | Positive |
| Scan Range | n/a | Capillary Exit | 250.0 V |
| Scan Begin | 50 m/z | Hexapole RF | 90.0 V |
| Scan End | 3000 m/z | Skimmer 1 | 45.5 V |
| | | Hexapole 1 | 25.0 V |
| | | Set Pulsar Pull | 337 V |
| | | Set Pulsar Push | 337 V |
| | | Set Reflector | 1300 V |
| | | Set Flight Tube | 9000 V |
| | | Set Detector TOF | 2093 V |

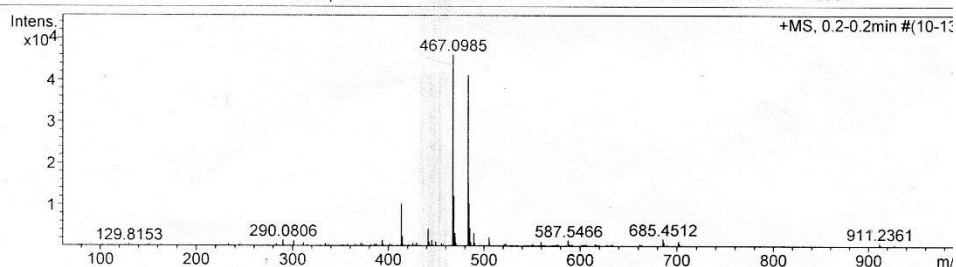


Figure A.35 HRMS spectrum of F5.

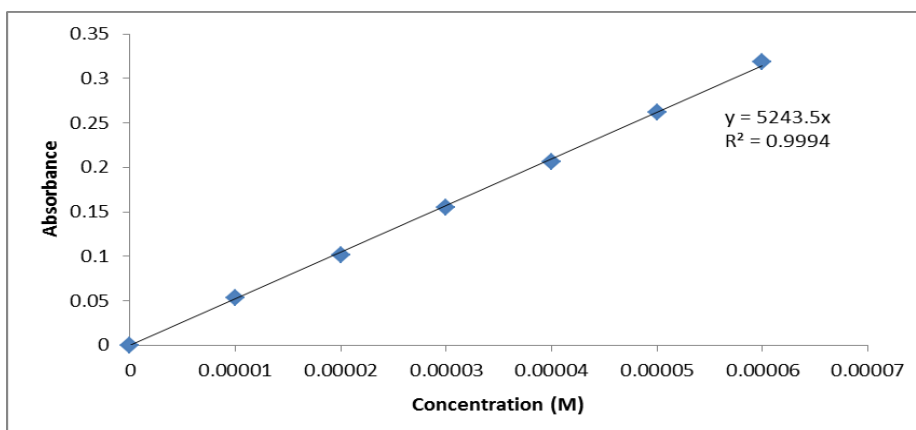


Figure A.36 Molar absorption coefficient plot of F1 in CH₃CN.

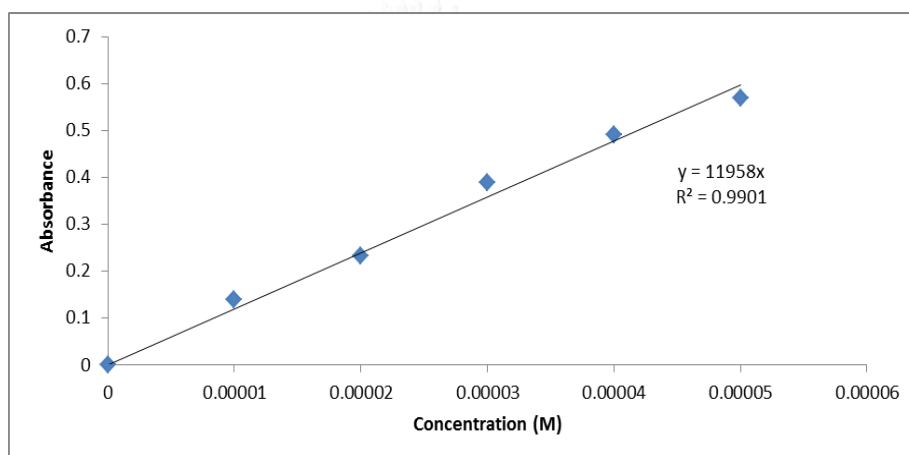


Figure A.37 Molar absorption coefficient plot of F2 in CH₃CN.

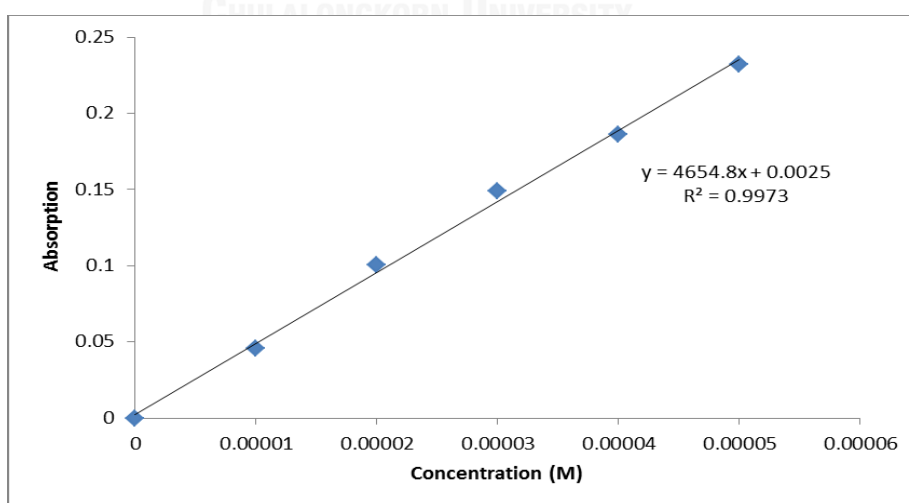


Figure A.38 Molar absorption coefficient plot of F3 in DMSO.

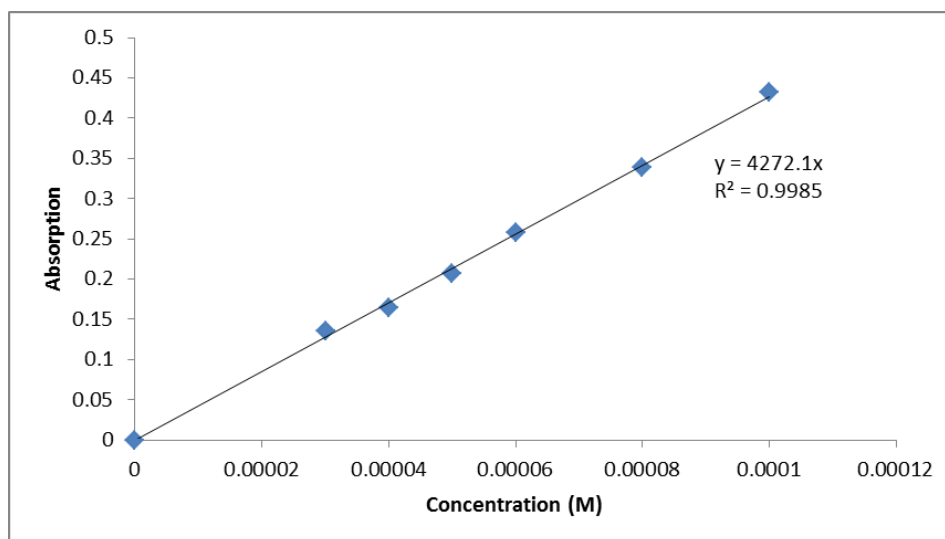


Figure A.39 Molar absorption coefficient plot of F4 in DMSO.

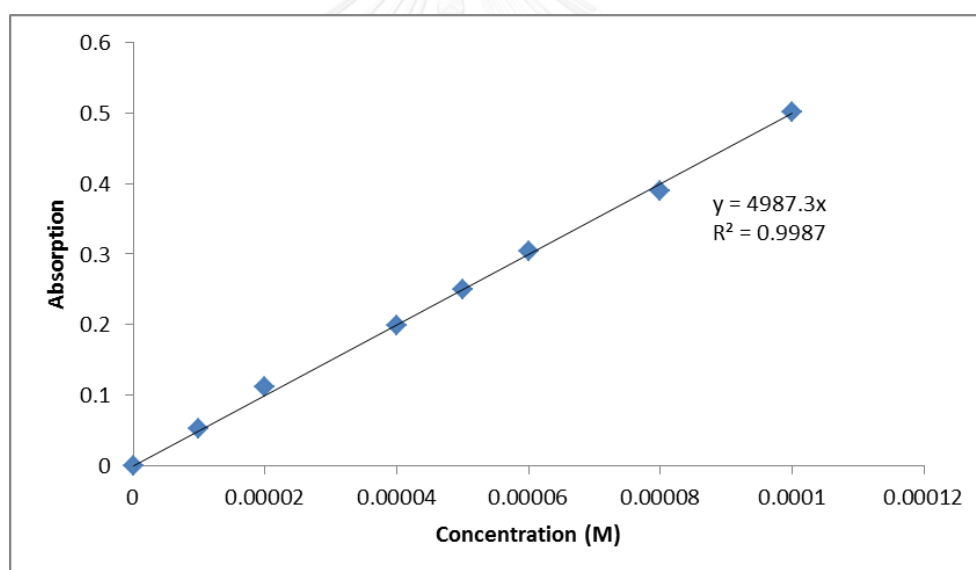


Figure A.40 Molar absorption coefficient plot of F5 in DMSO.

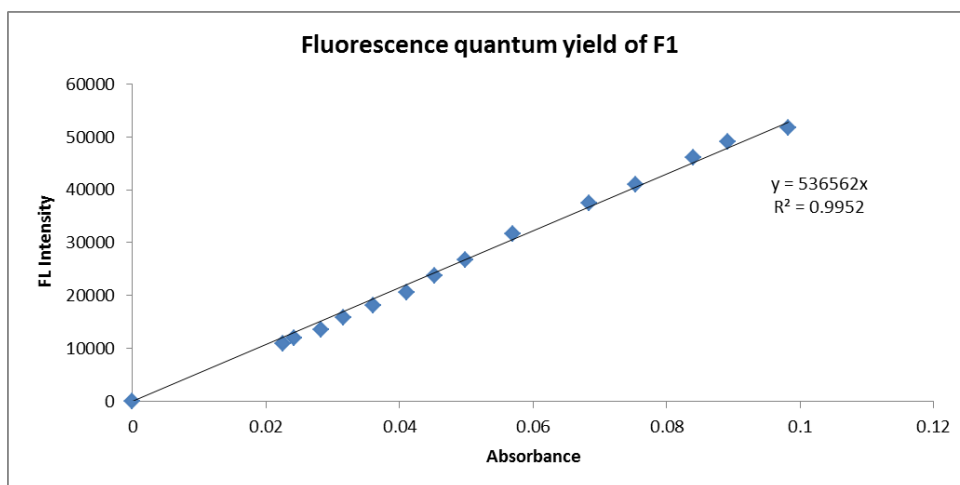
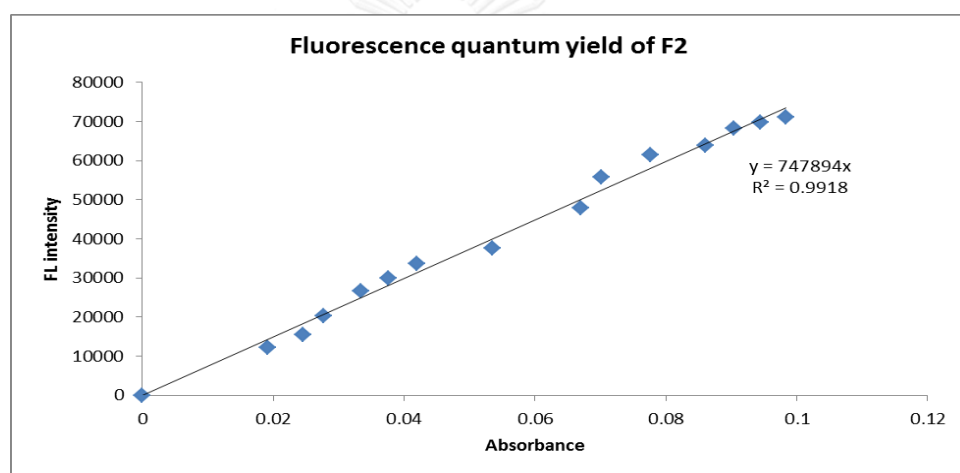
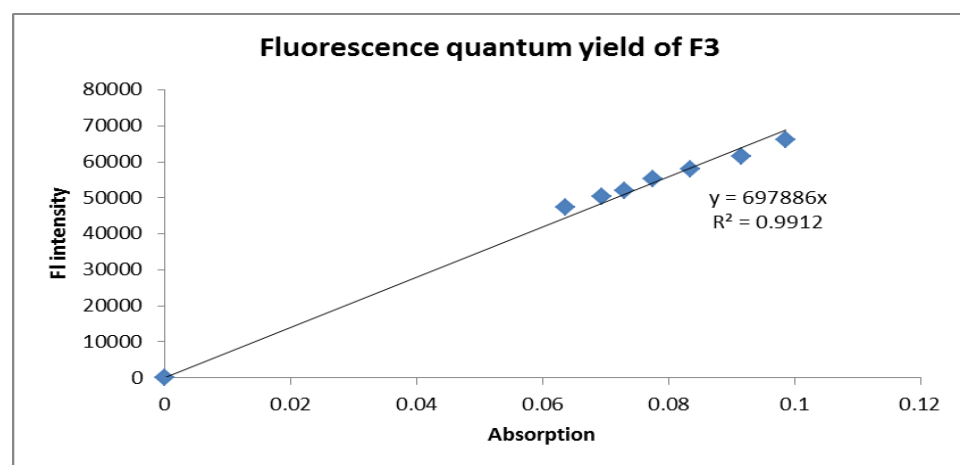
Figure A.41 Quantum yield plot of F1 in CH₃CN.Figure A.42 Quantum yield plot of F2 in CH₃CN.

Figure A.43 Quantum yield plot of F3 in DMSO.

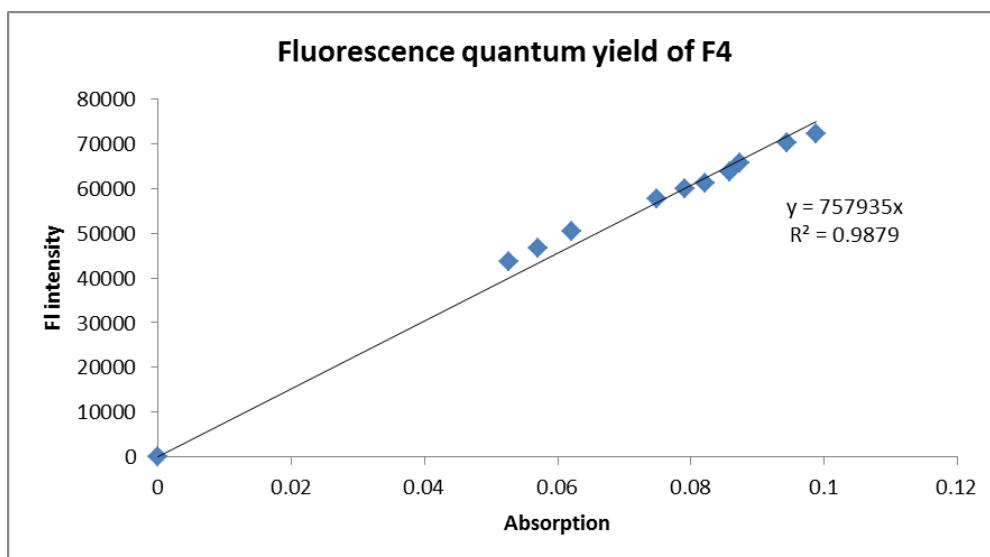


Figure A.44 Quantum yield plot of F4 in DMSO.

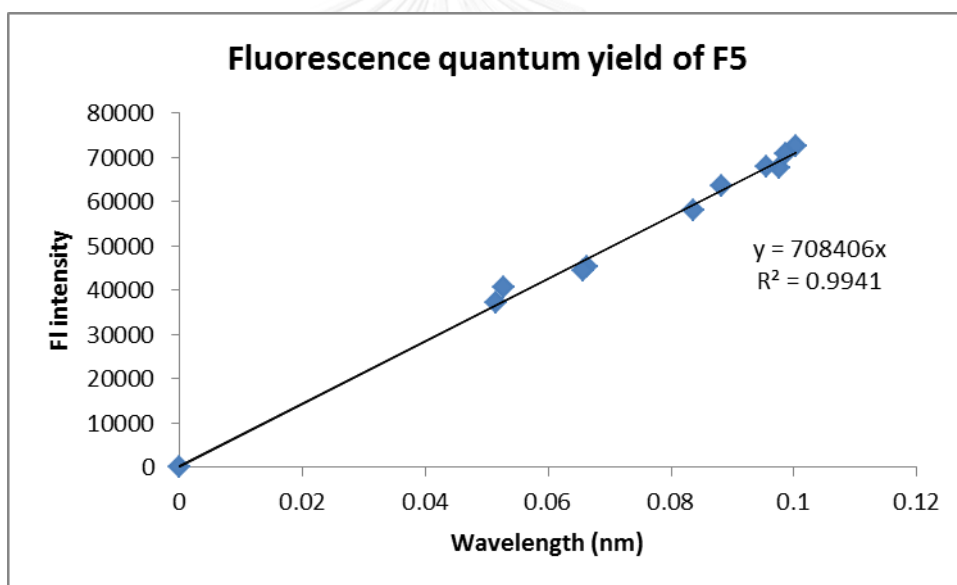


Figure A.45 Quantum yield plot of F5 in DMSO.

VITA

Ms. Chittranuch Pengsawad was born on February 5, 1988 in Uthaitani, Thailand. She graduated with high school degree from Nongchang Wittaya School, Uthaitani in 2006. In 2010, she got a Bachelor's Degree of Science with a major in Chemistry from Srinakharinwirot University. In 2013, she started her a Master's Degree in Petrochemistry and Polymer Science program, Chulalongkorn University. During her master course, she joined Material Advancement and Proficient Synthesis (MAPS) group under supervision of Assoc. Prof. Dr. Paitoon Rashatasakhon. She has presented her research at Pure and Applied Chemistry International Conference 2015 (PACCON 2015), Bangkok, Thailand on January 22nd 2015.

Her address is 115/226 Moo 7, Beauty House 5, Suanpuk road, soi suanpuk 50, Chimplee, Taling chan, Bangkok, 10170, Thailand.